Development of a Passive Lower Body Exoskeleton with Novel Compliant Joints for Walking Assistance

Design of Mechanical Systems

Master Thesis

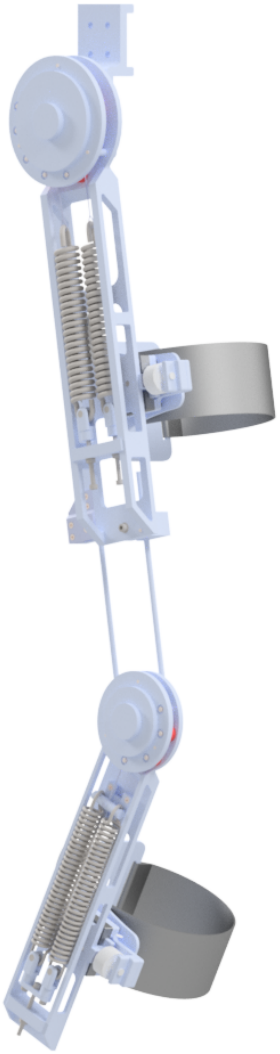

Participants
Jørgen Bjoner
Roger Hole

AALBORG UNIVERSITY

Supervisor
Shaoping Bai

Abstract

This project presents the development of a passive lower body exoskeleton. The exoskeleton is designed with the rehabilitation of post-stroke patients in mind, where an exoskeleton could be utilized as a wearable assistive device for regaining a natural gait cycle. The project base its research in the general trend of existing devices to be unnecessary heavy, and possibly unsafe due to the lack of a compact mechanism.

The scope of this project limits itself to an exoskeleton designed to overcome the gravitational and inertial effects during walking. A simplified dynamic design tool, developed by the authors in a previous project, is utilized for estimation of the generated torque in the lower limb joints. The simplified model has been modified further to include, and more accurately portray, the effect of ground reaction forces during the stance phase. These effects will however not be considered in the design of the exoskeleton.

The passive mechanism proposed is a carefully designed pulley system used to convert the tension force of built-in springs into torques, for overcoming the gravitational and inertial loads during gait. The configuration of the mechanism is optimized with respect to the torque requirements. From this analysis, it's discovered that high stiffness springs with a substantial pretension is required. This lead to the choice of using practical linear tension springs in the design.

The hip and knee exoskeletons share a similar design which consist of an aluminium frame, where the linear springs are placed alongside the frame. This ensures a safe and compact design. To evaluate the structural integrity of the design are the critical load cases estimated by assessment of the cable tension in the system, in addition to the gravitational loads on the system. By structural analysis is the deformation of the frame discovered to be the most influential design factor.

Initial analysis of stress and strain energy indicates that the initial design have an unnecessary large weight. It's therefore decided to perform a topology optimization of the outer frame, which is seen to be the largest weight contributor. The result is a lightweight design where "frame walls" are designed to counteract the displacement, in addition to effectively shielding the springs from the environment. The weight is effectively reduced by 58% in the hip frame and 49% in the knee frame.

In the end is the assistive performance of the design simulated by import of the initial CAD to a multibody dynamic software. A simulation is performed of the complete exoskeleton attached to a humanoid model of the leg. The results shows that the average driving torque was reduced by approximately 66% in the hip and 72% in the knee.

AALBORG UNIVERSITY
STUDENT REPORT

Study Board of Mechanics and Physics
Fibigerstræde 16
DK - 9220 Aalborg East
Tlf. 99 40 85 32
snmp@mp.aau.dk
http://www.mp.aau.dk

Title:
Development of a passive lower body exoskeleton with novel compliant joints for walking assistance

Semester: DMS4, Spring semester 2020

Semester Theme: Master's Thesis

Project Period: 03.02.2020-03.06.2020

ECTS: 30 per participant

Supervisor: Shaoping Bai

Project Group: Group 23D

Jørgen Bjoner

Roger Hole

Number of Printed:	1 Pieces
Pages:	89 Pages
Appendix:	5
Date of Completion:	June 3, 2020

Synopsis:

This project presents the development of a passive lower body exoskeleton for use in post-stroke walking assistance. A simplified dynamic design tool, developed by the authors in the previous semester, was used to obtain the estimated torque requirements of the lower limb joints. The assistive joint mechanism consist of a pulley system used to convert the tension force in springs into balanced torques. The configuration of this mechanism was further optimized based on torque requirements. Structural analysis revealed that the initial design was subjective to deformation, due to the presence of a high pretension force. This was later accounted for by a topology optimized design. In the end was the assistive performance of the design investigated by import of the CAD model to a multi-body dynamic software. It was observed a substantial decrease in average driving joint torque, compared to not wearing the exoskeleton.

Preface

This report is a master thesis written by two students during the 4th semester at the master's programme: "Design of Mechanical Systems" at Aalborg University. This project considers 30 ECTS per student, and was carried out under the Department of Materials and Production, from the 3rd of February to the 3rd of June 2020. The thesis presents the design process of a passive lower limb exoskeleton used in gait rehabilitation. The authors would like to express their gratitude to project supervisor Shaoping Bai and Ph.D student Harun Leto for their valuable counseling during this project period.

Reading and Formalities
The report is divided by a system of three numbers (x,y,z), where x indicates the chapter, y the section, and z the subsection.

Harvard referencing [Surname of author(s), year of publication] is used throughout the report. The complete reference list is given at the end of the report. If the content described is based on a specific reference will this reference be stated in the beginning of the relevant section. If specific statements or external data are presented, the reference is displayed directly with this statement. Pictures and figures not referenced in the report are either captured or created by the authors.

Figures, tables and equations are numbered with respect to the chapter numbers e.g. the first figure in chapter 1 is displayed as 1.1, the second as 1.2 etc. The numbering is displayed underneath the respective figure/table along with a short description of what is presented. Numbered equations are displayed with a bracket e.g. (1.1), which is displayed in the right margin of the page, next to the equation.

The appendices are presented after the complete list of references. The appendix pages are organized by a capital letter indicating sections and numbers indicating subsections e.g. A1, A2 etc.

Extra Note
This thesis was written in the midst of the global COVID-19 outbreak. As a result have the report been limited to a purely theoretical approach.

Table of contents

1 Introduction

Dysfunctions in the lower limb is a common struggle for people throughout the world. Stroke, spinal cord damage, degradation of musculature and other injuries may cause a patient to undergo repetitive sessions of rehabilitation in order to regain natural movement in the lower limbs. For this application, exoskeletons are becoming a larger part of the health sector.

An exoskeleton is a wearable device, utilized to assist human motion performance. In the case of a lower body exoskeleton, it's typically used to assist in the human gait cycles, or it's designed for more specific tasks. Depending on their application may the exoskeleton include sensors and actuators (an active exoskeleton) or it may be completely passive. The actuators in the active exoskeleton is typically driven by electrical or hydraulic motors, and are able to produce a predefined motion. This motion is typically found from motion capture of the patients gait. Such active exoskeletons are able to assist with different power levels and are in wide use already. An example is the BLEEX exoskeleton, designed at the university of Berkeley. The main goal of this exoskeleton is to increase the carrying capacity of healthy humans and is aimed towards military applications. Hybrid Assistive limb or "HAL", developed by Cyberdyne, detects bioelectric signals from the brain and use these for generating the desired movement of the user. HAL was originally designed to assist disabled and elderly users, but have seen applications also in disaster rescue and construction.

(a) BLEEX, (Zoss et al. [2006])

(b) HAL-ML05, (Wall et al. [2014])

Figure 1.1: State of the art lower body exoskeletons.

Active exoskeletons are however limited by its usually heavy weight, high cost and the patients inability to influence the trajectory. In Belda Lois et al. [2011], it was proven that a patients ability to freely balance and constrain the motion is highly important for complete rehabilitation. An alternative is therefore the passive exoskeleton.

A passive exoskeleton typically uses a spring mechanism to assist the motion, without the need of any external power source. The springs can typically be used for two purposes. The first being to store and release energy per step, and the other to compensate for the gravitational forces caused by the weight of the limbs. With the latter being the most utilized, such exoskeletons have the advantages of being lighter and cheaper to produce. While a passive exoskeleton lacks the ability to computationally change the trajectory and accurately alter assist level, such exoskeletons may be designed for a specific medical case for a specific patient.

1.1 Applications of a Passive Exoskeleton

Passive exoskeletons are increasingly utilized in the industry, where wearable devices are used to reduce the fatigue build-up in a workers body. An example is the passive hip exoskeleton designed by Bosch et al. [2016] to reduce the loads in the lumbar region. Passive exoskeletons also sees application in assisting the elderly, whom may suffer from degradation of the musculature. A lightweight and easy to use exoskeleton could then potentially improve their quality of life. In addition may a lower body passive exoskeleton be used in more specific medical applications, which will be further investigated in this thesis.

This project of passive exoskeletons is in collaboration with doctors at Aalborg University Hospital (AUH). Some perspectives from doctors are thus:

1. Possible applications.
2. User acceptance.
3. Requirements.

1) Possible Applications
Some specific clinical cases considered including:

- **Over-extension of joints**
  A patient currently under treatment have a tendency to over-extend the knee joint. During human walking, this could provide difficulties in the stance phase. A passive exoskeleton could be designed to constrain this extension of the knee.
- **Aftermath of surgery**
  Bone extension surgery was mentioned as an example where a passive exoskeleton would be used in the recovery phase. In this case would the muscles be in tension after the bone extension and would require slacking. A passive exoskeleton could in theory assist with this problem.
- **Assist after muscle removal**
  Muscles may have to be removed from joints due to accidents or more specific cases such as tumor propagation. This could thereby be a joint specific case for which an passive exoskeleton could provide extra assistance in the joint.

- **Stroke rehabilitation**
  A common outcome after a stroke is hemiparesis of the right or left side of the body. Hemiparesis is a collective term and can occur on the entire side of the body or just in certain limbs, and to very different degrees of severity. The degree of paresis can be decreased through rehabilitation and during the later stages of rehabilitation are passive exoskeletons applicable.

2) User Acceptance
While an exoskeleton can be proven to provide assistance with the given medical case, it all comes down to the patients willingness to actually wear the exoskeleton. This is believed to not only rely on comfort when wearing it, but also the aesthetics and ease of use. The patient is additionally more likely to wear the exoskeleton if it's designed specifically for that person.

3) Requirements
The doctors states the size and weight of the exoskeleton to be the two most important design considerations on a general case. In the end will this heavily affect the patients ability and willingness to wear the exoskeleton as discussed in point **2)**. Other requirements are given from the medical case in accordance with performance goals.

1.2 Post Stroke Gait

From the possible applications discussed, have the authors chosen to focus on the rehabilitation of stroke patients. The application of exoskeletons in this field is not new and the positive effects have been well documented. Hemiparesis causes as mentioned paresis in one side of the body, and logically this affects the persons gait. People suffering from hemiparesis typically presents a gait that is a mixture of kinematic deviations from the weakened limbs and compensatory motions performed by the stronger limbs. Such a gait is unique in every patient and also highly dependent on the severity of the hemiparesis. However, there are some common kinematic deviations that occur during the different phases of gait. These are listed below:

Heel strike phase:

- Limited ankle dorsiflexion.
- Knee hyperextension, which is limited flexion of the knee.

Single support phase:

- Lack of knee extension, which means the knee remains more flexed compared to normal gait, and excessive ankle dorsiflexion occurs to compensate.
- Stiffening of Knee, which can lead to hyperextension.
- Excessive lateral pelvic shift.

Toe off phase:

- Lack of knee flexion and ankle plantar-flexion, which affects push-off and the beginning of the swing phase.

Swing phase:

- Limited knee flexion, which affects the ground clearance of the toe.
- Limited knee extension and ankle dorsiflexion which affect the heel strike and along with the weakened muscles can cause instability in the knee.

So how would a passive exoskeleton be of assistance in such medical cases?
Part of the rehabilitation could be to regain normal human gait, as is the focus of this thesis. On that consideration, it's possible that the patient might find it simpler to comprehend and adjust the correct movement if the gravitational loads where removed from the joints. This is not specific to stroke patients, but could also apply to the elderly. In conclusion, it can be stated that the medical field of application is wide, and the resulting effects is an area worth exploring.

1.3 Considerations of Human-Exoskeleton Interaction

A common goal of most rehabilitation exoskeletons is to reduce the metabolic cost of performing the required task. This is a challenging task as there is no general guide on how to achieve this most efficiently. The typical common opinion is that mass and inertia properties of the device are considered to be important influential factors. Another factor is how the users natural motion trajectory is altered when wearing the exoskeleton. This last point is tied with the kinematic compatibility of the exoskeleton and in turn the actuation system. Näf * et al. [2019] stated that the use of an exoskeleton can only be successful if the assistance is provided at the right moment, with sufficient magnitudes, to the right joints. By this statement, it's clear that it's next to impossible to obtain a design general to all applicants, since the average person does not exist in reality. In order to obtain the most efficient passive exoskeleton, would therefore the design have to be user defined and the kinematic compatibility with the human joints close to optimal.

The kinematic compatibility with human joints are typically obtained by one of two ways. The most optimal solution would be to mimic the anatomical joint, but requires significant implementation efforts. The most typical solution is an anthropometric exoskeleton where each degree of freedom (DOF) on the exoskeleton corresponds to a DOF on the human. In this case is the DOF usually represented by simple revolute joints. The placements of these joints are crucial to the success of the design, since wrongful alignment of axis of rotation may lead to the creation of parasitic forces and induced torques. These will in turn inflict discomfort and perhaps even long term injuries with continuous use.

1.3.1 Human Lower Body Kinematics

In a previous semester project was the functionality of the lower limb joints investigated. The investigation showed that the available DOF's and movements of the joints could be simplified to Table 1.1.

Joint	DOF	Plane	Motion
Hip	3	Sagittal	Flexion/Extension
		Frontal	Adduction/Abduction
		Transverse	Internal rotation/ External rotation
Knee	1	Sagittal	Extension/Flexion
Ankle	3	Sagittal	Dorsiflexion/Plantarflexion
		Frontal	Adduction/Abduction
		Transverse	Internal rotation/ External rotation

Table 1.1: Joint motions in their respective plane.

The human locomotion can in high regard be seen to take place in the sagittal plane. By that notion it's common practice to characterize the human gait as a 2D motion, (Kanjanapas and Tomizuka [2013]). When designing for a lower body exoskeleton, this means that only the revolute joints in the sagittal plane needs to be actuated.

1.3.2 Human Gait Cycle

The gait analysis is a study on how a human walks, and a gait cycle is measured from an optional gait event, until that same event transpires again. In this report, as with the previous semester project, its decided to utilize the formulation by Torricelli et al. [2016] to divide the gait cycle into different phases. An overview of the phases are illustrated in Figure 1.2.

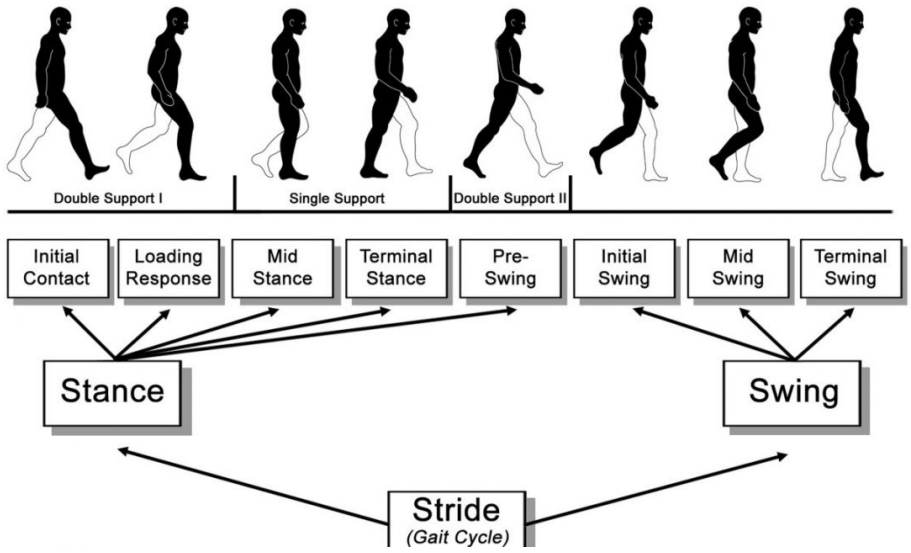

Figure 1.2: Illustration of the phases during a human gait cycle, (Torricelli et al. [2016]).

1.4 Influential Design Factors on Performance and Perception

The performance of the exoskeleton can be stated to be the most important design feature in an exoskeleton, but as pointed out by the doctors at AUH should the user acceptance be weighted as well. The user's perception of the design will in high regard decide if the exoskeleton will be used over longer periods. Some design factors have a direct influence on the mentioned assessments. These should be carefully considered during the design process and are listed in more detail below.

Weight
Researches have shown that the added effects of the inertia, due to the exoskeleton weight, are significant on the kinematics of the gait, (Zanotto et al. [2015]). In addition is the user more likely to wear the exoskeleton if it's light, which also improves its portability. A lightweight design should therefore be considered an important design criteria

Volume
The size of the exoskeleton is typically directly tied to the mass, and in turn the inertia effects. The users are also less likely to wear a bulky design, where their personal area is increased by the large design. In other words should the optimal design be compact and closely attached to the body to minimize the chance of interaction with the surrounding environment.

Safety
Safety simply indicates that the exoskeleton imposes no risk of harming the user during use.

Aesthetics and Ease of Use
These factors will not inflict the performance of the design, but are proven to have strong influence on user adoption, (Kintsch and Depaula [2002]). What's aesthetically pleasing is a subjective criteria, which is dependent on the target groups. It's therefore a factor that will not be evaluated in this report. "Ease of use" can be evaluated. Simply put, it determines if the design can be attached in a simple manner, without the need for multiple technical adjustments.

Comfort
How well the exoskeleton fits to the user, and the measured comfort are important design factors to consider for user acceptance. The comfort criteria does however introduce a new branch of design considerations which will be further assessed in Section 2.2.

1.5 Passive Exoskeleton Actuation

Utilizing a passive lower body exoskeleton for compensation of the gravitational effects during gait have been researched in numerous publications over the years. The designs does however present variable results in regard to performance, and the other influential factors mentioned in Section 1.4. This section presents the result of a literature study surrounding some existing

passive exoskeleton designs and passive joint actuation systems suitable for exoskeleton implementation. The designs are evaluated based on their reported performance and the design factors discussed in Section 1.4.

Banala et al. [2006] presents a hybrid method to balance the weight of the leg in all configurations during gait. This is achieved by locating COM geometrically and then placing springs in suitable positions so they completely balance the effect of gravity over the range of motion. The exoskeleton is designed for rehabilitation where it's fixed to a walking frame. The presented prototype can be seen to have a large volume and mass, in addition to springs attached between the limbs. There is a possibility for the springs to interact with the surrounding environment with such a configuration, which in turn could pose a risk to the user.

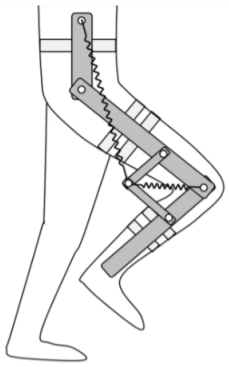

Figure 1.3: Compound rotating joint concept.

The solution presented by Banala et al. [2006], is an example of the many lower limb exoskeletons that are based on the simple gravity balancer. In these cases are typically a free-length springs placed between the payload and frame in order to compensate for gravity. Such exoskeletons are easy to wear, but requires some supplementary instrumentation (like walking frames) for real application. The springs utilized in such exoskeletons typically have a cross-link configuration, meaning that the springs operates outside the area of the limbs. These configurations pose a risk of harm to the user, as springs might interact with the environment. Research have been conducted in recent time for ways to avoid this risk. The prime solution has been to contain the mechanism and springs within the links of the exoskeleton.

Hung et al. [2017] proposes a gravity balancer as a compound rotating joint. The concept, illustrated in Figure 1.4a, utilizes an inverted Carden gear mechanism, with practical springs for achieving static balancing. The concept shows potential for perfect gravity balancing, and successfully limits its mechanism to the joint only. The concept is however limited by the fact that the free-length of the spring needs to be equal to the radius of the ring gear. The size of the joint will therefore increase with the required gravity compensation. For application in a lower body exoskeleton, the joint would be substantial in size.

Nakayama et al. [2009] presented a passive mechanism designed specifically for the lower limbs. Instead of a joint based design, was the entire mechanism contained inside the respective link, as seen in Figure 1.4b. In that way would the mechanism never disrupt the motion and avoid the large joint design which was the case for Hung et al. [2017]. The mechanism consisting of pulleys, gears and a spring, can however be seen as complex, too large and heavy for efficient performance. For efficient assist in the lower limbs will the weight and volume of the design have to be reduced.

A compact passive joint, designed with lower body exoskeletons in mind, was proposed by Zhou et al. [2020]. In this design is a pair of mating gears used to convert the tension force generated by the springs into torque. From Figure 1.4c, it can be seen that the mechanism and springs are fully contained within the links, hence achieving a compact and safe design. A prototype of a full lower body exoskeleton has been made with this concept. Further experimental testing have shown a lightweight design with adjustable pre-tension displacement of the springs, and the ability to obtain approximate gravity balancing of the hip and knee joints. The design can however be seen as unsatisfying large at this point, and should be made more compact for better user acceptance.

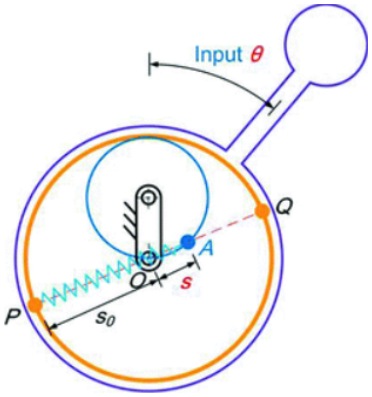

(a) Compund revolute joint by Hung et al. [2017].

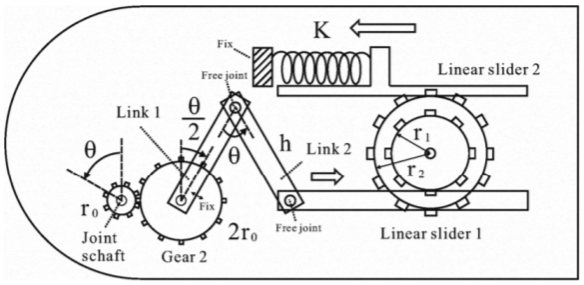

(b) Link with mechanism proposed by Nakayama et al. [2009].

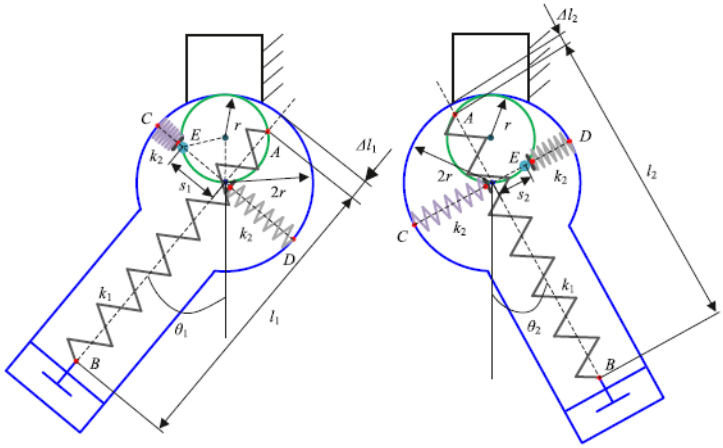

(c) Lower limb joint design by Zhou et al. [2020].

Figure 1.4: Illustration of existing solutions to passive actuation of exoskeleton joints.

From the above discussion it becomes clear that the field of passive gravity balancing is continuously explored and new solutions aims at finding new compact methods for assisting the lower limbs. Further investigations are however necessary for achieving a design capable of optimizing the mentioned factors in Section 1.4. This thesis aims to further add to this investigation, by considering a novel compliant joint mechanism for implementation in a lower limb exoskeleton.

2 | Task Clarification and Project Scope

This chapter specifies the design case and narrows down the scope of this report. Furthermore are the requirements of the medical device listed.

2.1 Design Case

This thesis aims to design a passive lower limb exoskeleton with the goal of assisting a patient in the rehabilitation process by compensating for the gravitational and inertial effects. As been discussed in Chapter 1, there are many possible medical applications for such an exoskeleton, but a passive exoskeleton is most effective when it's designed for a specific case.

This report will consider stroke patients during rehabilitation as its main motivation. Stroke patients suffering with lower limb implications are often not able to walk in the first weeks after suffering a stroke. They follow the general trend that the walking ability and speed increases with time passed since the stroke, (Kollen et al. [2006]). Therefore would the passive exoskeleton be most effective in the later stages of rehabilitation, where it could be used as an assistive device. The following assumptions are made about the design case:

Gait Cycle Kinematics:
The goal of the rehabilitation is to regain normal movement in the legs, the joint trajectories are therefore assumed to be equivalent of a healthy individual walking at normal speed (1.38 m/s). The joint trajectories are obtained from a motion capture study, which is detailed in an earlier semester project, (Bjoner and Hole [2019]). The joint angles of the hip and knee joints are shown in Figures 2.1 and 2.2.

Walking speed:
According to Kollen et al. [2006] is the walking speed after 18-20 weeks of rehabilitation about 0.5 m/s. This speed is chosen because the patient is likely to be able to walk to some degree without assistance. The use of the exoskeleton is then aimed at assisting the patient to regain a more normal gait.

Duration of Gait Cycle:
The duration of the gait cycles is calculated from the assumed kinematics, walking speed and geometry of the lower limb of the patient.

Patient Parameters:
Since a specific patient is not provided and it's not within the time scope of this report to fit the exoskeleton to an actual patient, are the anthropometric parameters based on one of the authors of this report. The parameters are given in Table 2.1. The limb lengths are obtained

from measuring between the markers of the previously performed motion capture study. The mass properties are calculated using an approximated method in (Bjoner and Hole [2019]).

	Trunk Human	Thigh Human	Calf Human	Foot Human
Mass [kg]	46.84	10.5	4.75	1.43
Length [m]	0.56	0.5	0.47	0.23
CM [%]	0.56	0.43	0.43	0.43
Inertia [kg m^2]	3.46	0.19	0.083	0.017

Table 2.1: Parameters of subject 1

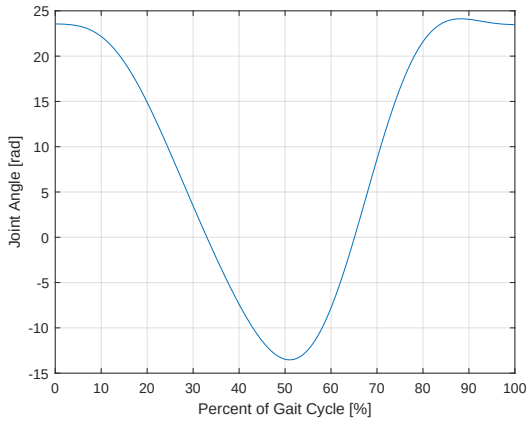

Figure 2.1: Hip joint angle during the gait cycle.

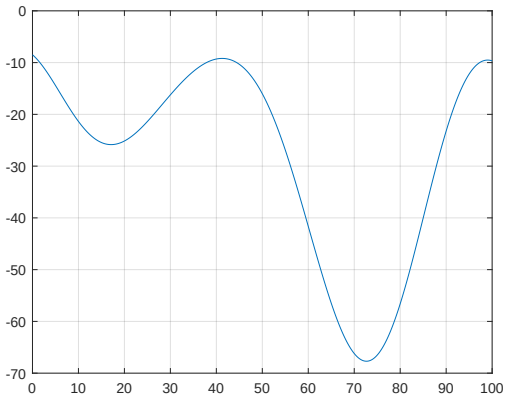

Figure 2.2: Knee joint angle during the gait cycle.

2.2 Problem Scope

The authors have chosen to divide a typical lower limb exoskeleton into 7 sections. The full list is presented bellow with numbers and colours indicating the different sections in Figure 2.3:

1. Attachment to human, trunk
2. Thigh assembly*
3. Attachment to human, thigh
4. Calf assembly*
5. Attachment to human, calf
6. Foot assembly*
7. Attachment to human, foot

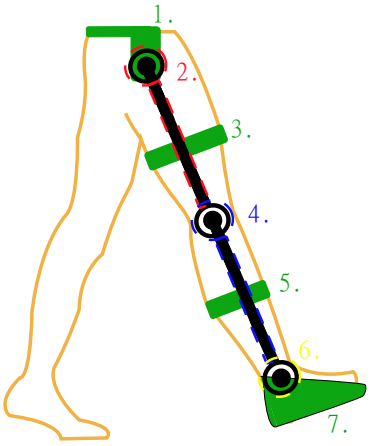

Figure 2.3: Illustration of the components in a full lower body exoskeleton.

*The assemblies are stated to include the respective joint mechanism and linkage.

Chapter 1 presented the need and potential applications for passive lower limb exoskeletons. As this thesis considers gravity and inertial compensation during the gait cycle, there are numerous options for design, but it is beyond the scope of this thesis to consider all of the listed categories.

There are examples in literature of passive ankle exoskeletons, such as the one presented in Dežman et al. [2017], that are designed to aid ankle propulsion. Such exoskeletons typically has the purpose of storing and returning energy. When designing for gravity compensation is the ankle joint typically left out of the design altogether, and the extra foot mass is instead compensated for in the calf assembly. This thesis will follow a similar approach where the final design does not include part 6 and 7 in Figure 2.3.

The attachments to the human introduces a new branch within the design process, namely ergonomics. With the nature of exoskeletons, the authors define ergonomics as the study of comfort and compatibility between the human body and exoskeleton. With the focus being on the joint performances, has the choice been made to utilize the cuffs designed in a previous project by Christensen et al. [2019] at AAU. This design decision is taken to further narrow the scope of the project.

In conclusion will the focus of this thesis revolve around sections 2 and 4.

2.3 Design Guidelines

The performances of exoskeletons are typically tied with safety considerations when designing. The utilisation of the device might cause harm to the user e.g. by wearer strain, despite achieving the performance goals. The question is then how the exoskeleton instead should be designed to be safe. Unfortunately, there are no safety- or performance standards for medical exoskeletons at this point. As an approximate solution, Bostelman and Hong [2018] extracts common performance metrics from industrial robotics, covering task-oriented human-robot interaction that could also be relevant for exoskeletons. They divide them into the following categories; Navigation, perception, management of tasks, manipulation and lesser effects such as duration and ease of use. Additionally, requirements and guidelines for the safe design and protective measures of personal care robots have been presented in ISO [2014]. Here, exoskeletons are referred to as physical assistance robots, and rehabilitation purposes are not considered to lie within this category. Relevant metrics from the mentioned literature have contributed to the specification of requirements in this report.

2.4 Selection of Requirements

There are three main questions to consider when designing a medical device:

- Does the device achieve the necessary objective?
- Is the device safe to use for the patient?
- Does the patient actually want to utilize it?

With this in mind have authors decided to categorize the design requirements in three categories, namely: Performance, Safety and User requirements. An evaluation of the selected requirements within each category will be conducted, before a full list of the selected design requirements are presented.

2.4.1 Performance Requirements

In a rehabilitation case such as this is it unnecessary to design for perfect balancing of the gravitational and inertial loads. Instead it's deemed sufficient if the exoskeleton achieves approximate balancing. The torque provided by the exoskeleton throughout the gait is therefore allowed to depart from the torque requirements a certain range. This torque residual may equal the uncompensated torque which the patient has to provide, but also overcompensation in some areas of the gait. In any case, it should be as low as possible. This is enforced by stating a upper/lower bound for the mean torque residual. The authors have chosen to specify approximate gravity balancing as achieving between 85-115% of the actual torque requirements.

2.4.2 Safety Requirements

The safety requirements are in this project defined as the design specifications necessary to ensure that there is no risk of harming the user, when using the exoskeleton for its prescribed purpose. As explained in Section 2.2, this will not include the interaction between the exoskeleton and user in the attachments. Instead will the safety requirements be focused on avoiding interaction between the mechanism components and user/environment, in addition to support the static loading that acts on the exoskeleton during use.

2.4.3 User Acceptance Requirements

Based on the discussion in Section 1.1, it was clear that the user is more likely to wear the exoskeleton if it's lightweight and aesthetically appealing. While it's difficult to specify individual opinions, a general trend would be to avoid a bulky and complicated design. Ergonomics also lies in this category, but this has been deemed to be outside the scope of this thesis.

2.5 List of Requirements

A full set of requirements have been listed based on the discussion in Section 2.4. Some of the entries in the list are specified as requirements, other as goals. As the name suggest, these entries are not critical for the success of the design, but reflects important design considerations still.

Requirements:	Description	Unit	Criteria
1	Joint mechanism is able to provide approximate gravity compensation	Nm	$0.85\tau_R < \tau < 1.15\tau_R$
2	The design must be compatible with existing body attachments		
3	The exoskeleton must fit the anatomical dimensions of the test person		
4	The design must withstand the critical load cases experienced during use		
5	The design should be simple to manufacture		
6	Should avoid expanding the user's personal area i.e have a compact design	mm	$D_{knee} < 100$ $D_{hip} < 120$
7	Range of motion of exoskeleton must allow level walking of the patient	degree	$ROM_{hip} > 25/-15$ $ROM_{knee} > 0/-70$
Goals:			
1	The exoskeleton should be lightweight	kg	< 3
2	The design should be aesthetically pleasing to the user		
3	The exoskeleton should be applicable to users of different sizes		
4	The design should utilize as much standard components as possible		

Table 2.2: List of design requirements for the passive lower body exoskeleton.

2.6 Design Process

This thesis follows a general approach for the engineering design process as described by Pahl et al. [2007]. The structure of the report can be seen to follow the flowchart drawn in Figure 2.4.

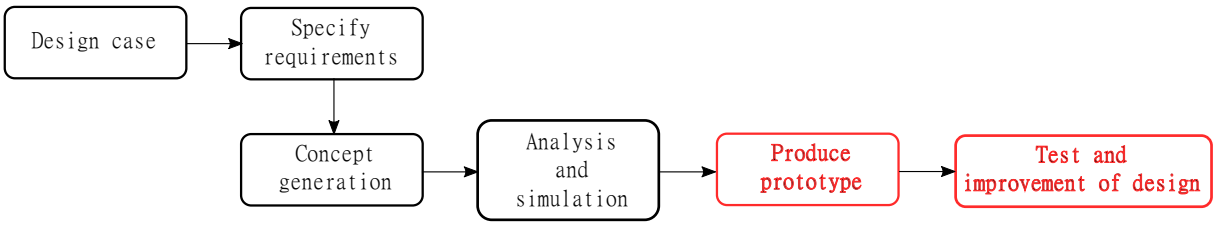

Figure 2.4: Flowchart that illustrates the design process followed in this report.

The first part of the design process will consider specifying the performance requirements of the design. These will be specified by a simplified computational design tool, simulating the proposed application scenario. This design tool is a dynamic model of the human leg wearing the exoskeleton, based on simplified assumptions in regard to both exoskeleton and human. The gait properties of the human are obtained from a motion capture experiment conducted in a previous semester project.

Part two of this report is assigned for generating a design suitable for the requirements stated. The design process will be based on a novel compliant concept previously utilized in conjunction with an active exoskeleton. A torque model developed for this concept will be utilized for optimizing the expected performance of the design with respect to the requirements.

Part three of the report evaluates the structural integrity of the initial design proposed in part two. The topology of the design shall further be optimized with respect to the requirements.

In the end is the performance of the design evaluated by import of the CAD design to a multibody dynamics software.

Ideally, a prototype of the lower limb exoskeleton would be used to conduct experiments and validate the design and/or improve upon the design. However, due to the extraordinary events mentioned in the preface note, such experiments are not feasible during the time of which this thesis is written. The full approach of the thesis can be seen visualized in Figure 2.5.

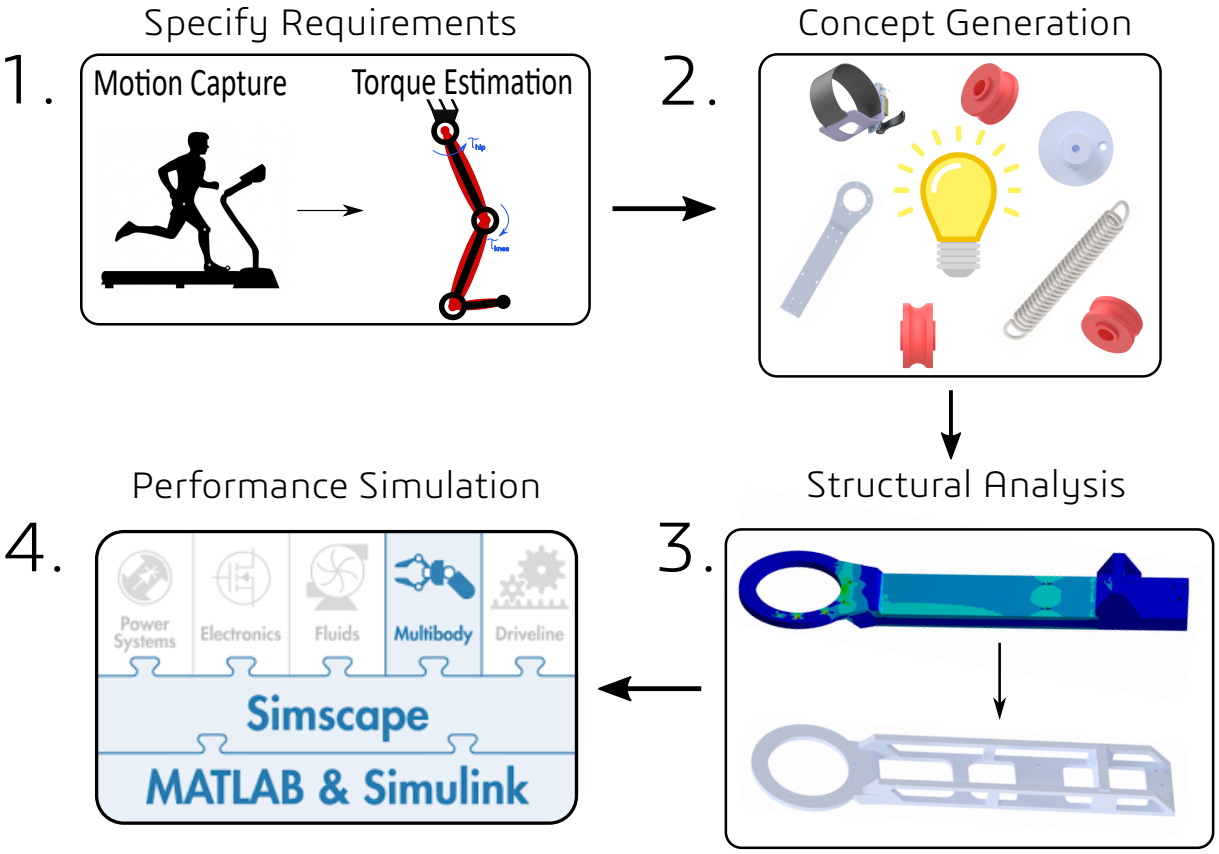

Figure 2.5: Flowchart that illustrates the procedure of the thesis.

3 | Simplified Dynamic Model

This chapter introduces the computational dynamic model developed in a previous semester project. This model is utilized for estimating the performance requirements of the design case presented in Chapter 2. The model saw some performance flaws in parts of the gait cycle, when including the effects of ground reaction forces. These are further assessed and attempted improved in this chapter.

3.1 Computational Dynamic Models as a Design Tool

Virtual models of an exoskeleton-human system can be seen as a powerful tool in regard to the analysis and design process. It makes it possible to test variations in configuration without having to produce an actual prototype, gain technical insight and hence reducing time and cost. In order for this to be possible, the model will have to resemble the actual system with sufficient accuracy. The methods for obtaining the models can vary from utilizing simplified models to more realistic muscoelastical human models. Examples of their use can be seen in state of the art exoskeletons such as BLEEX, (Zoss et al. [2006]), where a model have been used for control purposes, or the ATALANTE exoskeleton where a hybrid control system have been used to simulate human walking.

In an earlier project, the authors of this report developed a simplified human-exoskeleton dynamic model for use in the Axo-suit project at AAU. The goal of this project was to develop a simple and robust model for estimation of performance requirements in lower limb exoskeletons. It was initially specified to be utilized in design cases involving simple human walking. The model can be modified to fit the design case presented in Chapter 2, for obtaining performance characteristics of the joints. This chapter will also further build upon the previously developed model to improve its realistic presentation of human walking.

The full development process of the computational model in its current state is detailed in (Bjoner and Hole [2019]). A short synopsis of the theoretical description of the computational model is still presented in Section 3.2 in order to provide the reader the necessary background insight. A more detailed description of the kinematic and dynamic calculations can also be found in Appendix D.

3.2 Theoretical Background to the Computational Model

The computational model is a 2D inverse dynamic model with a body coordinate formulation based on Newton-Euler equations, as detailed in Nikravesh [2018]. The following description is modelled entirely in Matlab. The model considers a single human leg, wearing an exoskeleton. The human leg is considered to consist of 3 different parts, namely the thigh, calf and foot, illustrated in red in Figure 3.1. In the same manner is the single exoskeleton leg considered to

consist of three parts, illustrated in black. As the goal has been to investigate the full gait cycle, has the model been divided into two phases. During the swing phase and the stance phase, the model has two different formulations, by assuming different fixations to the ground. This has been illustrated in Figure 3.1. From the figure can it be seen that an additional body has been added in the stance phase, labelled as "Trunk", which is a simplified representation of the upper body.

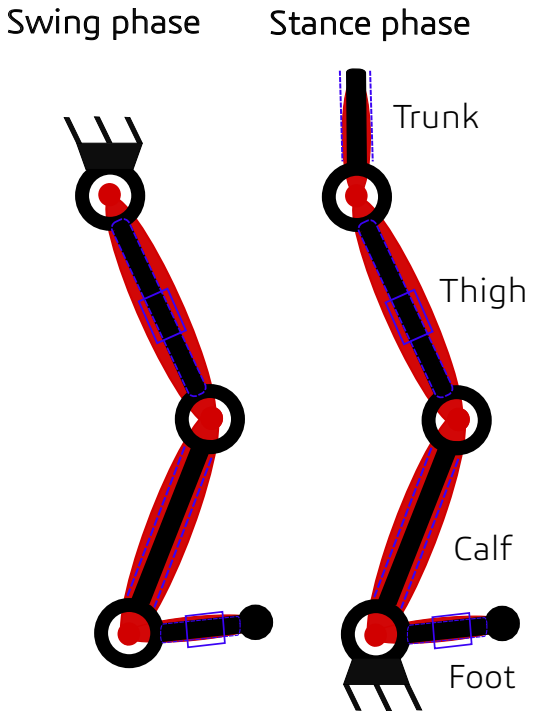

Figure 3.1: Illustration of the formulation of the computational model in the two phases.

3.2.1 Kinematic Considerations

The body coordinate formulation assigns an equal number of coordinates to each rigid body and systematically formulates the joint constraints between the body coordinates. This is done by setting up a set of nonlinear algebraic equations equal to the number of body coordinates, i.e 3 equations per body.

The bodies in each individual system (exoskeleton and human) are connected by revolute joints in accordance to the 2D sagittal plane assumption. The two systems are together linked by translational joints and parallel constraints. Figure 3.2 illustrates the kinematic relationship between bodies in the stance phase. Two revolute joints have been applied in the ankle. The first allows for motion between the ground and calf, the other for motion between the foot and calf. At two locations have parallel constraints been utilized instead of translational joints in order to not over-constrain the system. The kinematic spesifications of each phase are summarized in Table 3.1.

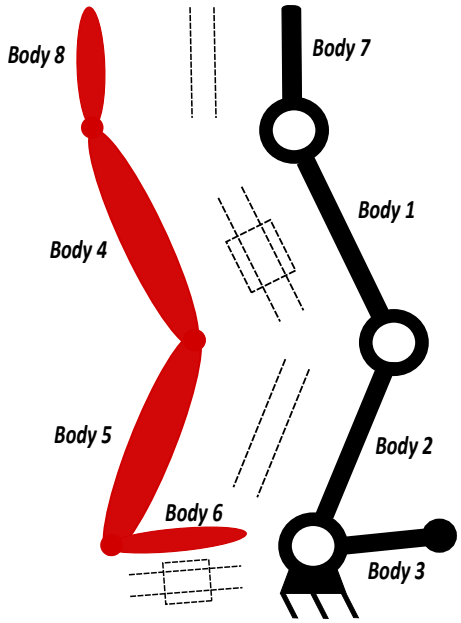

Figure 3.2: Kinematic formulation in the stance phase.

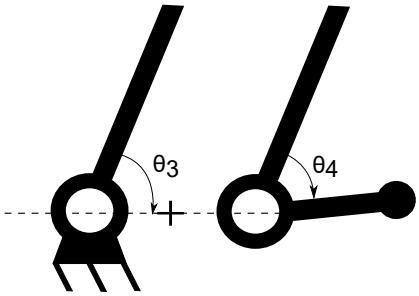

Figure 3.3: Illustration of ankle revolute joints.

By referring to the work done in (Bjoner and Hole [2019]) have the kinematic specifications been listed below, dependent on phase.

	Swing	Stance
Number of bodies	6	8
Revolute joints	5	7
Connectors	2 translational 1 paralell	2 translational 2 paralell
Fixation point	hip	ankle
Motion drivers	hip, knee, ankle	hip,knee 2 in ankle

Table 3.1: Kinematic considerations in the two phases.

3.2.2 Constraint Equations

The joints are seen as constraints equations. These constraints are lower kinematic pairs, which means that information in regard to the shape of the body is not necessary in order to determine the constraint equations. In this case are the equations only defined by the position of the joint with respect to the connecting bodies. This model does however utilize a prescribed motion, set by the authors. This motion is governed by the driving constraints, which are functions of time appended to the original kinematic constraints.

The driving constraints in this case are functions describing the angular position of the joints with respect to time. These functions have been obtained by a motion capture experiment conducted in a previous semester project. The experiment is visualized in Figure 3.4, where

the markers were placed strategically at the joints of interest. In the post-process where driver functions obtained for the angles illustrated in Figure 3.5.

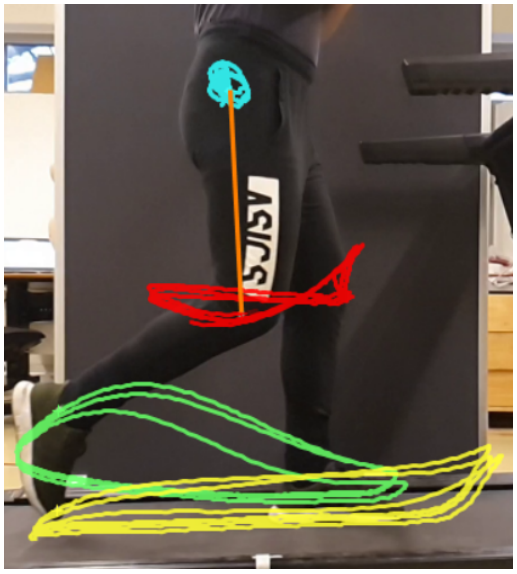

Figure 3.4: Marker trajectories in motion capture experiments.

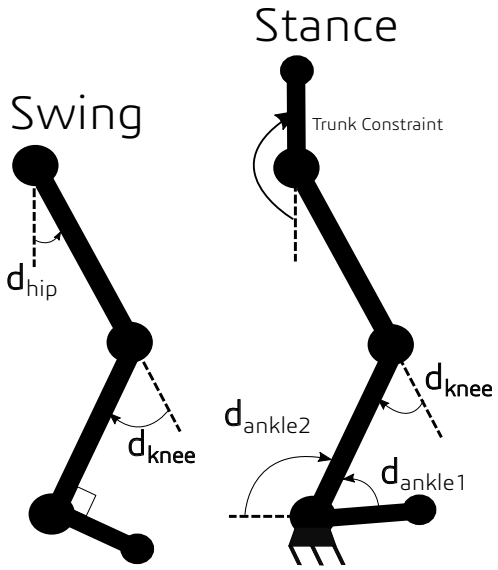

Figure 3.5: Illustration of the obtained drivers from mo-cap experiment.

Three tracked gait cycles are shown in Figure 3.4. The teal colour illustrates the path of the hip, the red colour is the knee path, the green is the ankle path and the yellow is the path of the toe. No markers were placed for capturing the relative motion the trunk. Instead is the trunk constrained to remain stable in its vertical position.

Constraint Matrices

The full set of constraint equations presented in Figure 3.6) has been evaluated in detail in (Bjoner and Hole [2019] and are only reported here for consistency with the new work done.

Notations applied in the constraint equations:

The following notations are applied when defining all the constraint equations in this chapter.

- r_i is the vector from the global coordinate system to the local coordinate system of body i.
- r_0 is the ground fixing point.
- s_{iX} the local coordinate of a given point in body i. X is the notation for a given point, where H is the hip, K is the knee, A is the ankle and T is the toe.
- A_i is the rotation matrix of body i.
- B_i is the rotation matrix, but rotated 90°.
- Φ_i constraint equation number i.
- x_i, y_i and ϕ_i are the body coordinate of body i.
- $\dot{\phi}_i$ is the time derivative of the angular body coordinate (angular velocity).
- $\mathbf{p}_1$ is a vector between the human thigh and the exoskeleton thigh defined as $\mathbf{r}_1 + \mathbf{A}_1\mathbf{s}_{1H} - \mathbf{r}_4$.
- $\mathbf{p}_2$ is a vector between the human foot and the exoskeleton foot defined as $\mathbf{r}_3 + \mathbf{A}_3\mathbf{s}_{3T} - \mathbf{r}_6$.
- d_{pos} is the driver function at the positions illustrated in Figure 3.5.

Swing phase

$$\left.\begin{aligned}
\Phi_{1,2} &= \mathbf{r}_0 - \mathbf{r}_1 - \mathbf{A}_1\mathbf{s}_{1H} \\
\Phi_3 &= \phi_1 - d_{hip} \\
\Phi_{4,5} &= \mathbf{r}_1 + \mathbf{A}_1\mathbf{s}_{1K} - \mathbf{r}_2 - \mathbf{A}_2\mathbf{s}_{2K} \\
\Phi_6 &= \phi_2 - \phi_1 - d_{knee} \\
\Phi_{7,8} &= \mathbf{r}_2 + \mathbf{A}_2\mathbf{s}_{2A} - \mathbf{r}_3 - \mathbf{A}_3\mathbf{s}_{3A} \\
\Phi_9 &= \phi_3 - \phi_2 - 90^\circ \\
\Phi_{10} &= \phi_4 - \phi_1 \\
\Phi_{11} &= (\mathbf{A}_1\mathbf{N})^T\mathbf{p}_1 \\
\Phi_{12,13} &= \mathbf{r}_4 + \mathbf{A}_4\mathbf{s}_{4K} - \mathbf{r}_5 - \mathbf{A}_5\mathbf{s}_{5K} \\
\Phi_{14} &= \phi_5 - \phi_2 \\
\Phi_{15,16} &= \mathbf{r}_5 + \mathbf{A}_5\mathbf{s}_{5A} - \mathbf{r}_6 - \mathbf{A}_6\mathbf{s}_{6A} \\
\Phi_{17} &= \phi_6 - \phi_3 \\
\Phi_{18} &= (\mathbf{A}_2\mathbf{N})^T\mathbf{p}_2
\end{aligned}\right\} = 0$$

Stance phase

$$\left.\begin{aligned}
\Phi_{1,2} &= \mathbf{r}_1 + \mathbf{A}_1\mathbf{s}_{1K} - \mathbf{r}_2 - \mathbf{A}_2\mathbf{s}_{2K} \\
\Phi_3 &= \phi_2 - \phi_1 - d_{knee} \\
\Phi_{4,5} &= \mathbf{r}_2 + \mathbf{A}_2\mathbf{s}_{2A} - \mathbf{r}_3 - \mathbf{A}_3\mathbf{s}_{3A} \\
\Phi_6 &= \phi_3 - \phi_2 - d_{ankle1} \\
\Phi_{7,8} &= \mathbf{r}_g - \mathbf{r}_3 - \mathbf{A}_3\mathbf{s}_{3A} \\
\Phi_9 &= \phi_3 - d_{ankle2} \\
\Phi_{10} &= \phi_4 - \phi_1 \\
\Phi_{11} &= (\mathbf{A}_1\mathbf{N})^T\mathbf{p}_1 \\
\Phi_{12,13} &= \mathbf{r}_4 + \mathbf{A}_4\mathbf{s}_{4K} - \mathbf{r}_5 - \mathbf{A}_5\mathbf{s}_{5K} \\
\Phi_{14} &= \phi_5 - \phi_2 \\
\Phi_{15,16} &= \mathbf{r}_5 + \mathbf{A}_5\mathbf{s}_{5A} - \mathbf{r}_6 - \mathbf{A}_6\mathbf{s}_{6A} \\
\Phi_{17} &= \phi_6 - \phi_3 \\
\Phi_{18} &= (\mathbf{A}_2\mathbf{N})^T\mathbf{p}_2 \\
\Phi_{19,20} &= \mathbf{r}_1 + \mathbf{A}_1\mathbf{s}_{1H} - \mathbf{r}_7 - \mathbf{A}_7\mathbf{s}_{7H} \\
\Phi_{21} &= \phi_7 - \phi_1 - 90^\circ \\
\Phi_{22,23} &= \mathbf{r}_4 + \mathbf{A}_4\mathbf{s}_{4H} - \mathbf{r}_8 - \mathbf{A}_8\mathbf{s}_{8H} \\
\Phi_{24} &= \phi_8 - \phi_7
\end{aligned}\right\} = 0$$

Figure 3.6: Constraint matrices for the swing and stance phase.

3.2.3 Kinematic and Dynamic Analysis

There are three properties required to describe the motion of the lower limb, namely the positions, velocities and accelerations. Now that all the constraints are specified is there an equal amount of coordinate variables and constraint equations. This means that the system is fully determined, and the system of nonlinear equations can be solved by the Newton-Raphson solution method for obtaining the positions. This requires the Jacobian, which is defined as the partial derivative of the constraint vector with respect to the generalized coordinates. The velocities and accelerations are found by calculating the first and second time derivative of the positions, respectively.

The system follows a trajectory set by the gait cycle. The objective with this model is then to determine the torques and forces necessary for generating this motion. This is what is called an inverse dynamic analysis. Gravity is the only external force applied to the system, and the kinematic properties are known from the previous calculations. The reaction forces are then calculated in accordance with the approach presented in Appendix D

3.3 Torque Requirements for the Passive Exoskeleton

In this thesis is the dynamic model utilized for obtaining the torque requirements of an exoskeleton applied to the design case presented in Chapter 2. Since the goal of the passive exoskeleton is only to compensate for the gravitational and inertial effects during gait, are the influential ground reaction forces not considered. This means that the model can be simplified to only have one configuration during the entire gait-cycle, namely that of the swing phase. The swing phase has been validated by comparison to external literature. This formulation is therefore deemed correct.

The scope of this thesis does not include an ankle exoskeleton so this is removed from the previously defined formulation. In order to have a fully determined system are the parallel joint in the calf region exchanged with a translational joint. The exoskeleton hip is fixed to the ground by a revolute joint. The constraint equations of the configuration are given in Equation 3.1 and the body numbers of the configuration is given in Table 3.2.

$$\left.\begin{aligned}
\Phi_{1,2} &= \mathbf{r}_0 - \mathbf{r}_1 - \mathbf{A}_1\mathbf{s}_{1H} \\
\Phi_{3,4} &= \mathbf{r}_1 + \mathbf{A}_1\mathbf{s}_{1K} - \mathbf{r}_2 - \mathbf{A}_2\mathbf{s}_{2K} \\
\Phi_{5,6} &= \mathbf{r}_2 + \mathbf{A}_2\mathbf{s}_{2A} - \mathbf{r}_3 - \mathbf{A}_3\mathbf{s}_{3A} \\
\Phi_7 &= \phi_1 - d_{hip} \\
\Phi_8 &= \phi_2 - \phi_1 - d_{knee} \\
\Phi_9 &= \phi_3 - \phi_2 - 90^\circ \\
\Phi_{10} &= \mathbf{A}_1\mathbf{N}^T\mathbf{p}_1 \\
\Phi_{11} &= \phi_3 - \phi_1 \\
\Phi_{12,13} &= \mathbf{r}_4 + \mathbf{A}_4\mathbf{s}_{4K} - \mathbf{r}_5 - \mathbf{A}_5\mathbf{s}_{5K} \\
\Phi_{14} &= \mathbf{A}_2\mathbf{N}^T\mathbf{p}_2 \\
\Phi_{15} &= \phi_5 - \phi_2
\end{aligned}\right\} = 0 \tag{3.1}$$

Body description	H.Thigh	H.Calf	H.Foot	Exo.Thigh	Exo.Calf	Exo.Foot
Body number	1	2	3	4	5	6

Table 3.2: Body numbers of the configuration used for design.

3.3.1 Exoskeleton Properties

The simplified model performs the dynamic analysis based on realistic dimensions and weight properties of the two systems. The anthrometric data of the human is specified in Section 2.1, along with the weight properties. The exoskeleton on the other hand needs a qualified guess on the final exoskeleton design weight, COM and inertial properties. It's been decided to utilize the maximum weight requirement (3kg) for the estimation of exoskeleton mass

in the dynamic model. The hip exoskeleton is typically larger and heavier than the knee exoskeleton due to the increased torque requirements for carrying the full leg. A point mass of 1.7 kg is therefore estimated for the hip and 1.3 kg for the knee exoskeleton. The COM is estimated to be mid-length of the links, which have the same lengths as the human limbs. The inertial properties are then calculated based on simplifications to the geometrical shape of the exoskeleton. This shape has it foundation in an active exoskeleton previously developed at AAU. More detail on the inertia estimation can be found in Appendix D. The estimated exoskeleton properties are presented in Table 3.3. The COM is presented as a percentage of the part length.

	Unit	Hip (exo)	Knee (exo)
Mass	kg	1.7	1.3
Length	m	0.5	0.46
COM	%	0.5	0.5
Inertia	$kg * m^2$	0.043	0.0219

Table 3.3: Estimated exoskeleton properties.

3.3.2 Requirement Estimation

An inverse dynamic analysis was performed with hip and knee drivers based on the angular distribution presented in Figure 2.1 and Figure 2.2 in Section 2.1. The resulting joint torques with respect to time are presented in Figure 3.7 and Figure 3.8 for the hip and knee joints, respectively.

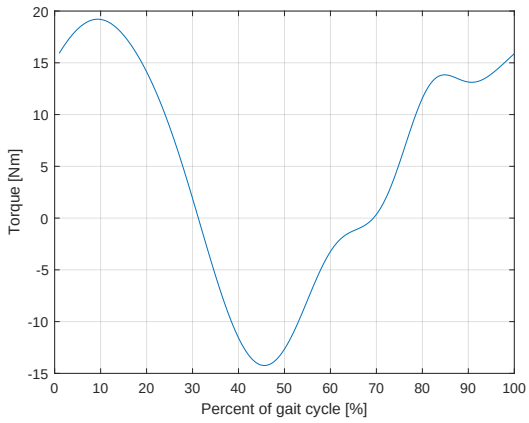

Figure 3.7: Torque requirements in the hip joint throughout the gait cycle.

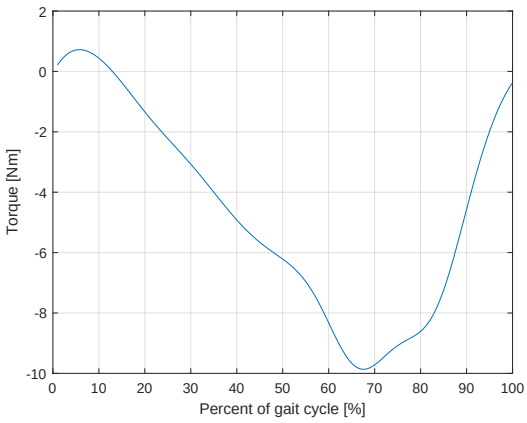

Figure 3.8: Torque requirements in the knee joint throughout the gait cycle.

The above plots presents the torque requirements in the joint influenced by the gravitational and inertial effects. The torque produced by the exoskeleton design will aim to counter this torque as well as possible. In other words should the exoskeleton joints produce a torque distribution similar to these, but of opposite values. This "flipped" torque distribution will from this point on be referred to as the "Torque requirements".

3.4 Model Refinement

For utilization in more complex design cases, the stance phase is modelled to include the effects of ground reaction forces. At completion of the previous semester project did however the model portray some flaws in the double support phases. This section presents an evaluation of the previously developed model and the refinements done to improve the model. It was decided to remove the exoskeleton for two reasons, namely to limit possible sources of error and because more external documentation is available when only considering the human.

3.4.1 Current Stance Phase

The model calculations have previously been validated by the multi-body dynamics software MSC Adams, and the obtained torque profiles are compared to similar cases in external literature for an evaluation of the results.

The previous work on this model concluded in an overall good correspondence with reality in the two phases, but the model presents high peak values in the transition between the two phases e.g. the double-support phases. As discussed in (Bjoner and Hole [2019]) is this likely caused by neglecting the foot movement. Figures 3.9 and 3.10 aims to illustrate the flaws of the model by simulation of the stance phase. The double support phases are highlighted in red. The specifications of the test person is presented in Table 3.4.

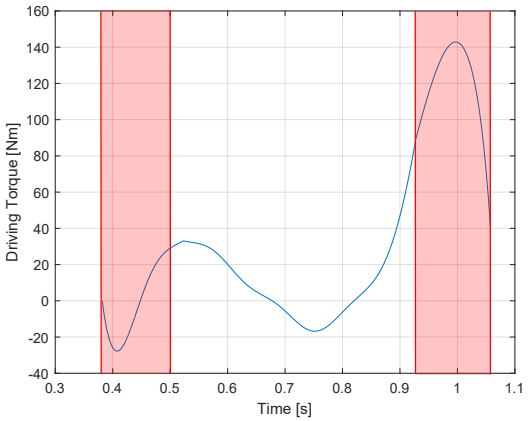

Figure 3.9: Hip torque from previous model.

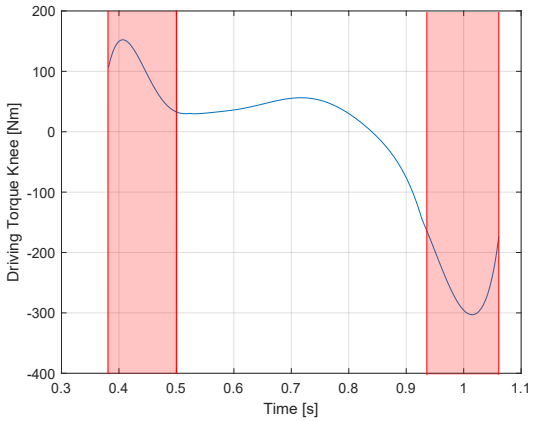

Figure 3.10: Knee torque form previous model.

Thigh (cm)	50.1
Calf (cm)	47.1
Foot (cm)	22.7
Body height (cm)	188
Body mass (kg)	100
Walking Speed (km/h)	5

Table 3.4: Specifications of test subjects.

3.4.2 Inclusion of Foot Movement

To better capture the foot movement relative to the ground, its been suggested by Mahmoodi et al. [2013] to model the foot sole with a roll-over shape. In this case is the center of pressure imagined to change with the shape of the foot, as illustrated in Figure 3.11.

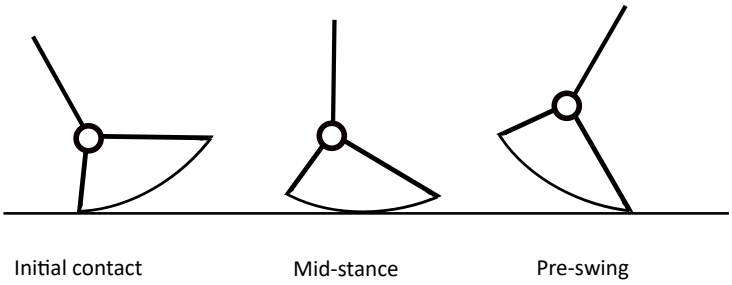

Figure 3.11: Illustration of the rollover foot shape.

This approach is implemented in a Matlab configuration by basing the necessary constraint formulations on a point follower cam constraint presented by Nikravesh [1988]. A point follower cam pair, where the ground is the point follower and the foot is the cam body, allows the point of rotation in the foot to smoothly change while it's still attached to the ground.

The same base formulation is utilized. The bodies trunk, thigh, calf and foot (bodies 1,2,3,4), are connected together by three revolute joints, which are assigned driver constraints. The configuration is visualized in Figure 3.12, and the rollover foot constraint is described in more detail in Section 3.4.3.

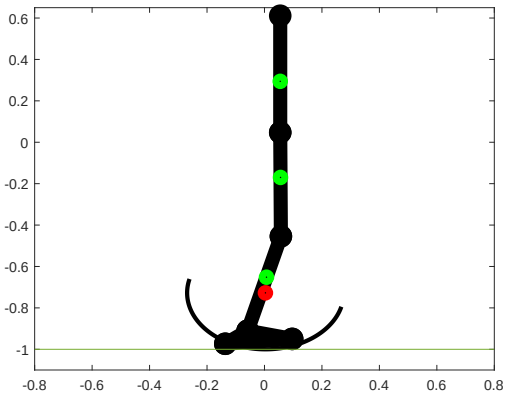

$$\left.\begin{aligned}
\Phi_{1,2} &= \mathbf{r}_1 - \mathbf{A}_1\mathbf{s}_{1H} - \mathbf{r}_2 - \mathbf{A}_2\mathbf{s}_{2H} \\
\Phi_{3,4} &= \mathbf{r}_2 + \mathbf{A}_2\mathbf{s}_{2K} - \mathbf{r}_3 - \mathbf{A}_3\mathbf{s}_{3K} \\
\Phi_{5,6} &= \mathbf{r}_3 + \mathbf{A}_3\mathbf{s}_{3A} - \mathbf{r}_4 - \mathbf{A}_4\mathbf{s}_{4A} \\
\Phi_{7,8} &= \mathbf{r}_{ground} - \mathbf{r}_4 - \mathbf{A}_4\mathbf{curve}_4 \\
\Phi_9 &= \phi_1 - 90^\circ \\
\Phi_{10} &= \phi_2 - d_{ankle2} \\
\Phi_{11} &= \phi_3 - \phi_2 - d_{knee} \\
\Phi_{12} &= \phi_4 - \phi_3 - d_{ankle1}
\end{aligned}\right\} = 0 \tag{3.2}$$

Figure 3.12: Visualization of refinement model.

3.4.3 Rollover Foot Constraint

The rollover shape is applied to the model by altering the constraint between the foot and the ground. Previously this constraint was a revolute joint, and it is replaced by a cam-follower constraint. The constraint does not affect the amount of DOF in the system, since the cam follower also constrains movement in both x- and y-direction. The cam constraint is formulated as a point follower cam, which has the general equation:

$$\mathbf{r}_i + \mathbf{A}_i \begin{bmatrix} s\cos\theta \\ s\sin\theta \end{bmatrix}_i - \mathbf{r}_j - \mathbf{A}_j \mathbf{s}_{jP} = \begin{bmatrix} 0 \\ 0 \end{bmatrix} \tag{3.3}$$

where i indicates the cam shaped body, j indicates the follower body and $\mathbf{s}_{jP}$ is the position of the contact point given in the local coordinates of the follower body. The term inside the bracket is used to describe the cam surface, where s is the distance between a set point and the cam surface. θ is an artificial coordinate introduced to simplify the expression of the surface. This method is applied to the model by considering the foot as the cam shaped body and a fixed point in ground to be the follower. The constraints implemented in the model are then:

$$\mathbf{r}_{ground} - \mathbf{r}_4 - \mathbf{A}_4 \left[\mathbf{s}_{4C} + \begin{bmatrix} R\cos\theta \\ R\sin\theta \end{bmatrix} \right] = \begin{bmatrix} 0 \\ 0 \end{bmatrix} \tag{3.4}$$

$\theta = -\phi_4$ to ensure no part of the cam surface penetrates the ground. The contact surface is described as a circle with a radius of $0.2726m$ and the center point is offset from the ankle by $0.015m$ and $0.1926m$ in the local x- and y-direction, respectively. The specific values are obtained from the height normalized values presented in, Hansen et al. [2004].

Weight Scaling
Since the model only includes one leg is it not able to capture the weight transfer between the legs in the double support phase without applying some form of scaling to the mass parameters. From literature, Ren et al. [2005], it is found that the weight distribution of both legs display a close to linear increase or decrease depending on which double support phase the leg is in. Therefore it was decided to have the mass of the system scaled linearly in the double support phase. Additionally the inertia of the trunk is scaled in the same manner as the mass, but the inertia of the thigh, calf and foot is not altered.

3.4.4 Fixed Ankle

The first refinement of the model implemented the rollover shape on a foot which was rigidly connected to the calf, by a relative angle of 90°. The torque profile in the knee and the ground reaction forces resulting from this formulation is presented in Figure 3.15. Two main observations are made from the evaluation of this model refinement, which is that the torque magnitudes of the knee joint is still too large and that the ground reaction force does not display two clear peaks. From these observations it was decided to apply a driver function to the ankle joint, in order to better model the push off effect of the foot.

3.4.5 Driven Ankle

The driver represented as d_{ankle1} in Figure 3.5 was applied to the ankle in order to provide the movement of the foot relative to the calf. From the knee torque in Figure 3.15, it's clear that the addition of the driver magnifies the second peak. The ground reaction force now has two clear peaks, but the magnitude of the second peak is significantly larger, and additionally the first peak is shifted and occurs later in the gait cycle. These tendencies are not in accordance with literature and is believed to be caused by the use of an inaccurate ankle driver function.

3.4.6 Constant Hip Velocity

As an alternative to the use of the inaccurate ankle driver was a constant velocity constraint applied to the hip joint. This is a substantial assumption, but from the results presented by Jansen et al. [2013], it's observed that the maximum lateral acceleration of the COM during normal walking has a magnitude of about $1m/s^2$. Hence is the assumption believed to be reasonable. The constant velocity constraint is applied as $\Phi_{10} = r_1(1) + s_{1H} - \frac{5}{3.6}t$ to ensure the trunk moves forward with a constant velocity, and thereby significantly reducing the lateral accelerations. The results from applying this constraint are observed to yield a realistic torque distribution, however the magnitude of the torque is too small, especially in the beginning of the gait cycle. The small magnitude here is believed to be caused by the applied scaling.

Evaluation of the Refinement Trials

To evaluate the effects of the updates on the model, the results are compared to the knee torque and vertical ground reaction force obtained from Fukuchi et al. [2018]. This is done in order to have a realistic benchmark. The knee torque and vertical ground reaction force presented in Figure 3.13 and 3.14, are based on the mean values of 42 healthy subjects, and is normalized with respect to total body weight. The shades of blues in the figures represents different walking speed, where the darkest shade corresponds to the highest walking speed.

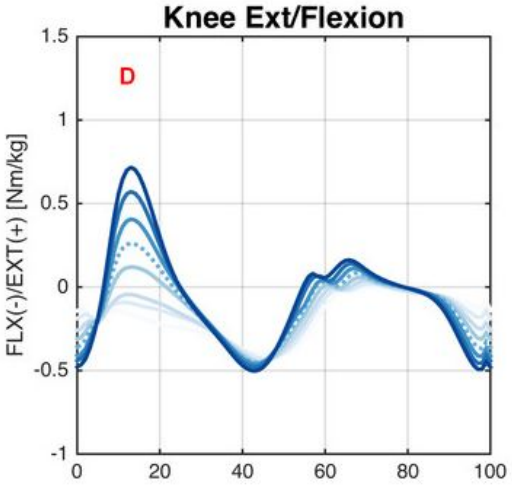

Figure 3.13: Knee torque, Fukuchi et al. [2018].

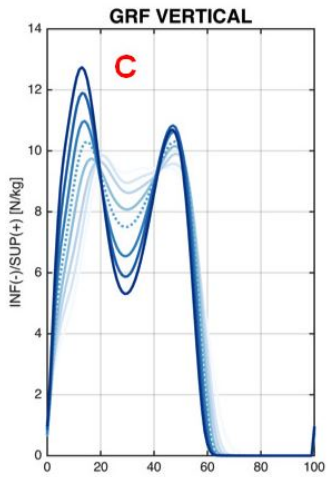

Figure 3.14: GRF, Fukuchi et al. [2018].

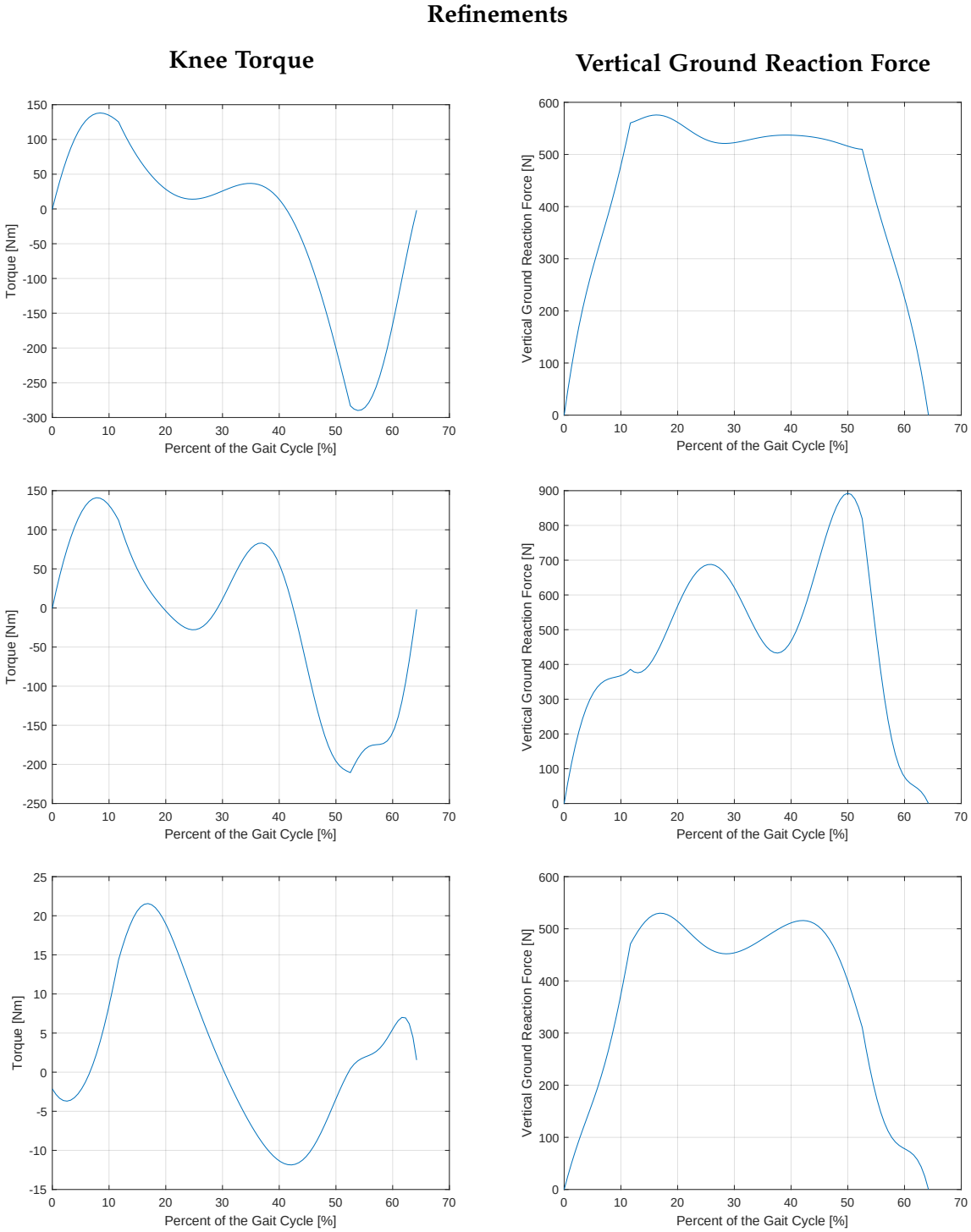

Figure 3.15: Results: Fixed ankle, Driven ankle and Constant hip velocity model presented in descending order.

3.4.7 Conclusion to Refinement Process

The use of a constant hip velocity and rollover shaped foot was observed to resemble a somewhat realistic behaviour in the knee. A similar investigation have been conducted on the hip joint, but the results showed a general inconsistency with the literature. This is most likely due to the simple nature of the driving constraint applied between the thigh and the trunk, and the scaling applied. The inclusion of a rollover shape to a single leg model can therefore be concluded in mixed results. To avoid issues with weight scaling should a second leg be applied to future models.

This marks the end to the consideration of ground reaction forces. The rest of the report will consider the performance characteristics of the design case presented in Section 3.3.

4 | Design Concept

This Chapter builds upon the design case and requirements stated in previous chapters to conduct the designing process of the lower limb passive exoskeleton. The chapter is divided in two parts; namely design of the joint mechanism in the knee and hip joints. Also link designs are evaluated in this chapter. The two parts follow a step-by-step procedure where the joint design concept are first presented with an explanation of the underlying theory. The implementation of the design concept is then driven by the torque requirements of the respective joints. In the end of the chapter is an initial CAD design presented for each joint, which will serve as a basis for the structural design.

4.1 Compliant Joints

Compliant joints, within the topic of exoskeletons, are stated as mechanisms that include compliant properties from a non-rigid actuation system and/or a structure, (Sanchez-Villamañan et al. [2018]). In a passive exoskeleton does the compliant properties typically come from springs, as seen in the literature study in Chapter 1.

Compliant joints are also utilized more and more in active exoskeletons for increasing safer interaction between human and exoskeleton, and for better adaption to the environment (shock absorption etc.). A compliant joint may have a fixed compliance, such as those who employ series elastic actuators (SEAs), or it could employ variable stiffness actuators (VRAs). The latter has experienced a large increase in developments in the recent years, because its nonlinear behaviour enable for more flexibility in shaping the torque -and stiffness-deflection profiles. Systems employing VRAs are able to mechanically modulate the output characteristics of the joint (e.g.torque, stiffness). Such a system could therefore theoretically be able to reproduce the human-like stiffness and torque profiles.

4.2 Presentation of Design Concept

At AAU there has been developed a novel compliant revolute joint design by the department of materials and production. Presented in Li and Bai [2019], this design is able to produce a variable stiffness behaviour with three working modes showing hardening, softening and linear behaviour. In addition does its reconfigurable design make for a wide variety of adjustments to the output profile. The design is originally intended to be utilized in collaboration with an electrical actuator, but it is of interest to investigate if the concept can be translated to a completely passive mechanism. This section will describe the underlying theory of the concept before moving on to design implementation in the following sections.

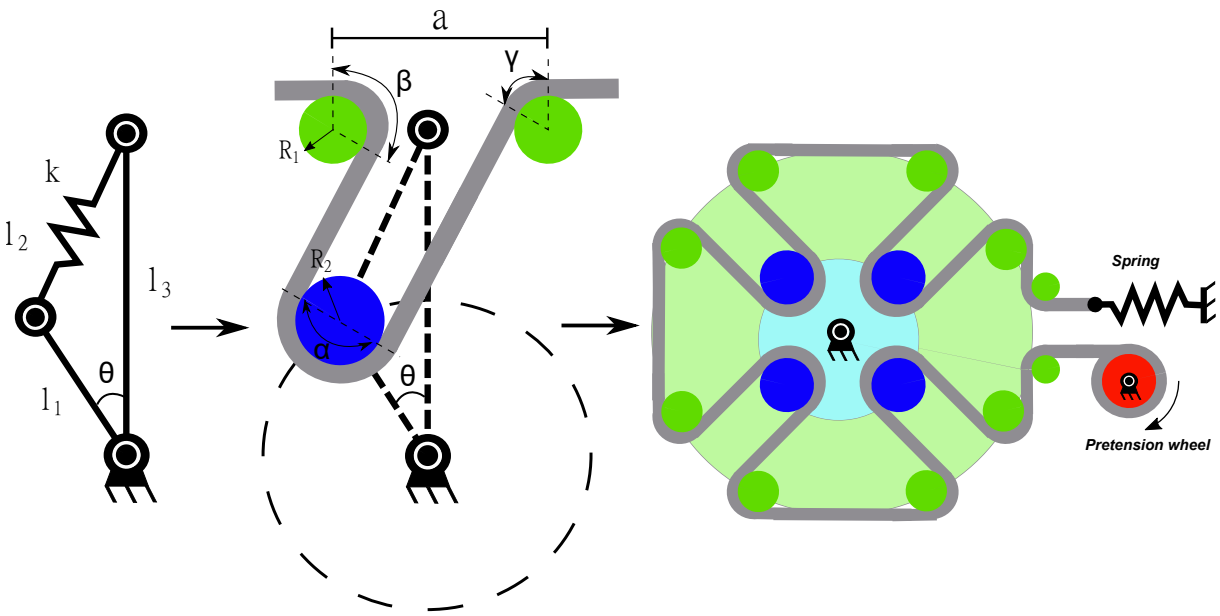

Figure 4.1: Illustration of the compliant joint concept and JVSR mechanism.

Figure 4.1 illustrates the concept of the compliant joint by a simplified 3-bar linkage and the design solution. The theory behind the concept, including full torque and stiffness models, is fully described in the paper by Li and Bai [2019], hence will only the basics be presented here.

The compliant joint is created by replacing the rigid link l_2 by an elastic element. Depending in the rotation angle θ will the joint experience a variable stiffness. This principle has been implemented in a revolute joint mechanism by a cable wrapped on three pulleys. Two of these pulleys (presented in green) are located on the input shaft, while one (blue) is located on the output shaft. One end of the cable is reeled to a fixed position on the input shaft while the other end is connected to a spring with spring stiffness k and pretension F_0. The cable and other structure components are considered rigid, so a change in rotation angle will lead to an elongation/contraction of the spring. The spring is therefore seen as the only compliant element in the system.

Figure 4.1 also shows the JVSR mechanism (proposed by Li and Bai [2019]), where the design concept has been implemented repeatedly. This mechanism is reconfigurable by the number of pins utilized and the pattern of which these pins are wrapped. By design is the number of pins on the input shaft, twice the number on the output shaft. This is then one possible configuration. As seen from the figure are the two coaxial shafts coupled through the cable, which is connected by a spring in one end and reeled in the other.

The paper also presents a way of calculating the output torque and stiffness generated by the concept with varying design configurations. In this project is it of interest to utilize the torque model to investigate if the torque response of the concept can be closely matched to that of the torque requirements. Therefore only the torque model of the compliant design is necessary to complete the design process. The torque model is presented in Section 4.2.1.

4.2.1 Torque Model

The torque model for the JVSR is based on the simple four bar linkage system as explained in Section 4.2. The complete derivation of the torque model is explained in detail in the paper by Li and Bai [2019]. The model is therefore only presented with a sufficient amount of detail to present the design parameters and implementation in a MATLAB script. The design parameters utilized in the following description is visualized in Figure 4.1. The torque of the JVSR concept is given as:

$$T = J_1 F \tag{4.1}$$

where T is the torque, J_1 is the jacobian of the linkage, and F is the internal tension force. Then by introducing N pins and splitting the tension force into two terms, one for the pretension and one for the elongation of the spring, the torque model becomes:

$$T = N^2 k_l \delta l J_1 + N F_0 J_1 \tag{4.2}$$

where k_l is the spring stiffness of a linear spring, F_0 is the pretension force, and δl is the change in length of the cable, due to the change in angle θ.

$$\delta l = l(\theta) - l(\theta_0) \tag{4.3}$$

The cable length l is given as:

$$l = \frac{a \cdot \alpha}{2} + |\overrightarrow{DB}| + |\overrightarrow{EG}| \tag{4.4}$$

Here the term $\frac{a \cdot \alpha}{2}$ is the cable length which is in contact with the inner and outer pins, where $a \approx 4R$ and α is given by Equation 4.7. The two last terms is the cable length which is not in contact with the pins, where:

$$|\overrightarrow{DB}| = \sqrt{l_2^2 - a l_1 sin(\theta)} \quad \text{and} \quad |\overrightarrow{EG}| = \sqrt{l_2^2 - a l_1 sin(\theta)} \tag{4.5}$$

These terms are dependent on the length of the elastic link, l_2, given as:

$$l_2 = \sqrt{l_1^2 + l_3^2 - 2 l_1 l_3 cos\theta} \tag{4.6}$$

The parameters $a, \alpha, \beta, \gamma, R, l_1, l_2$ and θ are visualized in Figure 4.1. The final undefined parameter of the torque model is the Jacobian which is defined as $J_1 = \frac{\partial l}{\partial \theta}$.

$$\begin{aligned} \alpha &= \beta + \gamma \\ \beta &= \arccos\left(\frac{a - 2l_1 \sin\theta}{\sqrt{4l_2^2 - 4al_1 \sin\theta + a^2}}\right) - \arccos\left(\frac{a}{\sqrt{4l_2^2 - 4al_1 \sin\theta + a^2}}\right) + \frac{\pi}{2} \\ \gamma &= \arccos\left(\frac{a + 2l_1 \sin\theta}{\sqrt{4l_2^2 + 4al_1 \sin\theta + a^2}}\right) - \arccos\left(\frac{a}{\sqrt{4l_2^2 + 4al_1 \sin\theta + a^2}}\right) + \frac{\pi}{2} \end{aligned} \tag{4.7}$$

4.3 Design Options

The simplified dynamic model in Chapter 3 originally utilizes relative angles for describing the movement between the thigh and calf i.e. the knee movement. Figure 4.2 attempts to describe the relationship between the dynamic model and the design concept regarding input angles. The design concept is simplified to focus only on the angle relationship. Hence does the configuration not represent the actual design chosen. As can be seen from the figure are the same relative angles used in both the computational model and torque model for the design concept. By the principle of opposite angles are the angles directly transferred to the concept. The use of relative angles as input are stated as *Design option 1*.

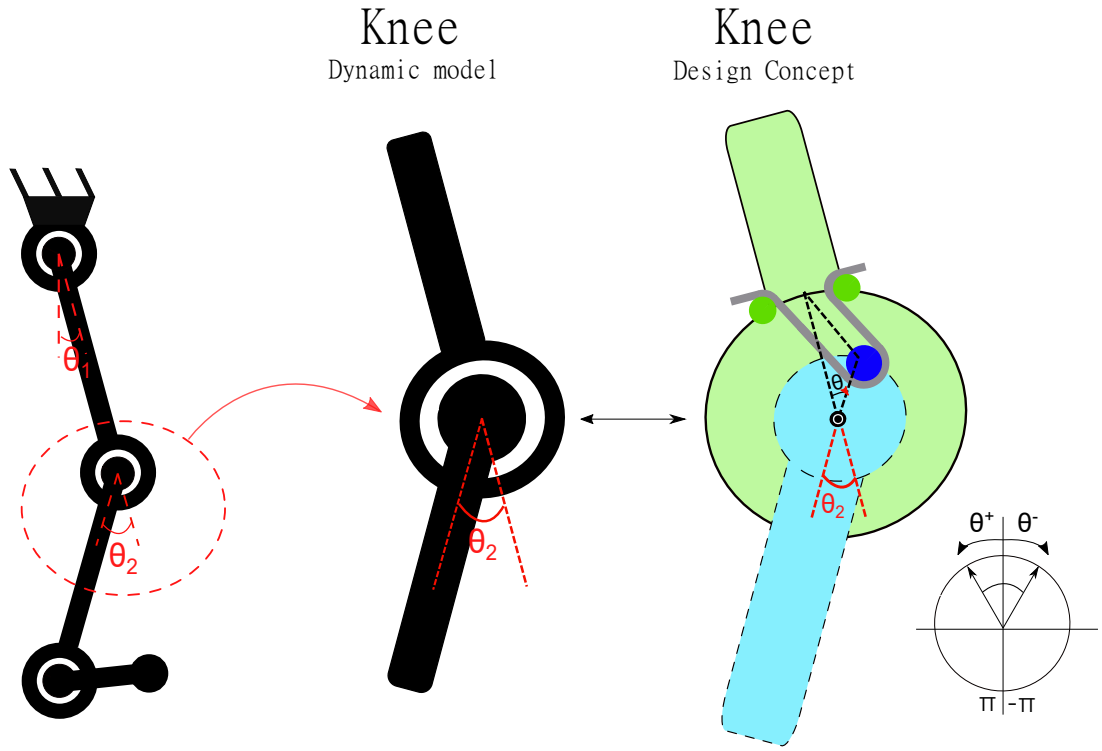

Figure 4.2: Illustration of the use of relative angles in both the computational model and concept.

Design option 2 considers the use of absolute angles in the knee joint. The idea behind absolute angles is that the knee base would remain parallel to the hip base which is fixed horizontally. This would require the installation of a parallel mechanism with an auxiliary link between the two bases, much like what is seen in Zhou et al. [2020], and illustrated in Figure 4.3. It is at this point unknown how the use of absolute angles will affect the torque profile, but the smaller angle interval should affect the configuration of the joint. An investigation in regard to the torque profile and possible joint configurations will be carried out for both design options.

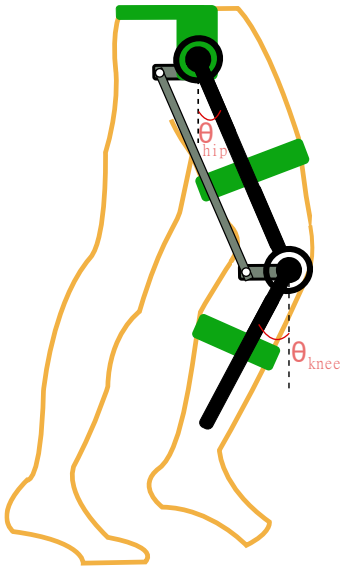

Figure 4.3: Illustration of a parallel mechanism necessary to obtain absolute angles in the knee.

4.4 Implementation of the Design Concept

By the description of the design concept it becomes clear that a direct implementation is not feasible for gravity compensation. An example of the torque-angle characteristics of the JVSR is used to see this more clearly. Figure 4.4 is provided by one of the authors of the JVSR, and is merely an example to illustrate the characteristic behaviour.

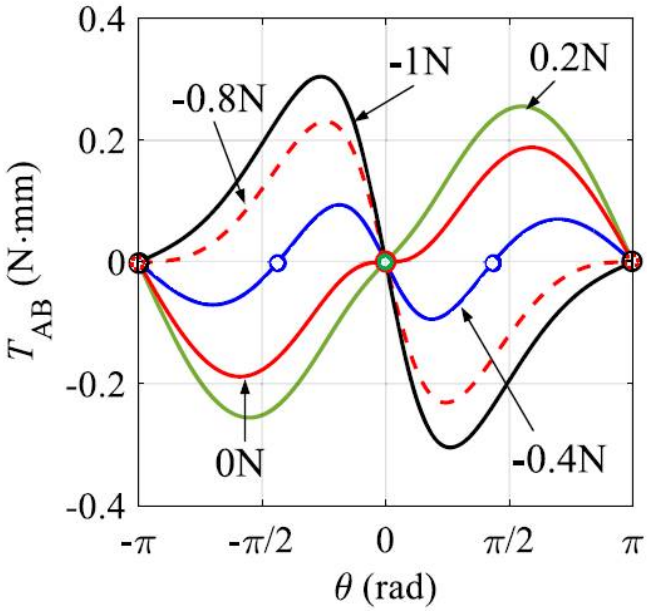

Figure 4.4: Influence of pretension on the torque behavior in the design concept, (Li and Bai [2019]).

An increase in the angle from neutral position (0 rad) leads to an increase in torque in either direction. The user would then need more efforts for the gait because he also needs to overcome the torque from the compliant joint when the joint angle increases. From Figure 4.4 we can however see this trend change as the torque profile reaches a maximum between $\pm\frac{\pi}{2}$ and $\pm\pi$. From this point the torque decreases until it reached the new unstable equilibrium at $\pm\pi$. In other words will the torque increase as the angle decrease in this region, which is the desired behavior. The goal is to find a way to exploit this last behaviour in the joint design. This may be achieved by introducing an initial angle and pretension to the concept. The idea is illustrated in Figure 4.5. By applying a positive initial angle, will a decrease in angle result in a positive torque.

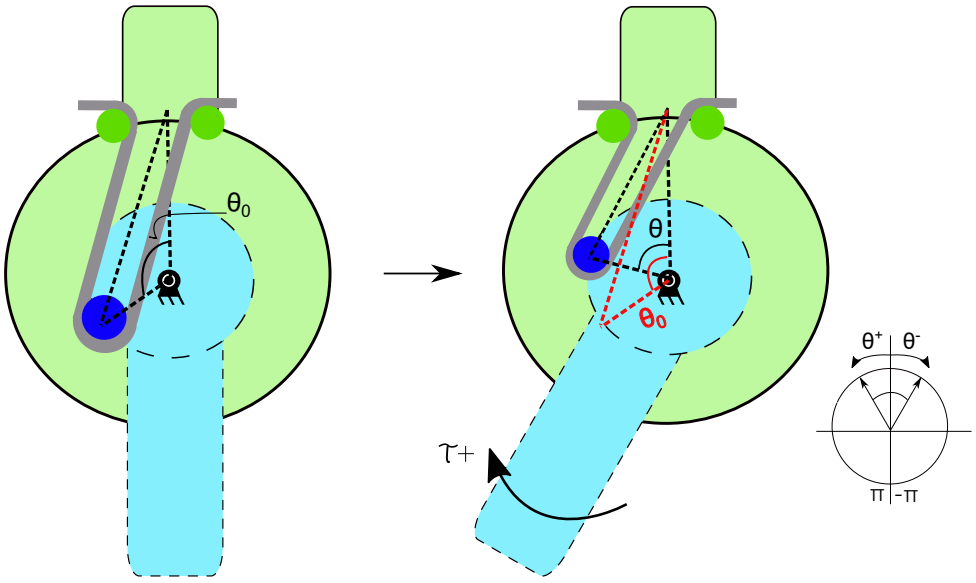

Figure 4.5: Illustration of the effect of introducing an initial angle.

This approach introduces several constraints to the concept, most significantly to the number of pins allowed. While this was a key parameter before, will the cables overlap if too many are used now. This depends on the input angles during the gait. The initial angle will therefore serve as an additional design parameter.

4.4.1 Joint Configuration

From the equations presented in Section 4.2.1 it is clear that the torque model of the design concept includes the following design parameters. A parametric analysis should be conducted to figure out what configuration best fulfills the torque requirement stated in Chapter 3.

Geometrical parameters

l_1	Length of bar 1
l_3	Length of bar 3
R	Radius of pulleys
R_t	Radius of spring pulley
a	Distance between coherent pulleys
d	Diameter of cable
N	Number of wrapped pulleys
θ_0	Initial/pre-rotated angle

Spring characteristics

k_l	Spring stiffness linear tension spring
k_t	Spring stiffness torsional spring
F_0	Pretension of the spring

Spring Selection

There are basically three options when selecting a spring. It could be linear, torsional or a customized nonlinear spring. The use of a nonlinear spring introduces more design parameters and the expanded investigation is deemed unnecessary within the scope of this thesis. Only a linear and torsional spring are then considered, each introducing new design considerations.

A linear tension spring has the advantage of simple implementation, and can be easily exchanged if that is required. To compensate for gravitational forces of these magnitudes it's likely that a large linear spring is necessary. It could possibly be located alongside the links. This introduces constraints to the elongation of the spring.

A torsional spring could be implemented in a similar way to what is seen in the JVSR design in the paper by Li and Bai [2019]. The torsional spring is here added directly on top of a new pulley. A design utilizing a torsional spring could theoretically enable for a more compact design. Additionally it allows for a greater range of configurations as both the radius of the pulley, and the spring characteristics affect the torque provided by the joint. Being located close to the main joint, this approach does however introduce size constraints and more complicated manufacturing considerations.

4.5 Optimization of Design Parameters

Due to the complexity of obtaining an optimal configuration with the amount of parameters, an optimization was performed. The goal is to minimize the residual between the torque requirements stated in Section 3.3.2 and the torque profile generated by this concept. The dependent design parameters of the configuration will vary with the use of a linear or torsional spring. The following description of the optimization algorithm is based on the use of a linear tension spring where the dependent parameters are N, l_1, l_3, k_l, F_0, R and θ_0.

4.5.1 Optimization Algorithm

The optimization is performed with the integrated MATLAB function *fmincon*, with the default settings applied. With default settings the function uses the interior point algorithm to find a minimum subjected to equality, linear and nonlinear inequality constraints. The objective function is stated in Equation 4.8.

$$\begin{aligned} \min f_{obj} &= \frac{\sum^{n}(\tau_{comp} - \tau_{dyn})^2}{n-1} \\ \text{S.T.} \quad & \mathbf{C} \end{aligned} \tag{4.8}$$

where T_{comp} is the torque generated from the compliant concept, calculated as in Equation 4.2. T_{dyn} is the torque obtained from the dynamic model, described in Section 3. Finally **C** is a set of constraints which is further explained below. The constraints vary slightly for the hip and knee joint, as the requirements are different for the two joints.

Constraint 1:

$$N = 1, 2 \tag{4.9}$$

The maximum of pins is set to two, as more than this is not feasible with the design idea presented in Section 4.4.

Constraint 2:

$$\text{Knee Constraint:} \quad l_1 + 2R \leq l_3 \leq 50 - R - 3mm \tag{4.10}$$

$$\text{Hip Constraint:} \quad l_1 + 2R \leq l_3 \leq 60 - R - 3mm \tag{4.11}$$

This constraint is based on the requirement that the outer diameter of the design must be less than $100mm$ in the knee and $120mm$ in the hip. The lower boundary is set to ensure there is no collision between the inner and outer pulleys.

Constraint 3:

$$R + 3mm \leq l_1 \leq l_3 - R - 3mm \tag{4.12}$$

The constraint is set to ensure that there is room for inner pulleys without any collision with each other or the outer pulleys.

Constraint 4:

$$k \geq 0 \tag{4.13}$$

The constraint is set because a negative spring constant is not feasible.

Constraint 6:

$$\text{Knee Constraint:} \quad 0 \leq F_0 \leq 500N \tag{4.14}$$

$$\text{Hip Constraint:} \quad 0 \leq F_0 \leq 700N \tag{4.15}$$

A negative pretension is not feasible, and a larger pretension seems excessive.

Constraint 7:

$$6.5mm \leq R \leq 15mm \tag{4.16}$$

The constraint is set because the obtainable pulleys have a radius within the range of $6.5 - 15mm$.

Constraint 8:

$$\frac{F0}{k} + \delta l \leq l_{spring} \tag{4.17}$$

Here, δl is the maximum elongation of the cable due to change in the joint angle, which is calculated with Equation 4.4, and l_{spring} is the maximum extension of the spring. The constraint is set up to ensure that the spring is not extended above its maximum limit.

4.6 Initial Design Results

This section presents investigations on the optimized joint configurations for both the knee and hip joints with their respective torque requirements. The torque profile may be influenced by the choice of spring as discussed in Section 4.4.1. The configuration utilizing a linear spring is first presented, with a torsional spring investigated in Section 4.7.1. The process of obtaining the configuration is general for the two joints. The knee joint will therefore be presented first in detail, while the hip configuration is evaluated more briefly towards the end of this chapter.

4.6.1 Knee Joint Configuration Using a Linear Spring

Two design options are considered based on the trajectory input. The use of relative angles, as described in Section 4.3, will firstly be presented, before absolute angles are considered. The optimization considering only one pin and relative angle input resulted in the torque profile seen in red in Figure 4.6. The corresponding configuration values are presented beside the Figure.

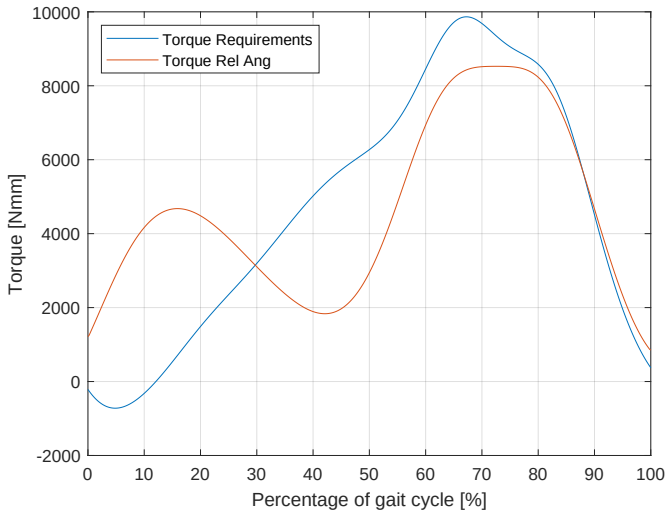

Optimized parameters		
Parameter	Unit	Value
N	#	1
l_1	mm	17.519
l_3	mm	30.519
k	$\frac{Nmm}{rad}$	10.000
F_0	N	500.00
R	mm	5
θ_0	rad	3.1416

Figure 4.6: Torque calculated from the design concept plotted against the torque requirements.

The use of relative angles can be seen to have a poor effect on the torque profile as it poorly follows the torque requirements during the first 60% of the gait cycle.

4.6.2 Absolute Angle Input

The same optimization algorithm is utilized, but the trajectory input in the knee is altered based on the design option described in Section 4.3. The optimization resulted in the torque profile seen in red in Figure 4.7, with the corresponding design configuration presented in the table.

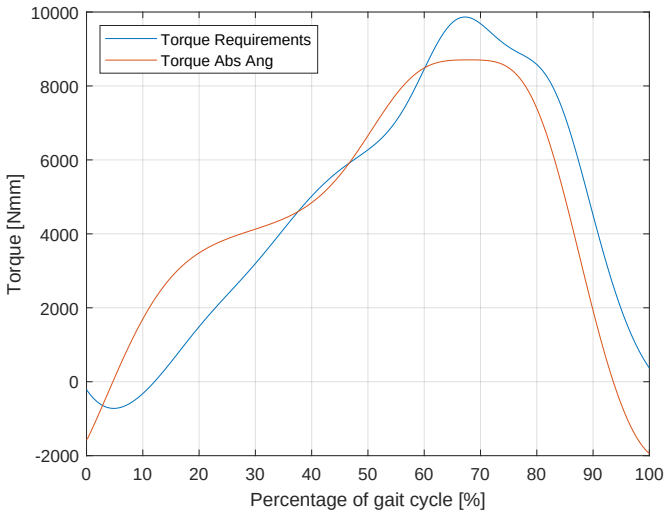

Optimized parameters		
Parameter	Unit	Value
N	#	1
l_1	mm	17.408
l_3	mm	33.408
k	$\frac{N}{mm}$	10.000
F_0	N	500.00
R	mm	6.5
θ_0	rad	2.9904

Figure 4.7: Torque calculated from the design concept plotted against the torque requirements using absolute angles.

The torque profile produced using absolute angles can be seen to much better follow the curve of the torque requirements. The profile does however experience some negative torque at the start and end of the gait cycle.

From the angular input in the knee, an opportunity for applying 2 pins in the design can be seen. However when using two pins, a new constraint is introduced to ensure that one inner pin does not interact with the cable of the other inner pin. For this to be possible must the maximum angle during gait not exceed π or $-\pi$. This constraint is given as:

$$\theta_{max} + sin^{-1}(\frac{R}{l_1}) \leq \pi \tag{4.18}$$

where:
θ_{max}= Initial angle (0) + maximum input angle (0.25 rad) from mo-cap
R= Radius of pulley
l_1= Length of link 1

The resulting profile is presented in Figure 4.8.

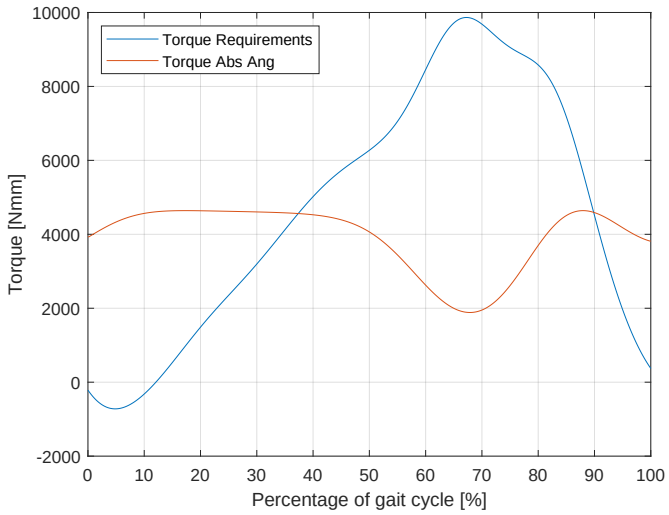

Optimized parameters		
Parameter	Unit	Value
N	#	2
l_1	mm	9.782
l_3	mm	35.782
k	$\frac{N}{mm}$	3.326
F_0	N	166.28
R	mm	6.5
θ_0	rad	2.0911

Figure 4.8: Torque calculated from the design concept plotted against the torque requirements using 2 pins

The optimized curve can be seen to poorly follow the torque requirements. The use of two pins are therefore disregarded as a design option from this point.

4.6.3 Discussion of the Design Options

The use of absolute angles in the knee joint are seen to be a better match for the torque requirements. The torque profile comes at the cost of increasing the manufacturing complexity and weight of the exoskeleton, but is deemed necessary to avoid undesired behaviour during the first 60% of the gait cycle. The 2-pin configuration is also disregarded due to the sub-optimal torque profile.

Due to the relatively high values of the required spring stiffness and pretension, it has been decided to apply two similar springs in parallel to share the stiffness and load. The parameters of the chosen spring(s) are presented in Table 4.1

Table 4.1: Spring parameters in knee joint.

Parameter	Unit	Value
OD	mm	19.05
L_0	mm	114.3
Max deflection	mm	45.97
k	N/mm	5.12
F_{max}	mm	258.21
Initial tension	N	23.24

4.6.4 Additional Design Considerations

The chosen linear springs are too large to include in the joint itself and must therefore be located elsewhere. The natural choice is to place them alongside the links to avoid possible interaction with the user and environment. This has been achieved by fixing the inner pin as the foundation, with the outer pins rotating relatively. By this alteration in design, the cable can be drawn directly out to the springs placed on the link. The full design of the knee joint is idealized in Figure 4.9.

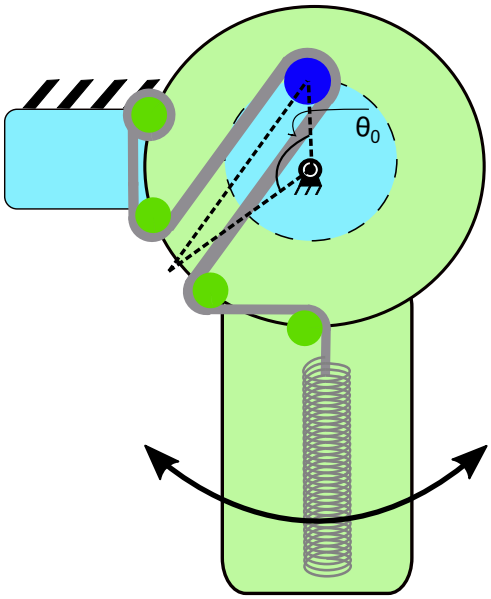

Figure 4.9: Illustration of the switch between bases in the design.

4.7 Configuration of the Hip Joint

An early conclusion can be drawn to the design options of the hip joint. The nature of the angular input in the hip joint can be seen to present relatively large negative and positive values (Presented in Figure 2.1). A direct 2-pin configuration will therefore not deem sufficient results due to the initial angle constraint previously described in Equation 4.18.

Initial investigations of the hip configuration applying one pin resulted in a satisfying torque profile, but very high spring stiffness and pretension values. The resulting tension forces would simply be too large for the pulleys to handle. For application in the hip joint, a design alteration was then necessary. The idea of the new design is to overcome the angle constraint when adding new pulleys by applying the pulleys on different levels. The simplest option is then to look at two separate pulley systems each producing separate amounts of torque due to the alteration of angles. Such a design would increase the outward size of the joint and weight. By adding together the produced torque profiles it was discovered that the torque profile presented in Figure 4.10 could be obtained by applying the corresponing configuration twice.

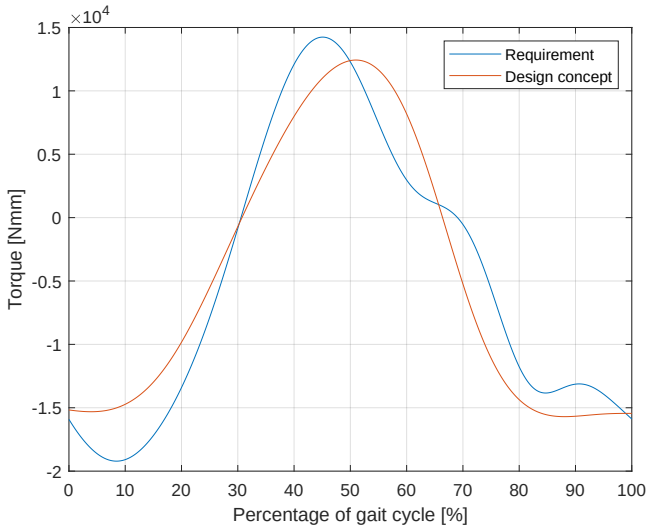

Optimized Configuration x2		
Parameter	Unit	Value
N	#	1
l_1	mm	30.0576
l_3	mm	46.0604
k	$\frac{N}{mm}$	26.1
F_0	N	646.38
R	mm	6.5
θ_0	rad	3.0952

Figure 4.10: Achieved torque profile by utilizing the same configuration twice.

The profile can be seen to not exactly achieve the optimal peak values, but still present a satisfying result. It is worth to mention that the optimization analysis was done in tandem with the spring options available. The design parameters of the final spring(s) chosen for the hip joint is presented in Table 4.2.

Table 4.2: Spring parameters in hip joint.

Parameter	Unit	Value
OD	mm	22
L_0	mm	138
Max deflection	mm	25.9
k	N/mm	25.99
F_{max}	mm	792.2
Initial tension	N	119.06

4.7.1 Evaluation of Torsional Spring Design

The use of torsional springs is evaluated since it potentially can be contained within the joint. The torsional spring is mounted on top of a pulley to allow the torsional spring to act as a linear spring in the torque model. The evaluation of the torsional design is done with the same base optimization algorithm as the linear design, but with a few alterations. The main alteration is a new constraint for the elongation due to the pretension:

$$\frac{F_0}{k_t} R_t^2 + \delta l \leq \theta_{maxSpring} R_t \tag{4.19}$$

Additionally a constraint was added to ensure the spring is load during the entire gait cycle. This constraint is formulated as:

$$l_{max} - l_{min} - \theta_{spring} R_t; \tag{4.20}$$

From the optimization, the design using a torsional spring would result in about the same torque provided by the concept as seen for the linear spring. In other words torsional springs is a viable option in theory. However, from investigating available springs it became clear that torsional springs with the desired strength has a thick wire diameter. This results in a tall spring with a large diameter. In turn, this would result in the spring extending far out from the base plate, about 50mm, which would violate the requirement of a compact design. Hence the concept of using a torsional spring is removed from consideration.

4.8 Initial Exoskeleton Design

The configuration of the initial exoskeleton design is based on the results from the optimization. The parts not affected by the optimization is based on intuition. The exoskeleton is divided into a hip and knee assembly, and a more detailed description of the two assemblies is given in the following subsections.

4.8.1 Hip Assembly

The full hip assembly is shown in Figure 4.11. The hip assembly can be divided into two sub assemblies, namely the hip joint and outer frame, an exploded view of the hip joint is shown in Figure 4.15.

Hip Joint
The hip joint design is mainly set by the radius of the inner and outer pin circles from the previous optimization. The thickness of the material is set by intuition, and is altered later in Chapter 6. A close up of the joint and the pulley system is presented in Figure 4.12. As seen from the figure, the joint contains a pin for mounting the cable, and two pulleys for routing the cables to the center of the springs. The cables are routed in two separate levels and connected directly to two separate springs.

Outer Frame
The outer frame is mainly governed by the parts attached to it, which is the auxiliary link, the springs and the cuff. The springs are mounted to the frame by a bracket, which contains a set screw that enables altering of the spring tension. The length of these springs is governing the length of the frame. The cuff is mounted to the frame with two bolts in the estimated position of the center of mass of the human thigh. The auxiliary link is mounted to a point in the hip joint and end of the frame which allows for rotation. It then work as a parallelogram, which ensures that the base of the knee joint is always horizontal.

Range of Motion
The range of motion of the hip joint is 45° degrees in both flexion and extension, which is well within the requirements set Table 2.2.

4.8.2 Knee Assembly

The knee assembly is similar to the hip assembly, but without the auxiliary link. The knee assembly and a closeup of the knee joint is displayed in Figures 4.13 and 4.14, respectively. As for the hip joint the knee joint is governed by the optimization results, and again the frame is mainly governed by the size of the springs. The springs are mounted in parallel at both ends, with a slider on the top to ensure each spring contributes equally.

Range of Motion

The range of motion of the knee joint is only limited by the frame colliding with the hip frame, resulting in a range of motion of 140° in both flexion and extension.

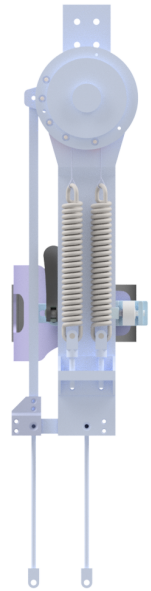

Figure 4.11: Hip joint assembly.

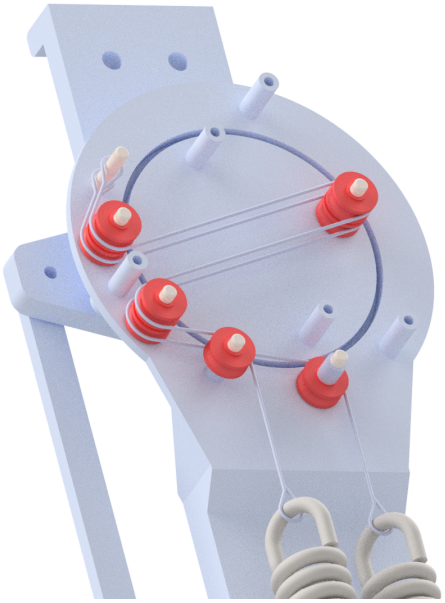

Figure 4.12: Detailed of the pulley system.

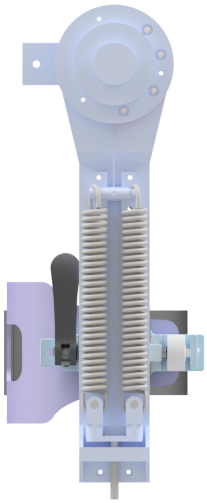

Figure 4.13: Knee joint assembly.

Figure 4.14: Detailed view of the pulley system.

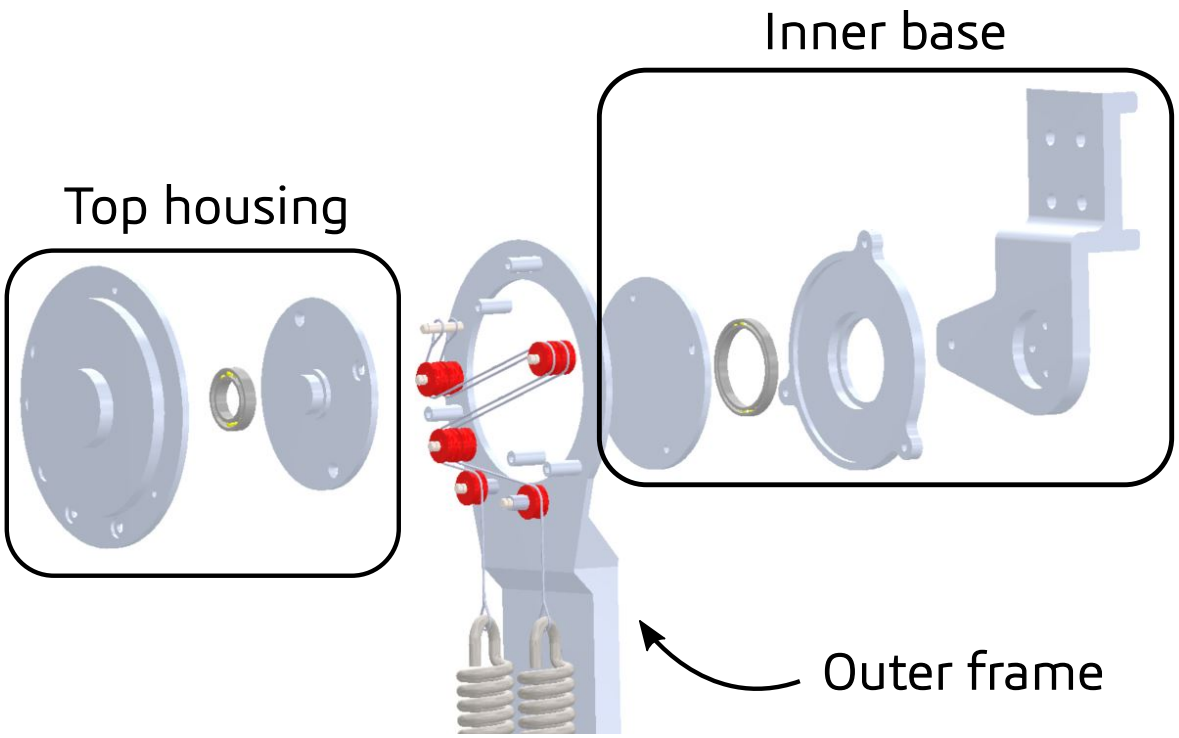

Figure 4.15: Exploded view of the hip joint.

5 | Load Considerations

Torque requirements were used in the previous chapter as a design guideline to the expected performance of the passive compliant joint. This chapter evaluates the assumed critical loading scenarios during the gait and how the estimated torque performance can be used to evaluate the structural integrity of the design. The loading cases will mainly be used for stress and deformation analysis of the design, but also as an evaluation of the structural integrity of standard components such as pulleys and bearings. The engineering design process is an iterative procedure which means that the results found at this stage could have a direct influence on the concept configuration described in Chapter 4.

5.1 Loading Scenarios and Critical Components

Without the opportunity to do physical testing of the reaction forces when wearing an exoskeleton, this section remains strictly theoretical with assumed critical load cases. The authors have chosen a component wise approach, were the model is divided in two main parts, namely the inner base and outer frame as visualized in Figure 4.15.

5.1.1 Force Evaluation

The authors imagine three different scenarios where the design experience critical static loads. The two joints share the same resemblance to being a revolute joint applied to a fixed base. This draws the assumption that although the specific loads change, are the load scenarios general for the two joints. The three cases will therefore be presented in a general manner in this section before the specific loads are found in Section 5.2.

Maximum Cable Tension
The torque produced by the joint is generated by the pulley-cable-spring relationship illustrated in Figure 4.9. The tension occurring in the cable is directly equal to the tension in the spring during the gait cycle. In other words will the maximum cable tension occur when the spring has the largest elongation. For both the knee and hip joint, this occur at $\theta=\pi$. The simplified free-body diagram in Figure 7.3 illustrates the situation. The cable tension is sometimes drawn as 1.8T to illustrate the effect of the cable wrapped around the pulley. They do not represent the accurate value or direction.

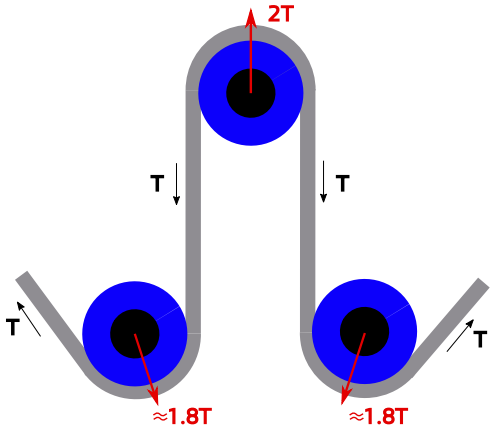

Figure 5.1: Simplified free-body diagram of pulley-system in joint mechanism.

This simple force calculation is necessary in order to investigate if the pulleys can handle the static force applied and how the inner pins and structure will react to the force.

Load Case 1

This load case only considers the outer frame. It's of interest to investigate its response to the critical loads experienced. The exoskeleton can be visualized to carry the human limbs in certain parts of the gait cycle. The critical reaction forces are then assumed to occur at the time during the gait in which the joint generates the maximum amount of torque. At this incident will the gravitational loads oppose the movement by a similar torque. In addition will the pins inflict a force on the part due to the cable tension.

It has been chosen to investigate this loading scenario by assuming the joint to be fixed and apply a gravitational force in the human attachment location. The forces due to the spring and cable tension are assumed bearing forces. The idea is illustrated in Figure 5.2.

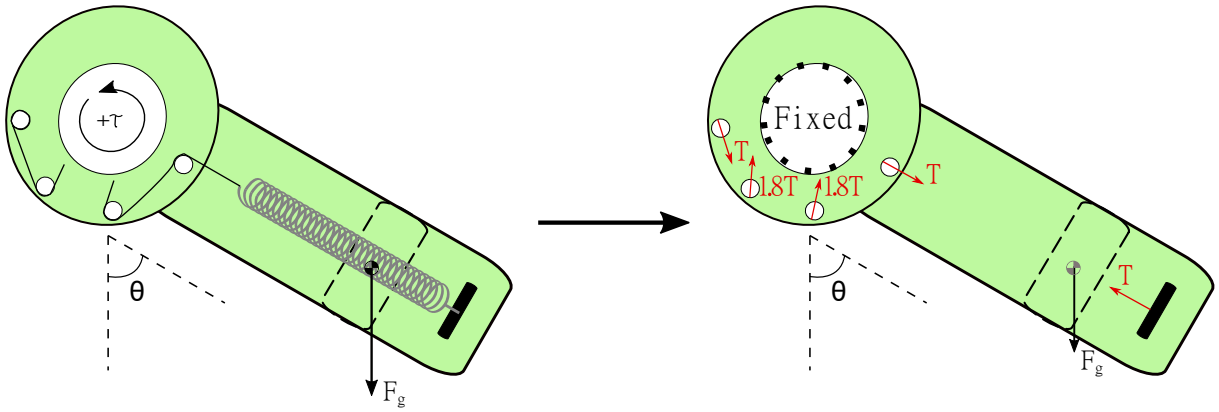

Figure 5.2: Illustration of the assumed load case 2.

Load Case 2

If still considering just the outer frame, it's noted that the cable tension is not at maximum in the previous case. As said introduction wise, this occurs when the total angle (θ+θ_0) is equal to π. At this point there will be no produced torque in the joint, and the case can be visualized to look like illustrated in Figure 5.3.

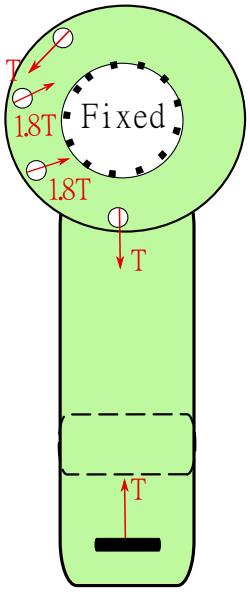

Figure 5.3: Illustration of the assumed load case 3.

Load Case 3

The inner base is at all times regarded as fixed, hence will the only varying force on the structure be the force due to cable tension and the torque around the shaft. As before will there be no torque when the cable has the maximum tension, but the part is also considered to carry the weight of the exoskeleton and human limbs at this point. In the other case will the shaft experience the maximum torsion due to the maximum torque applied during the gait cycle.

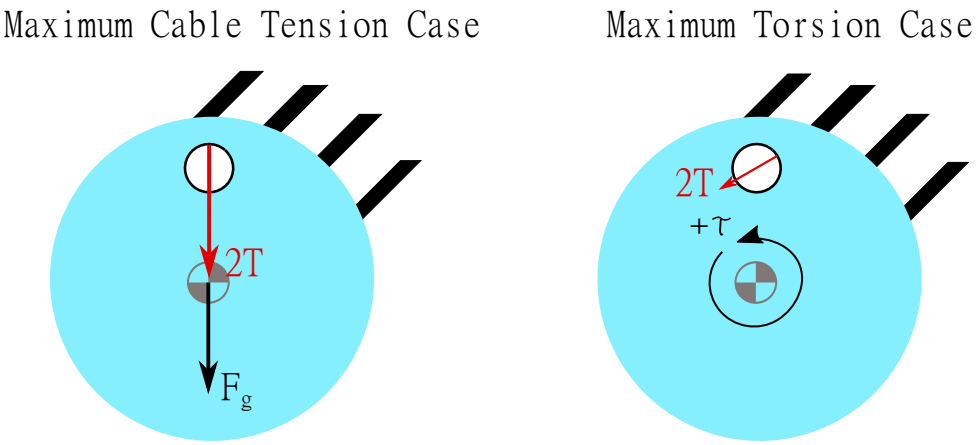

Figure 5.4: Illustration of the assumed load case 4.

5.2 Loads Evaluation for the Knee and Hip joints

The load cases are specified to the respective joints by considering the estimated performance of the joints throughout the gait cycle. The knee joint will be used as an example for calculating the cable tension in the respective scenarios.

5.2.1 Estimation of Cable tension in the Knee Joint

The angular input and elongation of the cable throughout the gait cycle are presented in Figure 5.5.

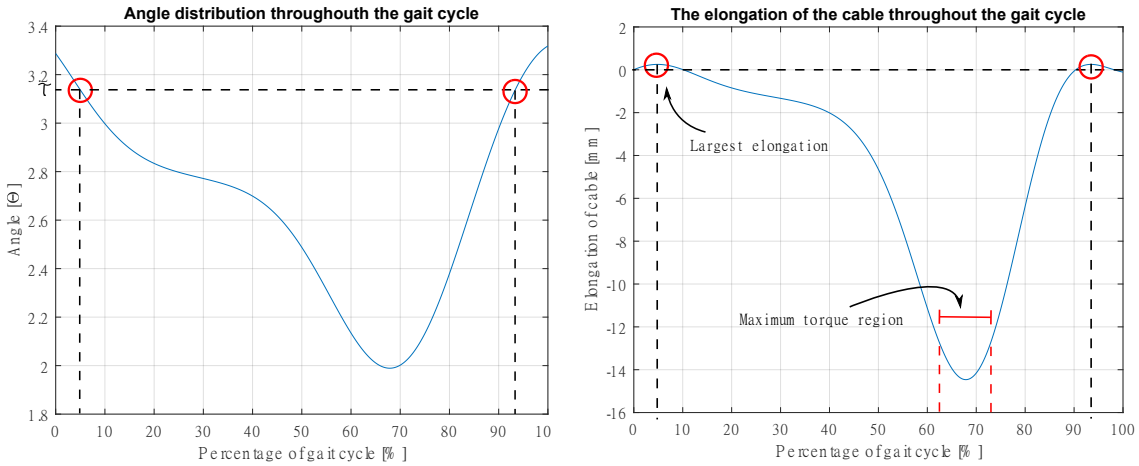

Figure 5.5: Illustration of the relationship between angular input and cable elongation.

The initial cable length is calculated from the initial angle, which is 2.99 rads in the knee joint. The total angle can be seen to reach π at two locations during the gait cycle, at approximately 5% and 94%. From the plot to the right it's clear that the largest elongation of the cable and hence spring elongation appear at the same incidents. The maximum cable tension is then calculated by Hookes law:

$$T_{max} = F_0 + k * \delta l_{max} \tag{5.1}$$

Considering *Load Case 1*, the cable tension will have a different value at the incident of maximum torque. From Figure 4.7, it can be seen that the joint produces a maximum torque in the period of approximately 62-72% of the gait cycle. The same region is illustrated in Figure 5.5, where the highest elongation is extracted and the cable tension is calculated similarly as before.

5.2.2 Gravitational Forces

During the load cases considering maximum torque incidents, will gravity oppose the torque generated by the joint with the same amount of torque in the opposite direction. The gravitational force can easily be found by division of the lever arm to the COM in both

the knee and hip cases. In the maximum cable tension case in *Load Case 3* will the gravitational force simply be weight, where the hip joint will carry the full weight of the exoskeleton and human leg, while the knee carries only the lower region.

5.3 Full Table of Loads

The full list of loads for each load case are presented in Table 5.1.

			Knee	Hip x2
	Load	Unit	Value	Value
Cable Tension	T_{max}	N	502	647
Load Case 1	T	N	370	581
	F_g	N	47	207
Load Case 2	T	N	502	647
Load Case 3	T_{max}	N	502	647
	T	N	370	581
	F_g	N	71	194
	τ_{max}	Nmm	8833	15700

Table 5.1: Table of the applied loads for the presented load cases.

The structural integrity of the design will be investigated by FEM of the last 3 load cases in ANSYS Workbench 19.2 in Chapter 6.

5.4 Additional Load Considerations

This report does not consider loads and effects due to potential misalignment of the joints. The resulting reaction forces of an improper fitting are likely seen in the attachments to the human and are not considered here. This is also the case for forces generated due to the passive elasticity of soft tissue and muscles.

The exoskeleton clearly experience cyclic load, as walking is a repetitive motion. This is an indication that fatigue should be considered. As a first iteration of the design, mainly serving as a proof of concept, it's not considered at this time.

6 Engineering Design of an Exoskeleton Leg

The concept design has been proposed and the critical load cases estimated. The next step in the engineering design process is to assess the structural integrity of the design, and further optimize with respect to the performance requirements. Before structural analysis is carried out will the components have to be assigned material specifications. The loading cases considers the main components of the design, namely the inner base and outer frame, hence will the material selection be focused on these components. The first part of this chapter will therefore provide an evaluation of the possible material candidates suitable. The discussion will have its foundation in the requirements presented in Chapter 2, but additional factors may be included as well.

6.1 Key Material Attributes

Chapter 2 presented the full list of requirements considered for the lower body passive exoskeleton. From this list is the material selection directly tied to the weight and manufacturing requirements. By referring to the works by Ashby [2011]; the design can be said to have one objective, namely to minimize weight while still performing the task. This objective is subject to constraints. The constraints are the material attributes necessary to ensure the estimated performance and safety of the user. The most important constraints are listed below and will in turn provide a material index useful for material selection.

Specific Strength
The material choice has the most direct impact on the weight of the design. In order to accommodate the goal of a lightweight design will the material have to present a high strength to weight ratio in order to also withstand the critical loading scenarios. The frame of the exoskeleton can be seen as a beam where the load, length and shape is specified. The material index evaluated for a minimum weight, yield-limited design is then $(\frac{\sigma^{\frac{2}{3}}}{\rho})$, (Ashby [2011]).

Specific Stiffness
While the material has to be strong enough to withstand the loads, it also have to be stiff enough in order to not bend or buckle. The main focus in this thesis is the estimated performance of the joints. By that notion is it in the first iteration of the design desirable to choose a material where the elasticity of the material will have little to no effect on the torque performance. The material selection should therefore only consider high stiffness materials. Constrained to stiffness, should the material index $(\frac{E^{\frac{1}{2}}}{\rho})$, where E is the Young's modulus, be evaluated when designing for a minimum weight, deflection-limited design, (Ashby [2011]).

Fracture Toughness
The exoskeleton might undergo rough treatment from the user e.g. by clashing with obstacles. For that reasons are brittle materials unacceptable for use in a exoskeleton design. The fracture toughness is a measure of this and should generally be high for allowing a higher fatigue life. The specific fracture toughness is evaluated by $\frac{K_{IC}}{\rho}$.

Ease of Manufacturing
The design process has so far in the report had this constraint in mind by developing a design consisting of relatively simple geometries without unnecessary tight protrusions and indentations. The chosen material will however introduce manufacturing constraints dependent on the geometry and loads on the component. Manufacturing considerations have a large impact on other key project points such as production time and cost, and is therefore regarded as an important attribute.

Cost
This thesis serves mainly as an investigation of the applicability of the compliant joint concept in an exoskeleton. In addition is it difficult to evaluate a cost constraint against the possible health benefits of such a device. Therefore are there no specified requirements to the cost of the exoskeleton design in Table 2.2. The cost may itself be seen as an objective function, such as the weight, but in this selection will it only be evaluated as an additional constraint.

6.2 Classes of Materials

A literature study was conducted as an initial screening of available materials. It becomes clear that the typical material classes utilized in exoskeleton design falls under the categories "Metals, Polymers and Composites".

6.2.1 Metals

From the load considerations in Chapter 5 it's seen that the largest loads, and hence stress concentrations will appear within the joint. This makes metal alloys the obvious first choice because of theirs high strength and stiffness. In addition can metals be assumed an isotropic material, where their material properties are equal in every direction. This allows the use of a general failure criterion. Metal alloys such as aluminium are also typically easy to machine by computer aided control (CNC), which allows for great ease in manufacturing. The aluminium alloys are popular in exoskeleton design due to their relatively low price, but Magnesium alloys have also been employed in state of the art exoskeletons such as HAL cite, because of their lower density. A general observation is that the higher yield strength the material has, the smaller can the frame be.
Based on the material attributes presented in Section 6.1, it has been decided to narrow down the search in metals to aluminium alloys. This is in accordance with the general trend of exoskeletons as they are cheaper than their opponents, but still maintain high strength.

6.2.2 Fibre Reinforced Composites

By investigating the respective Ashby charts it can immediately be seen that composite materials, with carbon fiber composites in the lead, presents improved specific strength, stiffness and toughness properties compared to metals. Unlike metals are composites referred to as orthotropic materials, where the material properties are direction dependent. Composites are well known as a combination of two or more constituent materials, typically a strong and stiff component. When developing strong lightweight structures are these constituents typically polymer resin/matrix reinforced with long continuous fibers. To accommodate the loads coming from various directions in the joint, would multiple fibre orientations be used to achieve the proper balance between strength and stiffness. The fibre system could then be specially altered to account for various load levels, unlike what is possible for isotropic metals.

Considering the load cases for the initial design it can be seen that relatively high forces are applied to the holes at the center disc, and stress concentrations are likely to occur here. A typical design rule when dealing with composites is to avoid stress concentrations as the stress concentration factor generally is much higher. Isotropic engineering metals such as aluminum are ductile enough to yield to accommodate for stress concentrations locally when close to a stress concentration. This is not the case with composites which are generally less ductile than isotropic metals. In other words does composites need careful consideration and should be part of the design process at an early stage. It is not within the time and scope of this thesis to investigate the effects of applying a composite material to the design, but the authors envision it for future iterations.

6.2.3 Polymers

Polymers have the advantage of typically low weight, low cost and simple manufacturing by either a mold or 3D printing. From the respective Ashby charts can it be seen that the material indices of polymers generally scores lower than aluminium alloys and fibre reinforced composites. It's still plausible that the chosen polymer would be able to withstand the load cases described in Chapter 5, but its been decided to not conduct stress analysis on polymer materials this time around. This is based on the fact that there is no narrow cost limitation to the design, and the focus is mainly on the performance of the joint mechanisms. Therefore has it been decided to utilize an aluminium alloy in the first iteration of the design.

6.3 Materials in Initial Design

This report distinguish between three categories of components in the exoskeleton design. The first being the standard components (pulleys, springs, bearings etc.), add-ons (cuffs, auxilliary link, trunk frame) and the joint components. The above discussion only considers the last category, where a single material is envisioned for all components.

From available alloys its been decided to utilize Al 7075 T6 as the main material. This is reasoned by the fact that it's an easily obtainable commercial material and presents higher strength and stiffness characteristics than e.g. Al 6061 T6 which is more ductile. This can more clearly be seen by comparing the material properties of the two alloys in Table 6.1. It should be noted that the lifted values are provided by the Aluminium association and represents typical values.

	ρ ($\frac{kg}{m^3}$)	σ_{yield} (MPa)	E (GPa)	K_{IC} (MPa$\cdot m^{\frac{1}{2}}$)	$\frac{\sigma^{\frac{2}{3}}}{\rho}$	$\frac{E^{\frac{1}{2}}}{\rho}$	$\frac{E^{\frac{1}{2}}}{\rho}$
Al 6061-T6	2700	276	68.9	29	1.6	3.07	1.07
Al 7075-T6	2810	503	71.7	18	2.2	3.01	0.63

Table 6.1: Comparison of two commonly used aluminium engineering alloys, (MatWeb [2020]).

The material indices are only used for comparison of the two alloys, so the units are not deemed important. From the table it can clearly be seen that the 7075 alloy provides higher strength characteristics and an increase in stiffness at the account of fracture toughness. The latter is however regarded as the least important of the three.

6.4 Static Structural analysis

The static structural analysis is performed based on the load cases that are considered critical, see Chapter 5. All of the static analyses are performed under the assumption of small deformations, i.e linear analyses. The following subsection presents the setup and analysis of the three defined load cases. The load cases are defined for both the hip and knee joint, however the following will mostly focus on the hip joint as it is subjected to the largest forces.

6.4.1 Safety Factors and Failure Criteria

Stress Safety Factor and Failure Criteria

It is considered good engineering practice to apply safety factors to the loads and material properties. Usually these factors are obtain from standards. However a standard for medical exoskeletons does not exist, so the factors must be obtained elsewhere. As the chosen material is aluminum, the standard *Eurocode 9: Design of aluminium structures*, (EN1999-1-1 [2007]), is a logical choice. The standard suggest a safety factor of 1.1 or 1.25, when assessing the structures resistance to failure, where 1.25 is for structures that are mainly tension loaded. The frame is assumed to experience an advanced stress state, especially where the limb connects to the frame, which makes the stress state difficult to determine. Hence the most conservative option of 1.25 is chosen. The definition of failure applied in this thesis is the von-Mises failure criterion, i.e failure occur when the maximum von-Mises stress is above the yield strength of the material. The yield strength of the chosen material is $503MPa$, and with the applied safety factor the maximum allowable stress is $402MPa$.

Deformation Failure Criteria

The initial design of the frame can roughly be defined as a flat plate connected to the inner disc and subjected to a compressive loading which induces bending. It is therefore considered plausible that the design can experience considerable deformations in the flat plate region. Hence it is desirable to define an upper limit of the deformation. The maximum deformation criteria is set to $1.5mm$, considered conservative. The limit is set conservative to ensure the exoskeleton can withstand possible unexpected loads during operation. Additionally is a low deformation of the frame desired, especially in the hip joint, since this deformation would lead to the knee joint being pushed outwards or inwards. This would result in the user experiencing increased reaction forces in the cuffs.

6.4.2 Analysis of Load Case 1 in the Hip Joint

Load case 1 for the hip exoskeleton focuses on the outer of the hip joint. The case is simulated as an assembly consisting of two parts, namely the outer frame and the spring bracket. The assembly is shown in Figure 6.1, where the bracket is highlighted in blue. The main reason for including the bracket is to ensure that the forces from the spring mounting point are applied in a realistic manner. The contact point between the frame and the bracket is not of interest for load case 1, hence the bracket and the frame is considered to be one part. This is done by sharing the topology of the two faces in contact. This simplifies the analysis, such that no contact formulation is needed. A detailed description of the setup, which includes element choice, mesh generation, loads and boundary conditions is provided in the following paragraphs.

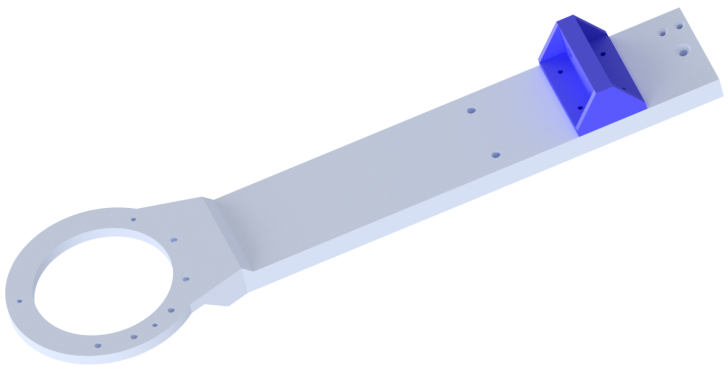

Figure 6.1: View of the analysed assembly.

Element Choice

The ANSYS Workbench software automatically chooses the element type, and for this part it chose the element called *SOLID187*. The *SOLID187* element is a 10 node tetrahedral element, which means the element is capable of displaying quadratic displacement behaviour. According to the ANSYS documentation (ANSYS [2019a]), the element is well suited to model irregular meshes, as is expected for this part. An irregular mesh is expected because, among others, there are both circular and rectangular areas on the same part, which results in irregularities in the structure of the mesh. Therefore it is decided to keep the elements that the software chose.

Mesh Generation

The part is meshed by using three different sections, these three sections share topology to ensure the meshes are compatible with each other on the inter-phases. The sections are illustrated in Figure 6.2 and highlighted in 3 different colors. Preliminary analyses revealed that the stresses in Sections 2 and 3 are low compared to Section 1. As a result Section 2 and 3 was meshed with a relatively coarse mesh with a base element size of $10mm$. However the mesh around the holes in the geometry was refined due to the loads being applied there. Section 1 has a base element size of $3mm$, and a significant refinement around the holes.

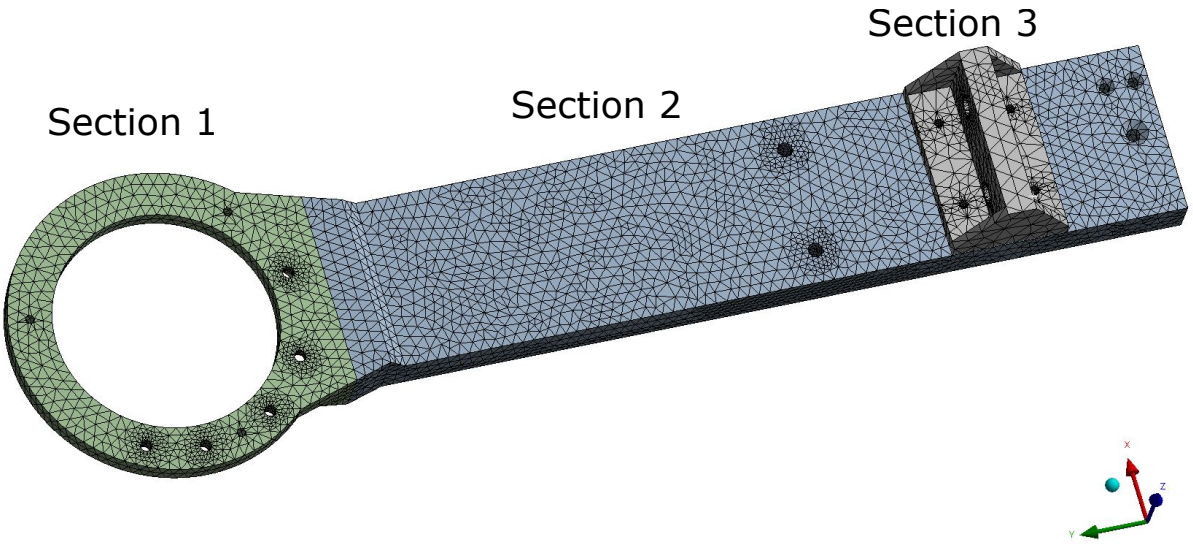

Figure 6.2: Generated mesh for converged model.

Loads and Boundary Conditions

The model is fixed in the inner ring of the housing, as explained in Section 5.2. The loads applied to the model are all applied at holes in the geometry. This is a simplification done to remove the pulley pins and bolts from the simulation. The applied loads are visualized in Figure 6.3, which illustrates the application hole and the direction of the loads. All loads, except for the ones applied in section 3, are applied as bearing loads. This is done because the bearing load option offers a more realistic representation of the load distribution. The load applied to the two holes in section 2 are distributed evenly between the two holes, even though only one force is visualized.

Figure 6.3: Setup of static structural analysis in ANSYS.

Mesh Convergence Study

The model is considered converged when the maximum deformation is not changing when the mesh is refined. The maximum deformation is chosen as convergence failure criteria because it's clear from the stress levels of the part that deformation is the main issue for failure. In order to obtain convergence is the mesh in section 1 and 2 refined. The results from the study is presented in Figure 6.4, and the model considered converged at about 100000 nodes, with a maximum deformation of 1.242mm.

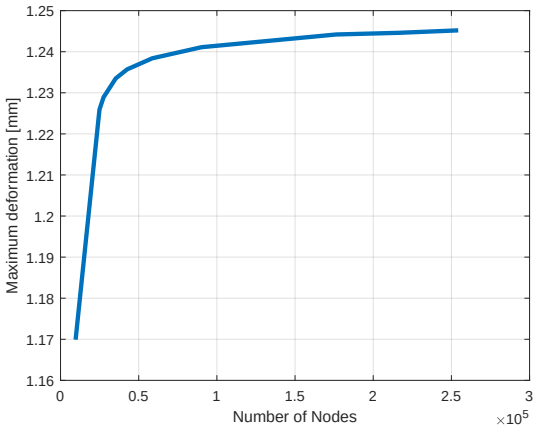

Figure 6.4: Mesh convergence of the thigh assembly

Deformation results

The total deformation of the frame is displayed in Figure 6.5. The deformation mainly occurs in the positive z-direction and has the same distribution as the total deformation. This deformation is caused by the bending moment induced by the mounting point of the springs being above the base of the frame. The maximum deformation in the x-direction is less than 0.1mm and is considered negligible, and therefore not presented. The maximum deformation in the y-direction occurs at the top of the spring bracket and is about 0.2mm.

Figure 6.5: Maximum total deformation of the initial design subjected to load case 1. The color bar is given with the unit meter.

Stress results

The stress distribution of the analysis is presented in Figure 6.6. From the analysis it is observed that the maximum stress is about $60MPa$ which is far below the yield strength of the material. This leads to the conclusion that failure due to stress is highly unlikely in the current design. From the figures it is clear that there are large areas of the part which has a low stress, which indicates that strategic removal of material could result in a more lightweight part with the same structural performance.

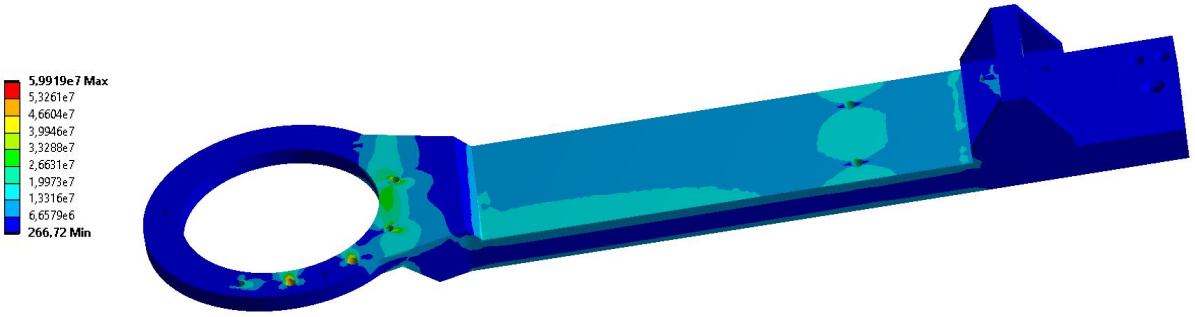

Figure 6.6: Stress distribution of the initial design. The unit of the color bar is Pascals (Pa).

6.4.3 Analysis of Load Case 2 for the Hip Joint

Load case 2 occurs when the spring tension is at a maximum. The analysis for load case 2 has a very similar setup as case 1. The model uses the same elements, mesh generation strategy, boundary conditions and mesh convergence criteria. The only difference is the magnitude and direction of the applied forces. The setup of load case 2 is visualised in Figure 6.7. A mesh convergence study is performed for load case 2, and it yielded similar convergence behaviour as case 1. The model is considered converged with a mesh of about 100000 nodes, and the maximum deformation is $1.33mm$. The deformation results are further explained in the following paragraph. The stress distribution is visualized in Figure 6.8. It is observed that the stress is similar to case 1, where there are large areas with low stress. Combining the stress results from both cases suggest that there is significant possibility for removing material. In Section 6.5 topology optimisation is applied as a tool to strategically remove material in an effective manner.

Figure 6.7: Setup of the analysis for load case 2.

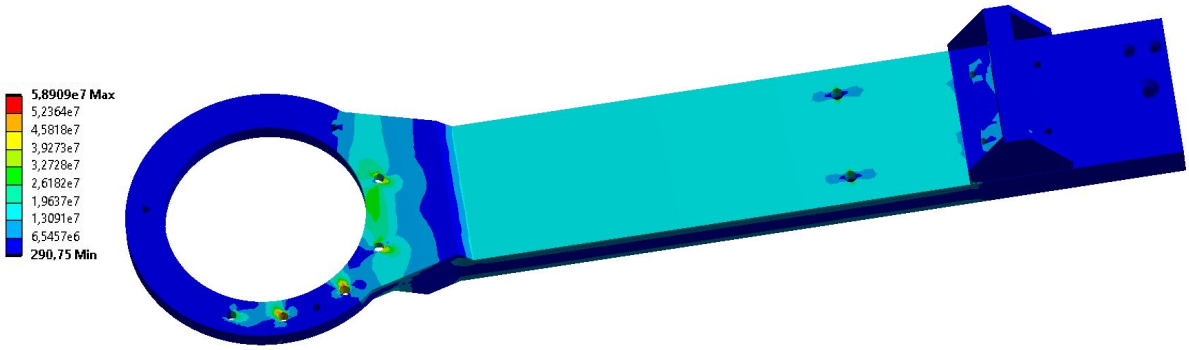

Figure 6.8: Stress distribution of the initial design. The unit of the color bar is Pascals (Pa).

Deformation results:
The global deformation of the initial design is shown in Figure 6.9. The deformation is presented with a true scale and the undeformed body is the shaded shape in the figure. The maximum deformation is observed to be 7.5mm, which is very large, and it displays a real chance of buckling.

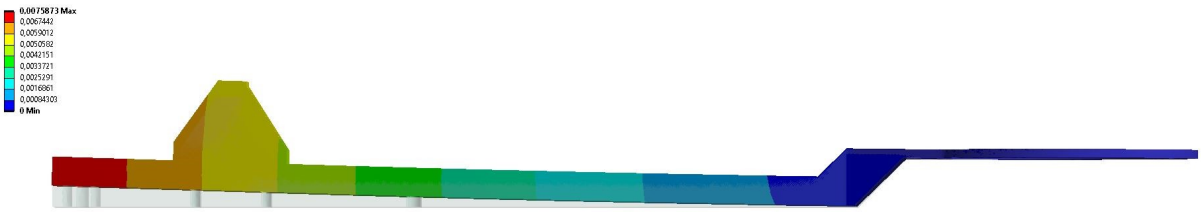

Figure 6.9: Global deformation of the thigh base plate.

The strain energy density of the model was investigated for a way to effectively add material. The strain energy density is a measure of each elements contribution to the stiffness of the model. Material was added until the resulting deformation was less than 1.5mm, which is considered acceptable. Material was mainly added by increasing the thickness of the flat rectangular plate. The deformation of the acceptable design is shown in Figure 6.10. The undeformed

body structure is shown with a black frame. The deformation is almost not noticeable and considered acceptable. The weight of the design is however increased ($890g$), and as seen from previous analyses is there a low stress distribution. Based on these observations was it later decided to use topology optimization as a tool to lower the weight of the assembly.

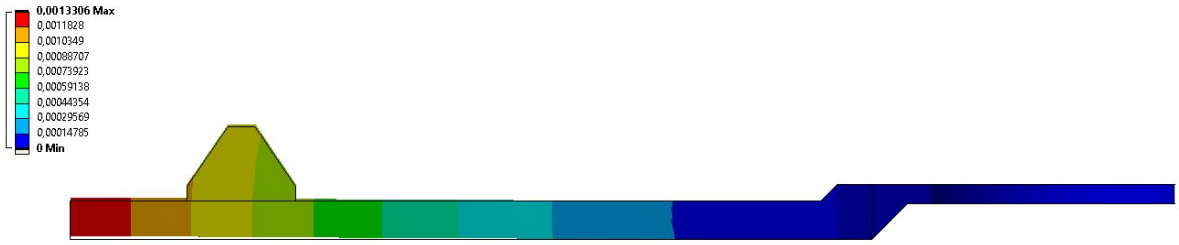

Figure 6.10: Deformation of the altered initial design.

6.4.4 Analysis of Load Case 3 in the Hip Joint

Case 3 occurs when the inner base plate is subjected to the maximum spring tension. This case has a simple setup where the axle surface is considered a fixed support, and a bearing load is applied to the inner pin hole. The setup is presented in Figure 6.11, where the blue surface is the fixed support and the red arrow indicates the direction of the bearing load. A convergence study is performed on the model. The maximum stress is $71.9MPa$, and the model is considered converged at about 60000 nodes. The deformation of the model is less than $0.01mm$, which is negligible and it is therefore not presented. The stress distribution in the model is shown in Figure 6.11.

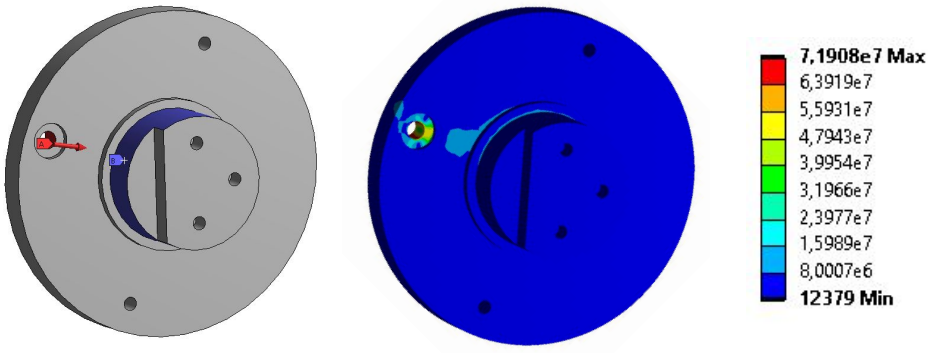

Figure 6.11: Stress distribution in load case 3.

6.4.5 Analysis of the Knee Exoskeleton

The initial outer frame and inner base of the knee shares the same design as the hip, only with other dimensions. The same approach for evaluating the load cases has therefore been conducted. A summarized list of the results are presented below, while the stress and deformation distributions can be seen in more detail in in Appendix A.

	Max. Stress		Max. Deformation	
	Unit	Value	Unit	Value
Load case 1	MPa	126	mm	1
Load case 2	Mpa	167	mm	1.24
Load case 3	Mpa	194	mm	0.01

Table 6.2: Result from structural analysis of initial knee design.

6.4.6 Conclusion of Strength Analysis

It's clear that the analysed parts are strong enough to withstand the critical load cases. The design can however be seen to be unnecessary heavy in its current state. The largest contributors are the hip frame at $890g$ and the knee frame at $466g$. To ensure a more lightweight design will topology optimization be used as a tool to strategically remove material.

6.5 Topology Optimization

A typical topology optimization analysis computes the optimal geometry of a selected region of a model, based on specific design objects subjected to a set of constraints. In this thesis, topology optimization is used as a tool to obtain a strong and yet lightweight exoskeleton design. The optimization will focus on the larger components in the design, i.e the outer frames of the hip and knee joints. The analysis is performed in ANSYS and utilizes the built in topology optimization options. The details of the optimization and the chosen algorithm is detailed in Section 6.5.1.

Topology optimization in ANSYS is based on a set of loads and boundary conditions set by a preceding linear static structural analysis. The discretization (mesh) of the geometry is also set by the preceding analysis. The mesh is effectively the resolution of the topology optimization as it evaluates whether to keep or remove material on an element level. In other words, a finer mesh generally results in a more detailed optimization. Additionally, if a feature in the model becomes as thin as one element, the algorithm may struggle to properly capture the design. Based on this and a limited options for contact formulations in the topology optimization framework, it was decided to optimize the components of the exoskeleton separately. The setup and results of the topology optimizations are presented in the following subsections.

The goal of the topology optimization is to find the best use of material for a part such that an objective criteria is maximized or minimized, while subjected to a set of constraints. Some typical objective criteria are global stiffness, natural frequencies, volume and mass.

6.5.1 General Topology Optimization Problem Statement

Topology optimization seeks to minimize or maximize the objective function (F_{OBJ}), while subjected to a set of constraints (C_j). To set the design variable of the optimization a is a discretized body required. The design variables are introduced by assigning a pseudo density η_i to each finite element in the discretized body. The pseudo densities varies from 0 to 1, where $\eta_i \approx 0$ represents that material can be removed and $\eta_i \approx 1$ representes that material should be kept. In simple mathematical terms the optimization problem can be stated as follows, (ANSYS [1999]).

$$F_{OBJ} = \text{a minimum/maximum w.r.t. } \eta_i$$

subject to:

$$0 < \eta_i \leq 1 \quad (i = 1, 2, 3 \ldots N)$$
$$LB_j < C_j \leq UP_j (j = 1, 2, 3, \ldots, M)$$

where:

$$N = \text{number of elements}$$
$$M = \text{number of constraints}$$
$$C_j = \text{computed jth constraint value}$$
$$LB_j = \text{lower bound for jth constraint}$$
$$UP_j = \text{upper bound for jth constraint}$$

From the above stated problem it is clear that performing a topology optimization would require an objective function formulated to be dependent on the pseudo densities and a set of constraints. Additionally it requires a method for solving the optimization problem by determining the pseudo densities of the elements. The following subsections will focus on the available options and choice of solution method, objective function and constraints. The available options are limited to what ANSYS Workbench 19 R2 offers.

6.5.2 Objective function

The available objective function options in ANSYS are to minimize the compliance, mass or volume. The objective function of interest is to minimize the compliance, i.e maximizing the stiffness. Minimizing compliance is the function of interest, because it was observed that the deformation was the main issue in the preceding analyses. The compliance is the default option in ANSYS when optimizing with a static stress analysis as the base. The formulation of the compliance objective function is given in Equation 6.1, where the function is transformed from a global formulation to a discretized formulation, (Perez [2012]).

$$c(\eta) = U^T K U = \sum_{i=1}^{N} u_i^T k_i u_i = \sum_{i=1}^{N} \eta_i u_i^T k_l u_i \tag{6.1}$$

Where U and K are the global displacement vector and global stiffness matrix obtained from the equilibrium of the FE-analysis. u_i and k_i are the element displacement vector and element stiffness matrix of the i-th element. Finally k_l is the stiffness matrix of an element with a pseudo density (η) of 1. An advantage of this formulation is that the stiffness is represented in the global equation of the FEM, which leads to a more convex problem for the optimization solver. A more convex problems generally leads to faster convergence, and a better chance for reaching the global optimum and not a local one.

6.5.3 Constraints

A wide range of constraints are available in ANSYS, however these constraints are limited based on modeling choices such as element choice and optimization method, (ANSYS [2019b]). In the general topology optimization problem, concerning a compliance objective function, there are three constraints present, which are the following:

$$0 < \eta_\mathrm{i} \leq 1 \tag{6.2}$$

which ensures the pseudo density takes on physical values.

$$KU = F \tag{6.3}$$

which ensures that the structure fulfills the global equilibrium equation.

$$m(\eta) \leq m_{req} \quad \text{or} \quad V(\eta) \leq V_{req} \tag{6.4}$$

where m is the mass of the structure, m_{req} is the required mass, V is the volume of the structure and V_{req} is the required volume. In ANSYS m_{req} and V_{req} are by default set as a percentage of the original mass or volume. The constraint ensure the mass or volume of the structure is reduced with the desired amount. Some other possible constraints are:

- Maximum displacement of a body or a node.
- Manufacturing constraint, limiting the minimum member size.
- Maximum global von-Mises stress.

6.5.4 Topology Optimization Methods

There are three available topology-optimization solution methods in ANSYS; Density based optimization, lattice optimization and level set based optimization. Some of the theory behind the density based optimization and the level set based optimization is presented in this subsection. The lattice optimization algorithm is not detailed, because it is aimed at additive manufacturing, and it is not the intention to limit the production method to additive manufacturing.

Density Based Optimization

In short this method performs the optimization based on the density of each element of

the model. This optimization employes the SIMP method which stands for "Solid Isotropic Material with Penalization". The method uses the pseudo densities (η_i) of each element as design variables. For this method, the pseudo density is defined as:

$$\eta_i = \frac{\rho_i}{\rho_0} \tag{6.5}$$

Where ρ_i is the density of the i-th element and ρ_0 is the density of the base material. The material properties of each element are then set to be dependent on the pseudo density of the element. This affects the objective function and the densities are altered in an iterative manner until convergence is reached. The solution convergence criteria is detailed in subsection 6.5.5. However as the goal is to determine whether there should be material in an element or not, the pseudo density is penalized by raising it to a power p. The default option in ANSYS is $p = 3$. As an example of the method, the Young's modulus E_i of the elements in the model then becomes:

$$E_i = \eta_i^p E_0 \tag{6.6}$$

Where E_0 is the material Young's modulus and E_i is the current modulus used in the optimization. As a result should the final design consist primarily of elements with a pseudo density of about 1 or about 0, i.e elements with or without material, Jain et al. [2015].

Level set based Optimization

The level set method uses a level set function to describe the boundary of the part within the optimization domain. The level set function is positive within the boundary, zero on the boundary and negative outside the boundary of the part. When applied to a discretized structure the level set function must satisfy the following equation.

$$\phi(p_i) = \begin{cases} > 0 & \eta_i = 1 \\ < 0 & \eta i = 0 \end{cases} \tag{6.7}$$

Where p_i is the center position of an element. The physical meaning of the equation is that the pseudo density is set to 1 inside the boundary of the part and 0 on the outside. This method modifies the pseudo density constraint to only allow for the values 0 and 1. The optimization is then performed by altering the described boundary by the use of an evolution equation given below:

$$\frac{\partial \phi}{\partial t} = v|\nabla \phi| - wg \tag{6.8}$$

In the above equation is t a fictitious time parameter, which indicates the direction of the evolution of the boundary. v is the normal velocity that determines the geometric velocity of the boundary, i.e how fast the boundary is changing. g determines the nucleation of new holes within the boundary and w is a positive number which regulates the influence of g. The evolution equation is a partial differential equation, which is solved numerically, Perez [2012]. More details on v and g is given in Appendix A. The advantage of using the level set method is that it generally results in smoother geometries ready for design validation.

6.5.5 Theoretical Background of the ANSYS Topology Optimization Analysis

Solver

The default solver of the topology optimization in ANSYS is the Sequential Convex Programming (SCP). SCP is an extension of the moving asymptotes method. This method approximates a solution for a topology optimization problem by solving a sequence of convex and separable subproblems. The subproblems are solved efficiently due to a special structure.

Solution Convergence Criteria

The analysis is considered converged when the solution reaches a stationary point where all constraints are satisfied. The convergence criteria when one constraint is applied is shown below.

$$\|\nabla L(\rho, \mu)\| = \epsilon \tag{6.9}$$

Where ϵ is the desired tolerance. This tolerance is user defined, but has a default value of 0.1%, and $L(\rho, \mu)$ is the Lagrange function which is defined as:

$$L(\rho, v) = f(\rho) - \mu c(\rho) \tag{6.10}$$

Where f is the objective function, and μ is the Lagrange multiplier which corresponds to the constraint c. However it can require a lot of iterations to reach the stationary point within the desired tolerance. Therefore ANSYS uses a relaxed convergence criterion, which states that the optimization stops when the following equation is true for three successive iterations.

$$\left| \frac{f(\rho_i) - f(\rho_{i-1})}{f(\rho_i)} \right| \leq \epsilon \tag{6.11}$$

Where ρ_i is the vector of pseudo densities of the i-th iteration. The above equation then states that if the pseudo densities are unchanged for three iterations in a row, the model is considered converged, (ANSYS [2019b]).

6.5.6 Topology Optimization of the Hip Outer Frame

There are two main observations from the static analysis, described in Section 6.4, that are used to guide the topology optimization of the hip outer frame. The first observation is that the main stress concentration is located on the disc containing the pins. The stress state here is advanced, and therefore is this region excluded from optimization. The second observation is that the stress level in the outer frame is generally low, and therefore it was decided to focus on this part of the geometry. The setup and results of the topology optimization is detailed in the following paragraphs.

Defining Optimization Region

The topology optimization algorithm in ANSYS only assesses whether or not to remove from the optimization region. The topology optimization algorithm can only remove material, and

is not able to add any material. The optimization region is therefore set bulkier than what the final design is expected to be. A significant limitation of the optimization is that the spring bracket and cuff still has to be attached to the structure. Hence the regions in the immediate vicinity of the mounting points are excluded from the optimization region. The optimization region is illustrated in blue in Figure 6.12, with the excluded regions in red. The optimized geometry is shown below in the same figure. The background for the optimization and the evaluation of results are discussed in more detail in the proceeding paragraphs.

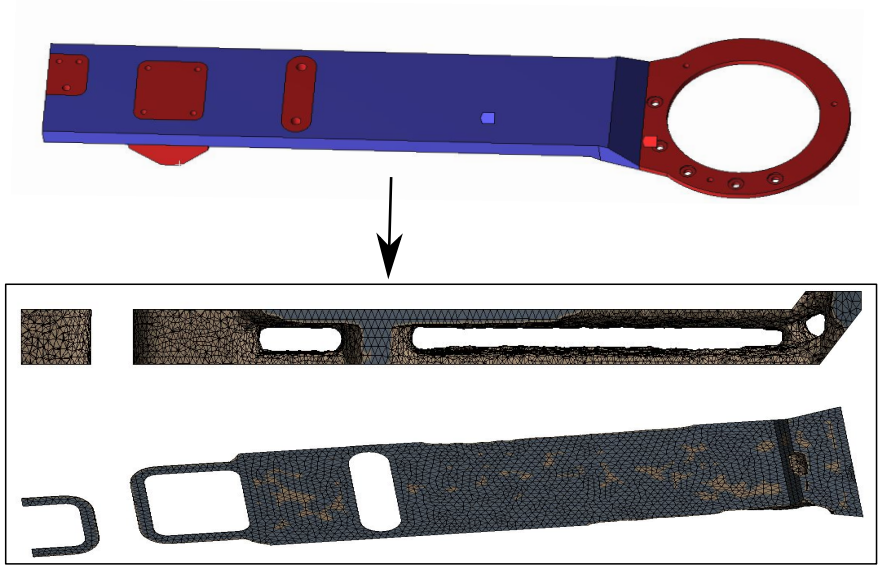

Figure 6.12: Optimization region, shown on the top figure in blue and exclusion region shown in red. The two bottom figures displays the resulting optimized geometry.

Setup of Static Analysis

The static analysis is set up with the same geometry, elements, loads and boundary conditions as load case 1, from Section 6.4. However the strategy for meshing of the model is rather different, as the goal is to have the mesh uniform in size and as fine as possible within the optimization region. A significant limitation to a fine mesh is the computational time, since a topology optimization is computationally expensive. It's therefore decided to limit the number of nodes to less than 250000, which also is the limit of the available ANSYS license. Design case 1 is chosen because it has forces acting on the limb that are not aligned with the longitudinal direction of the limb, and is therefore expected to give a better understanding of where material is needed to withstand the reaction forces from the human.

Objective Function:

The objective function is chosen as minimizing the compliance, i.e maximizing the stiffness. This objective function allows for a more robust optimization compared to for instance minimizing the stress. The robustness comes from the stiffness being a global variable in the static analysis and therefore yield a more convex problem. Minimizing the stress would be dependent on the derivative of a global values and therefore yield a less convex problem and increase the chances of ending in a local optimum instead of a global one.

Set Response Constraint:
This constraint determines how much of the original mass is kept. The default option in ANSYS is set to 50%, and it was decided to keep this constraint. This limitation is set because the optimization region is not very bulky and it was assumed that the algorithm could remove a limited amount of material without sacrificing the stiffness of the structure. An additional reason is the computational cost. The computational effort is often lowered when the constraints are looser because it generally requires less iterations to converge.

Choosing Optimization Method:
The level set based optimization method is chosen. This method is chosen because it generally results in smoother surfaces, and a part that is closer to being manufacturable by conventional machining. Therefore this method is more suited for our purpose as it is not desired to limit the production method to metal 3D-printing.

6.5.7 Topology Optimization Results

The topology optimization is carried out over two trials, where the results are presented in Figure 6.12 and Figure 6.14 for the first and second trial, respectively. The gray elements represent material that is evaluated to be kept by the algorithm, i.e the material is vital for the stiffness of the structure, or included in the exclusion region. The beige elements represents material that is less vital for the stiffness.

Evaluation of the First Optimization Trial
The first optimization trial was performed with the optimization region in Figure 6.12 and resulted in the geometry presented in the same figure. To verify that the algorithm removes material as intended, the strain energy density of the optimization region was examined, and is presented in Figure 6.13. From the figure is it observed that the material in the middle thickness of the plate has a stress energy density of about 0, meaning it does not contribute to the stiffness of the model. This indicates that the algorithm removes material as intended. Now taking a closer look at the optimized geometry is it clear that it mainly removes material in the middle of the structure. This geometry is hard to manufacture, and it would also result in a thick structure, where the springs are mounted further from the human leg. Therefore it was decided to perform another optimization with an an alternative optimization region.

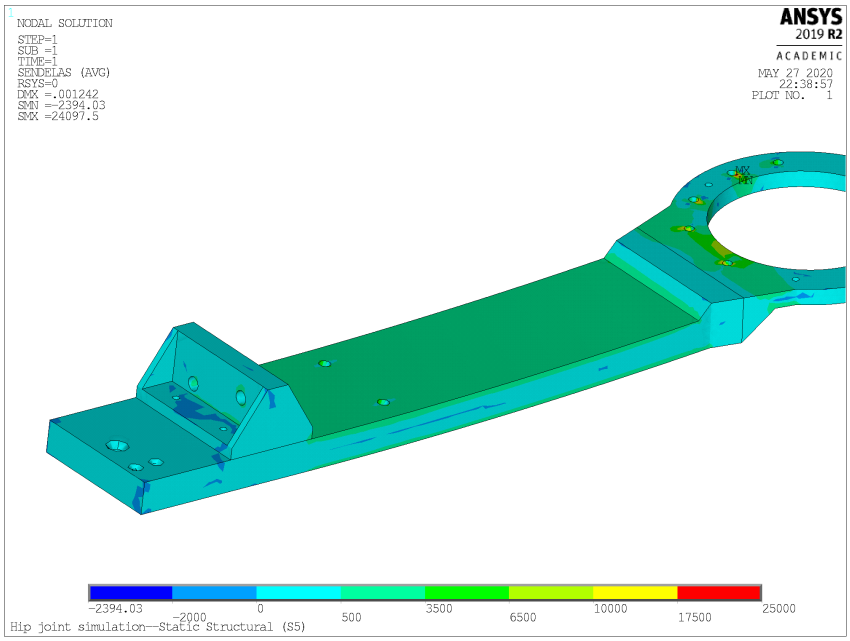

Figure 6.13: Strain energy density of the first optimization trial region.

Evaluation of the Second Optimization Trial

The new optimization region can be seen in Figure 6.14 along with the resulting geometry from optimization. The new region is based on the observation that a certain thickness of the part is necessary to obtain the desired stiffness, and the desire to mount the springs close to the leg. The side walls have a height of 20mm and the center region has a height of 5mm. The strain energy density of the optimization region is investigated and it is observed that the algorithm removes material where the density is lowest, as is expected. There are two main observations from the new optimized geometry that are used to guide the post processing and generation of a final design. The first observation is that most of the material of the base is removed, except for the exclusion ares. The second observation is that the material in the middle of the side supports is considered less vital for the stiffness.

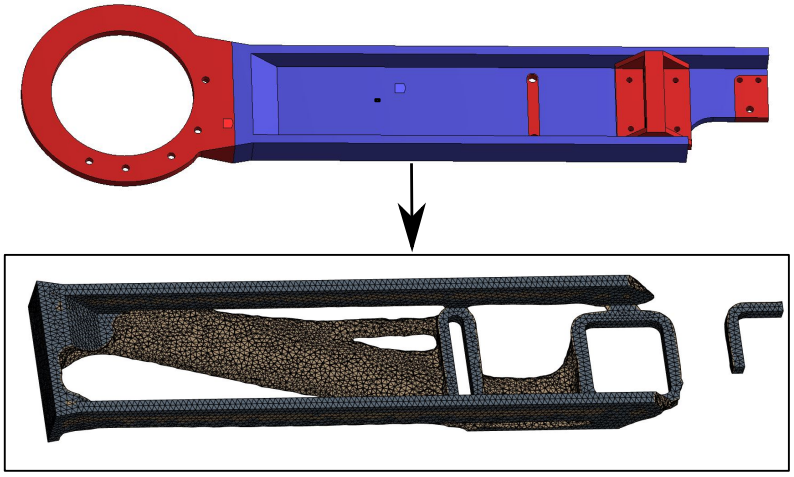

Figure 6.14: Optimization region, shown on the top figure in blue and exclusion region shown in red. The two bottom figures displays the resulting optimized geometry.

6.5.8 Post Processing of Topology Optimization in the Hip Joint

The post processing is focused on creating a lightweight design that is manufacturable within conventional machining. A symmetrical design is desired, since the design will experience forces from several directions during operation. The proposed design is therefore not only based on the optimization results of load case 1. The post processing was done as an iterative process, with several designs considered before settling on a final one. The weight and the maximum deformation of the different iterations of the part, subjected to case 1, is shown in Table 6.3. The stress is not highlighted here because the observed values where around $100MPa$, which is far enough below the yield strength of the material to make it an irrelevant failure criteria. Since the stiffness of the design is the main concern is the strain energy density along with the stress distribution used as guidance for adding and removing material.

Iteration	Weight [g]	Max Deformation [mm]
1	390	1.49
2	341	2.5
3	360	1.5
4	332	1.7
5	344	1.42
6	369	1.28
7	380	1.27
8	393	1.12
9	418	1.11
10	371	1.08

Table 6.3: Design iterations for the thigh limb.

The final geometry of the part is displayed in Figure 6.15. This part has a total mass of $371g$, which includes the bracket, since it's been integrated into the frame. It can be concluded that the optimization process resulted in a weight reduction of 58%, and a smaller max deformation, compared to the initial design. Design dimensions can be found in Appendix C.

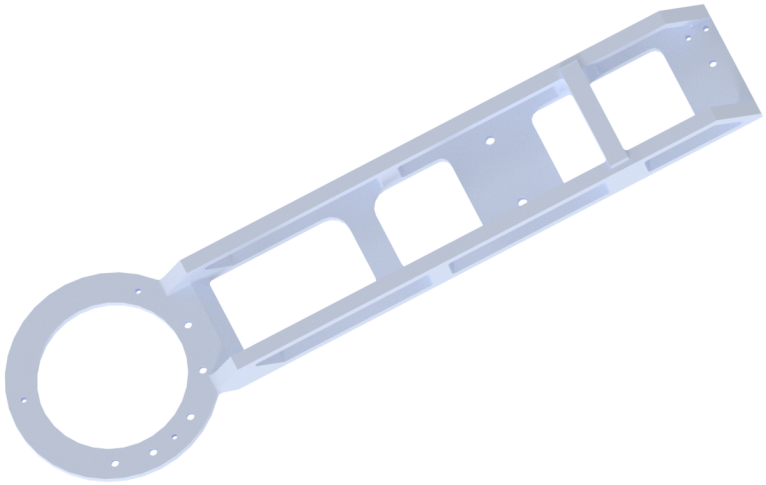

Figure 6.15: CAD model of the final design of the thigh limb.

6.5.9 Structural Integrity of the New Design

The design was guided by the simulations based on load case 1. To ensure that the design can endure all critical loads during operation has a mesh convergence study been carried out for both load cases. Since the design was guided by the simulations of load case 1, is load case 2 presented here for validation. The stress distribution and deformation due to load case 1 can be found in Appendix ... The convergence study was this time conducted by a nonlinear static analysis, to ensure that the deformation is not limited by the small deformation assumption.

The convergence study was carried out with both the maximum stress and maximum deformation as criteria. The deformation is assessed because it was observed to be the limiting factor of the part, and the stress is assessed because it often converges slower. The two convergence plots are shown in Figures 6.16 and 6.17, the model is considered converged at about 150000 nodes with respect to the deformations, with a maximum value of 1.154mm. The stress also converges at about 150000 nodes with a maximum value of 110MPa.

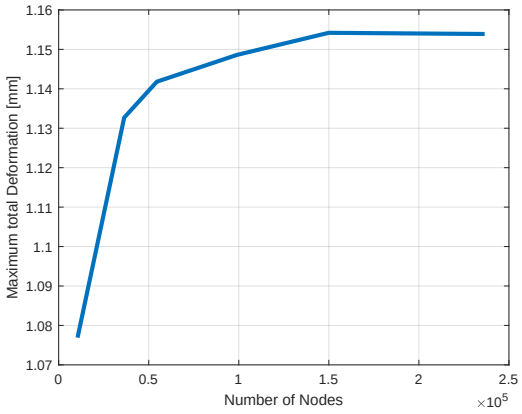

Figure 6.16: Mesh convergence study of the total deformation.

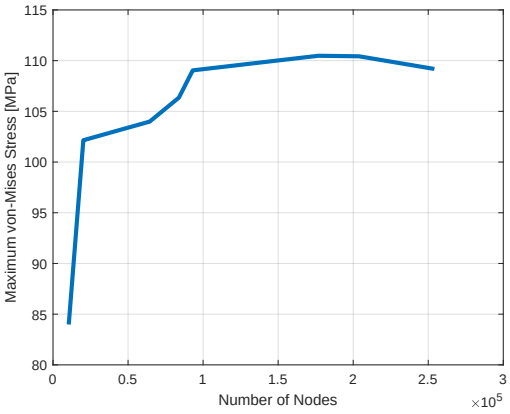

Figure 6.17: Mesh convergence study of the maximum von-Mises stress.

The total deformation of the final design, with a converged mesh, is shown in Figure 6.18. The deformation can be seen to be maximum 1.154mm, which is within the failure criteria.

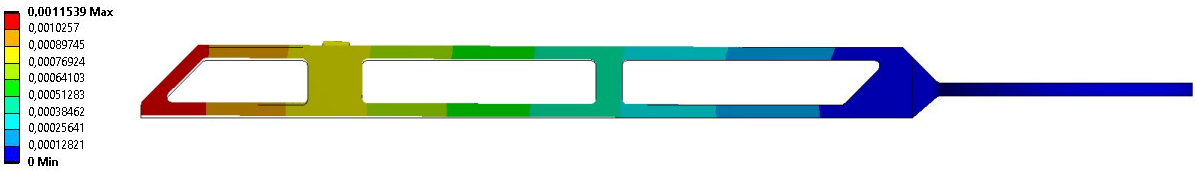

Figure 6.18: Maximum deformation of the final design subjected to load case 2. The color bar is given with the unit meter.

The stress distribution of the final design is shown in Figure 6.19. It is observed that the general stress level of the new design is generally higher than in the initial design. The maximum stress is still well below yield, and the part has a safety factor of about five.

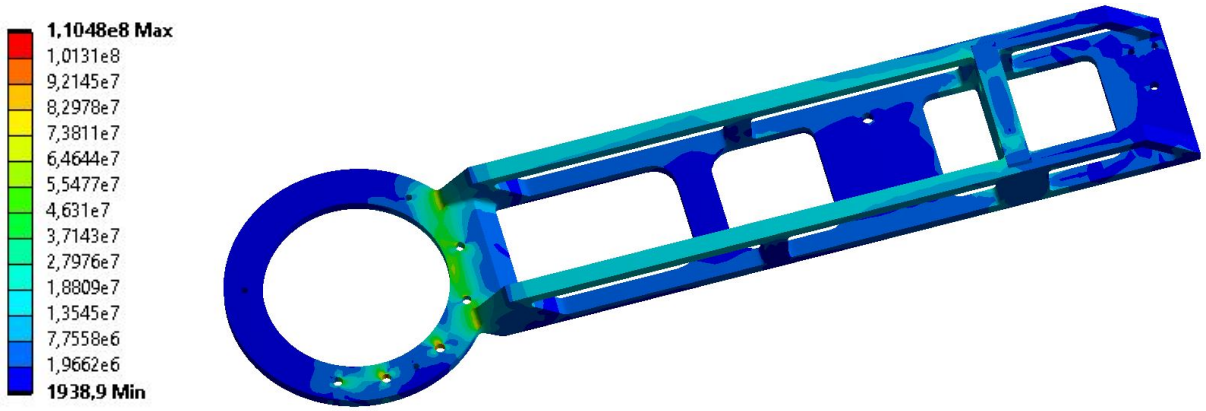

Figure 6.19: Stress distribution of the final design subjected to load case 1. The color bar is given with the unit Pascals [Pa].

6.5.10 Topology Optimization of the Knee Outer Frame

The topology optimization of the knee outer frame follows the same procedure as the one for the outer frame in the hip. The most significant difference between the two is the optimization region. The initial optimization region is based on the results from the hip outer frame, but an additional exclusion region is added in the bottom of the part. This region is to ensure that there is room to mount a slider connected to the springs. The geometry marked in blue in Figure 6.20 is the optimization region and the geometry marked red is the exclusion region.

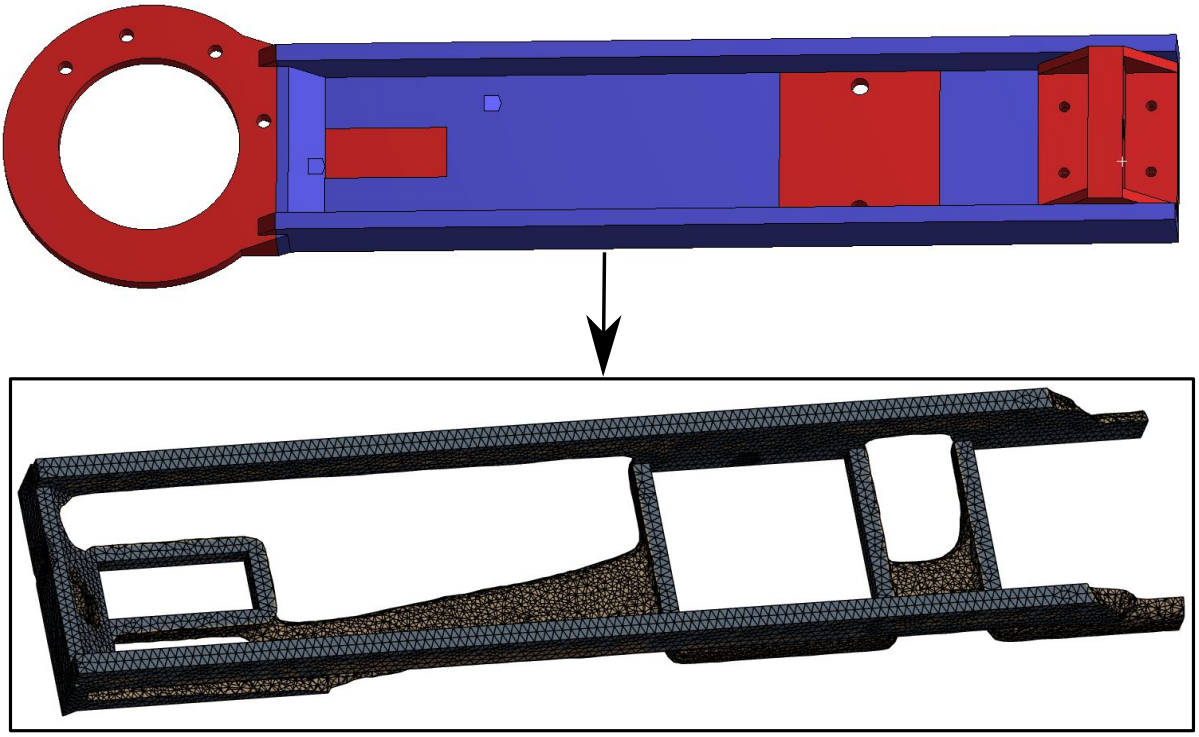

Figure 6.20: Optimization region, shown on the top figure in blue and exclusion region shown in red. The two bottom figures displays the resulting optimized geometry.

6.5.11 Post Processing of Topology Optimization in the Knee Joint

The post processing of the knee joint follows the same idea as the hip joint, where the design is subjected to load case 1 and the topology, stress and strain energy density results guides the design process. Inspiration to the design have also been drawn from the final hip exoskeleton design, which leads to the design shown in Figure 6.21, in only 3 design iterations. The weight of the design was reduced from $465g$ to $233g$, an approximate 49% reduction.

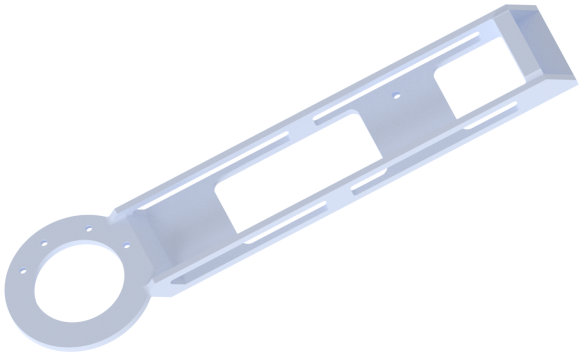

Figure 6.21: CAD model of the final design of the calf limb.

Structural Integrity of the New Design

As mentioned was the frame subjected to load case 1 to obtain the final design. From load case 1 the maximum deformation was found to be $0.57mm$, and the distribution was similar to hip frame (Figure 6.18). The maximum stress observed for case 1 is $66MPa$, and the stress distribution is shown in Figure 6.22. The structural integrity due to load case 2 was also seen to be safe within the requirements. Details can be found in Appendix ....

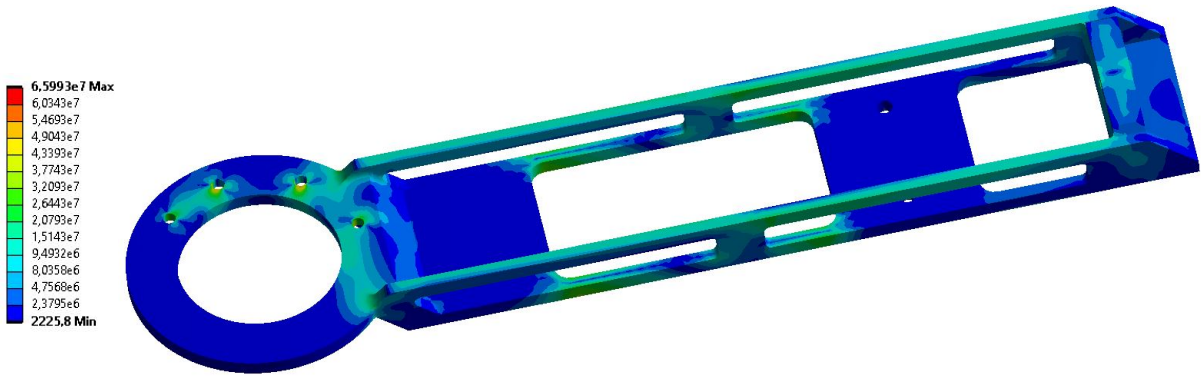

Figure 6.22: Stress distribution of the calf limb resulting from load case 1. The unit of the color bar is Pascals (Pa)

6.5.12 Evaluation of Final Geometry

A stiffness optimized geometry is recognized by having uniform strain energy density within the given constraints. The strain energy density of the final hip frame subjected to load case 1 and 2 is presented in the Figure 6.23. From case 2 is it observed that the strain energy density is rather uniform in the top of the side walls, which indicates an effective use of material. Areas with close to zero strain energy is typically seen to be the constrained areas, required to have material. The attachment point for the auxiliary link has extra support applied, since the loads experienced during operation are unknown. In general is an effective use of material seen in the new design, but the blue areas also indicate that more material could be removed for future iterations. The final geometry of the knee frame is similar to the one for the hip, and mainly the same behaviour is observed. It is therefore not presented, but effective use of material is also observed for the knee geometry.

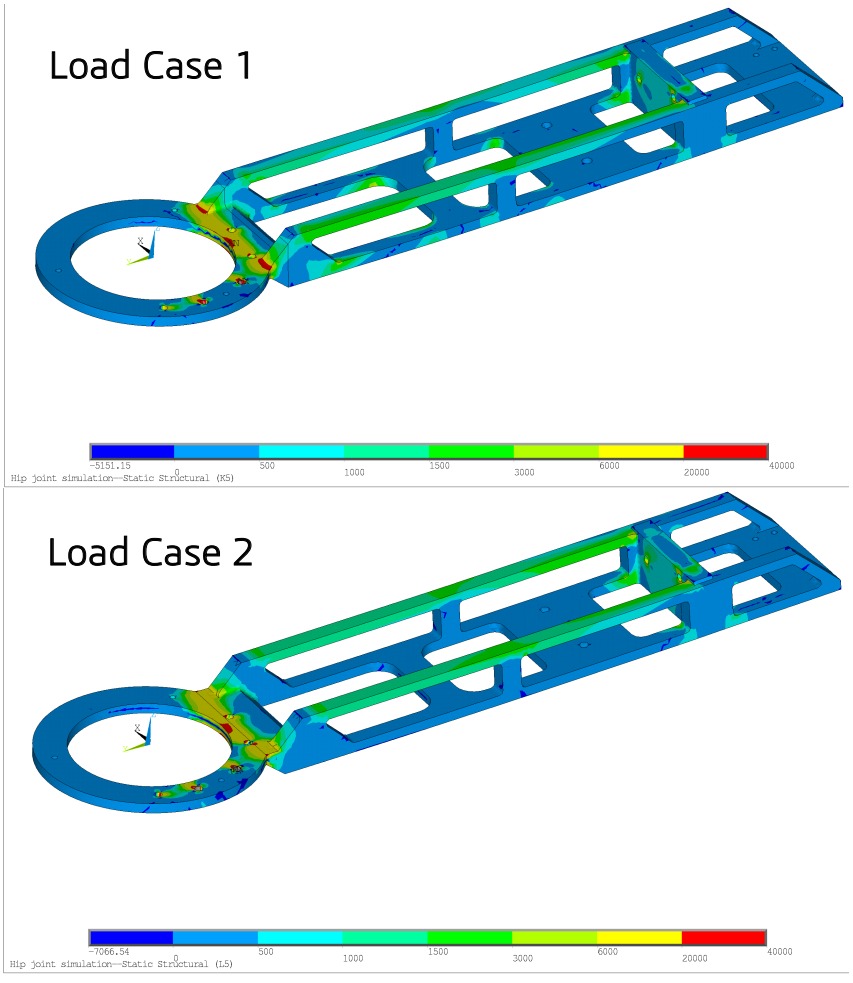

Figure 6.23: Strain energy density in hip frame.

As a conclusion is it observed that the topology optimization has resulted in a hip and knee frame which is about half the weight of the initial designs. Additionally displays the frames less deformation and allows for a more compact overall limb design.

6.6 Final Design

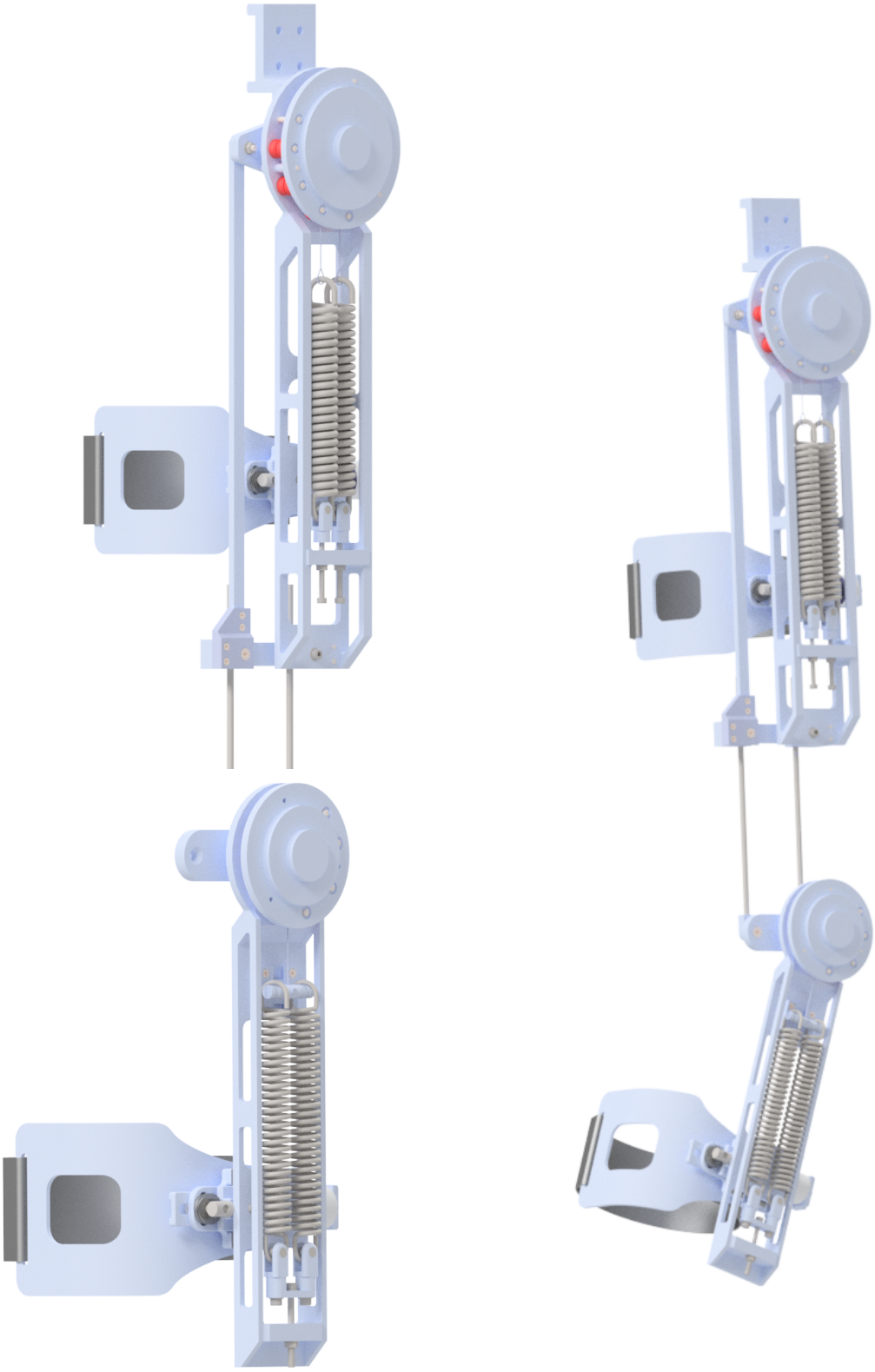

Figure 6.24: Presentation of the final design.

7 | Performance Simulation

After validating the structural integrity is the next step to evaluate the performance of the exoskeleton joint under realistic circumstances. The optimal method of investigation would be to create a physical prototype and conduct experimental testing. This process can however be time consuming and cost draining. It is of great benefit if the response of a virtual prototype could be analyzed beforehand, and in turn guide the design process. To accomplish this will the initial CAD be imported to a multi-body dynamics software where its response to human walking conditions will be simulated.

7.1 Simscape Multibody and Formulation of Model

The chosen software for simulation is Simscape Multi-body, a MathWorks product used in connection with Matlab. This is a simulation environment in which you can directly create geometrical solids or import 3D CAD models from softwares such as Solidworks. Once imported, the model can be seen as a block diagram, where blocks have been utilized for representing bodies, joints, constraints, pulleys etc. The CAD model is imported to Matlab by converting it to an XML file and a set of STEP files for visualization. Once imported are two files created; a SLX file contain the block diagram mentioned, and a M data file which contains the relative positions and orientations of each part. The accurate mass and moment of inertia of each part are also found in this file. The procedure is illustrated in Figure 7.1.

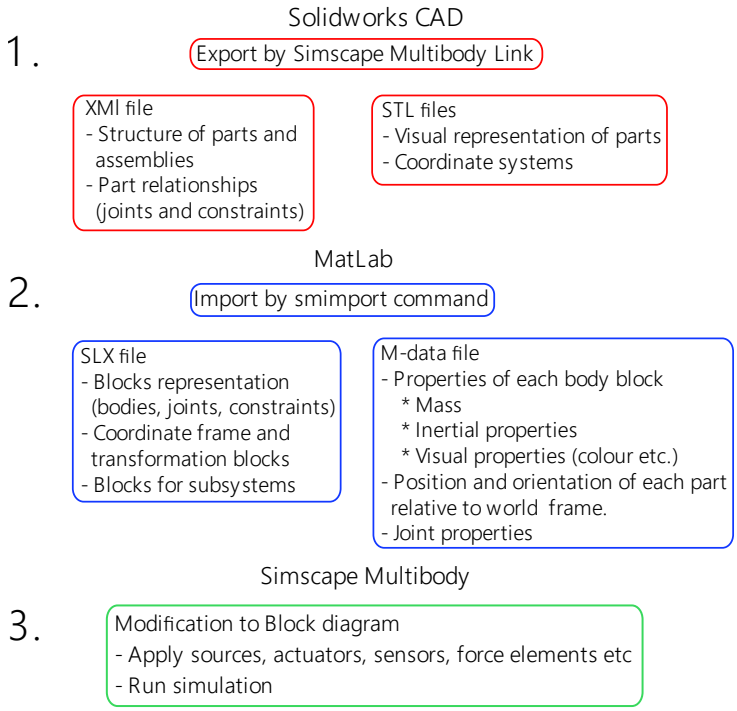

Figure 7.1: Illustration of the set-up process of the simscape model.

Once imported is the block diagram updated by applying sources, actuators, sensors, force elements etc. from the Simscape lock library. Simscape Multi-body formulates and solves the equations of motion for the complete mechanical system. So unlike what has been done in Chapter 3, is there no need for formulating these equations. The use of accurate mass center locations, and ideal mass and inertia properties makes this a valuable tool for evaluating the performance of the design without developing a physical prototype. More information in regard to how Simscape Multibody formulates and solves the equations of motion can be found in Appendix E.

7.2 Modelling Approach

This section will serve as a description of the modelling assumptions taken and procedure for formulating the dynamic multi-body model. The modelling of the exoskeleton hip and knee joints will be described first. Since the two joints are similar in design, will a general procedure be described, and joint specific configurations are evaluated when appropriate.

The blocks used to reconstruct the CAD assembly are extracted from the Simscape Multi-body library, so the relationships specified in Solidworks must be able to translate to blocks found in this library. This implies that features such as mate combinations needs to be carefully edited before import to Simscape. This is due to the limited number of standard constraints that are supported. In addition is Solidworks unable to portray the deformative characteristics of the spring and cable. Specific modelling procedures will therefore have to be conducted in the Simscape Multi-body environment. Figure 7.2 aims to illustrate the simplified modelling behind the Simscape model and will be referred to in the following sections.

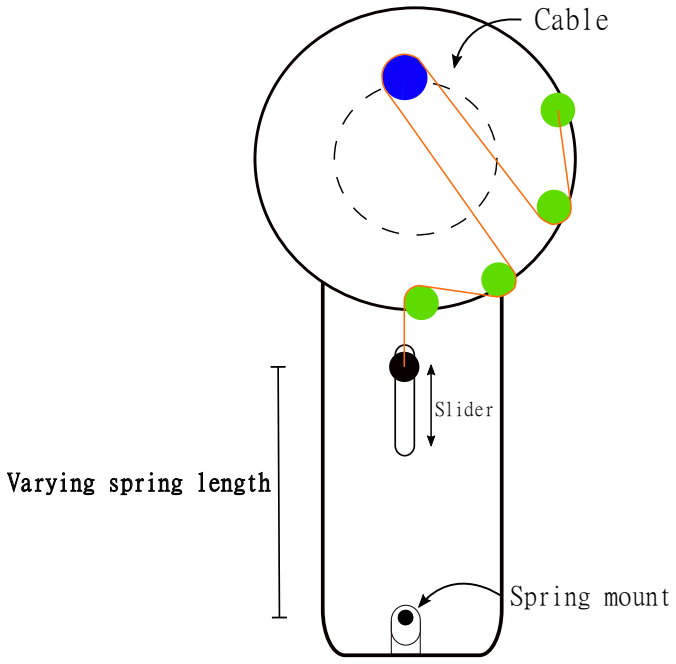

Figure 7.2: Illustration of the mechanics behind the knee Simscape model.

7.2.1 Modelling of Pulley System

Before import is the cable completely left out of the CAD model. Instead is the pulley-cable relationship captured by integrating blocks associated with the "Belts and Cables" section in the Simscape library. Each pulley from the CAD have been associated with a revolute joint and are assigned a block representing a pulley. The pulley block represents an ideal pulley, massless and frictionless, where there is no slip between the pulley and the cable. The cable itself is considered massless and not extendable. As illustrated in Figure 7.2 are the cable connected to a rigid end and the other end to the slider. The length of the cable is computed by the initial placements of the pulleys and fixation points. A section from the knee joint block diagram is presented in Figure 7.3 for visualizing the block representation of the pulley system.

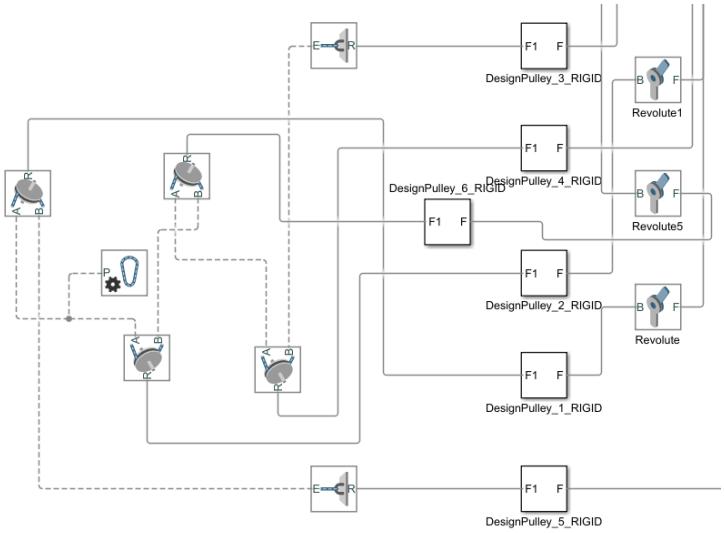

Figure 7.3: The pulley system as modelled in Simscape Multi-body.

7.2.2 Modelling of Springs

The geometry and mass properties of the springs are imported to the CAD from the developers website. The springs are therefore not able to issue spring characteristics in any way, and hence must this also be modelled in Simscape. The springs are included as part of the main assembly, fixed to the links, and therefore serves no purpose other than obtaining realistic weight and inertial values of the total assembly. The spring behavior is simply modelled by a block in the Simscape library called "Spring and Damper Force". This block applies a linear damped force between the two frames of which it is connected. The force is generated by specifying the natural length, spring stiffness and damping coefficient of the springs. Similarly to real springs is the force attractive if the spring length exceeds the springs natural length. The spring length and hence force was allowed to vary throughout the gait, by connecting one end of the force block to the slider. As the cable is connected to the same slider and in-extensible, will the spring length vary as the pulley relationship varies. The physical springs utilized is designed to have a built-in pretension. This is not possible to specify in the "spring block". To

compensate for this extra force is the initial length increased a distance corresponding to the elongation necessary to produce this force.

As a simplification to the knee joint was only one block utilized for both springs, corresponding to the spring stiffness sum of the two springs. The spring was further modelled to act along the centerline between the two springs, see Figure 7.4. In the hip joint was one block utilized for each spring, since the springs acts at different levels. The spring blocks were placed to act in the same location as their realistic counterparts.

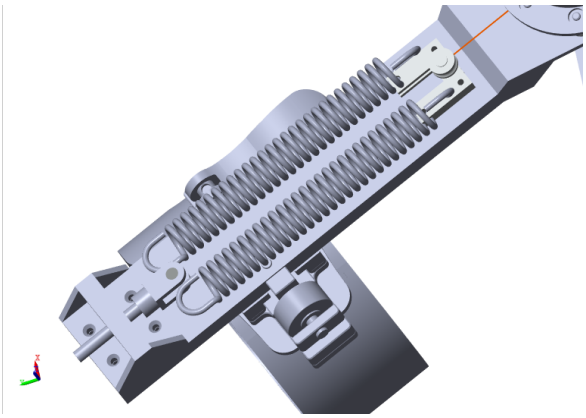

Figure 7.4: Illustration of the simplification to the springs in the knee joint.

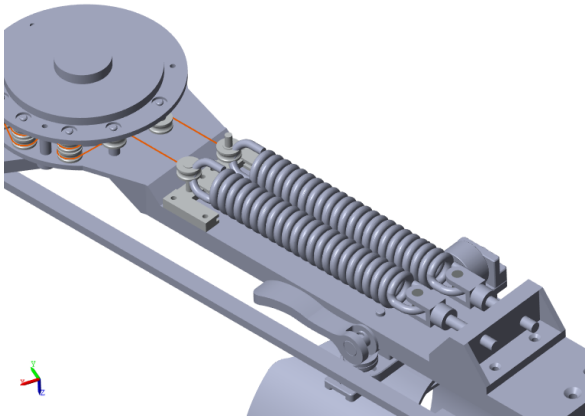

Figure 7.5: Illustration of the simplification to the sliders in the hip joint.

7.2.3 Modelling of Slider

When formulating the model is the initial position of the slider important, as the length of the cable is computed by the initial placements of the pulleys and fixation points. Only the function of the slider is deemed relevant for this simulation, so the slider has been given a simple geometry as seen in Figure 7.5, formulated as a prismatic joint in Simscape.

The slider has been simplified in the knee joint to only consider the attachment of one spring, in coherence with what's done with the springs in Section 7.2.2. This is illustrated in Figure 7.4. The hip joint doesn't utilize sliders in the real design, since the cables are directly applied to the springs. This is not possible to model in simscape, as the cable fixation points needs to be attached to a solid, not only a spring force block. The solution has been to apply sliders also for this joint. One slider is connected to each spring-pulley system, as visualized in Figure 7.5.

7.2.4 Modelling of the Human Leg

The geometry of the human limbs are acquired from an external source. The mass, location of the COM and inertia of the human limbs are based on the same calculation approach utilized for the simplified computational model presented in Chapter 3.

The model of the human is created entirely in solidworks and consists of the three bodies thigh,

calf and foot, and they are connected by revolute joints. The hip joint fix the thigh to a specific location in space.

By import to Simscape Multibody is a simple block diagram created, as seen in Figure 7.6. The revolute joints functioning as the hip and knee joint are actuated by specifying an input motion for each of the joints. The ankle is modelled fixed. The motion is characterized by the same relative angle input used for the calculation of the torque requirements in Chapter 3. The angle inputs are presented as A and B for the knee and hip joints, respectively, in Figure 7.6. A sensor is applied to the joints which writes the calculated torque values to a file in the directory. The design parameters are specified in Section 7.3.3.

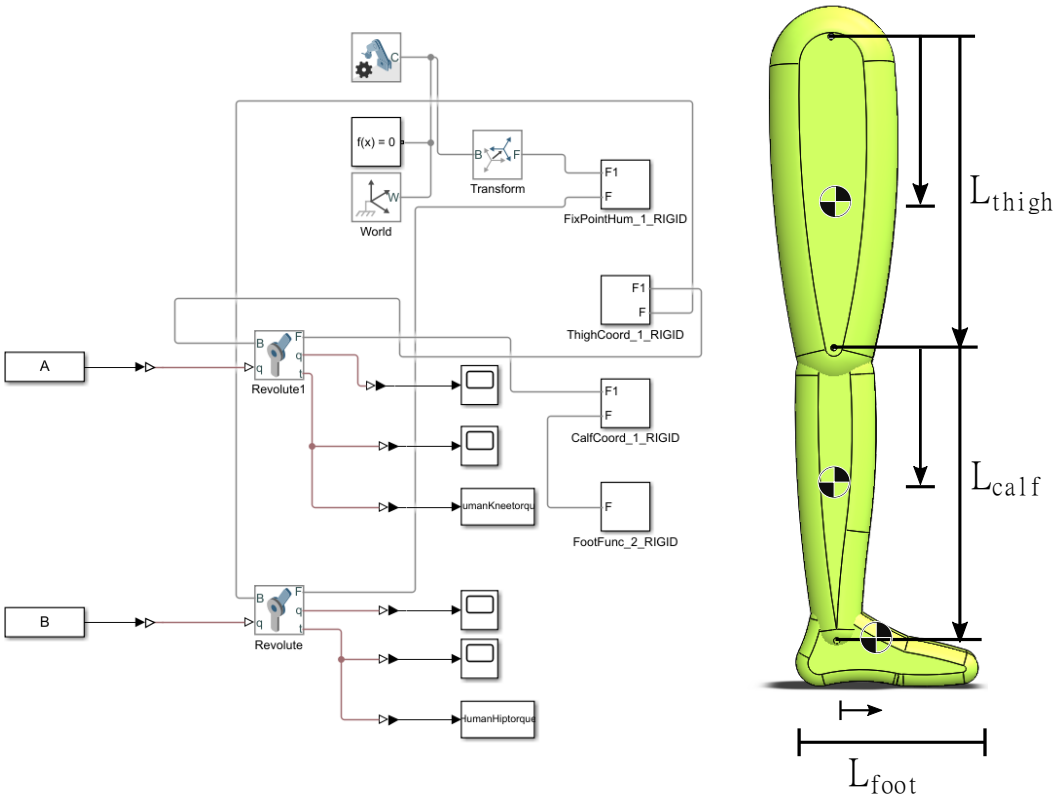

Figure 7.6: The complete block diagram and visual representation of the human model.

7.3 Simulation of the Individual Parts

Four individual Simscape Multi-body models have been developed for this project. These include the exoskeleton knee and hip, the human leg and a full assembly with the exoskeleton parts connected to the human. The simulation of the exoskeleton joints aim to investigate if the proposed joint configuration will produce similar torque profiles to what was evaluated in Chapter 4, when implemented in a real design. The simulations are conducted with a simple geometry of the exoskeleton, since this chapter mainly serves as a proof of concept.

The simulations are conducted in a similar manner for all models. The actuation is a position based input, which is acquired from a motion capture experiment of human walking. The duration of the gait is 2.39s, and the joints are actuated by hip and knee angle inputs. These are the same data sets that were utilized for the estimation of the design configuration in Chapter 4. The joints are also applied sensors, which outputs the actuated torque. More information on the blocks utilized for actuation and sensing of the joints can be found in Appendix E.2. By only simulating the exoskeleton should this reflect similar values to what was theoretically calculated in Chapter 4.

7.3.1 Simulation of the Knee Joint

The simulation of the exoskeleton knee joint was visualized in Simscape Multi-body as presented in Figure 7.7. The design parameters of the joint is presented in Table 7.1.

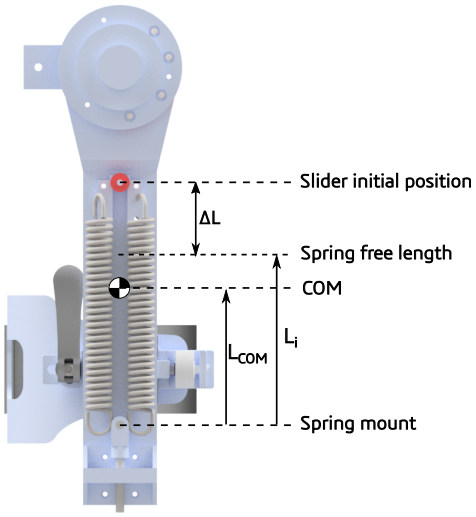

Figure 7.7: Illustration of design parameters utilized in knee joint simulation.

	Mass	L_{COM}	I_{zz}	k	L_i	ΔL
Unit	kg	mm	$kg * m^2$	$\frac{N}{mm}$	mm	mm
Value	1.19	93	0.0108	10.24	114	49

Table 7.1: Design parameters in the exoskeleton knee.

The sensed torque output from the joint is plotted against the calculated profile presented in Chapter 4.6.2, in order to investigate how well the concept translates to a realistic design implementation. The result is shown in Figure 7.8.

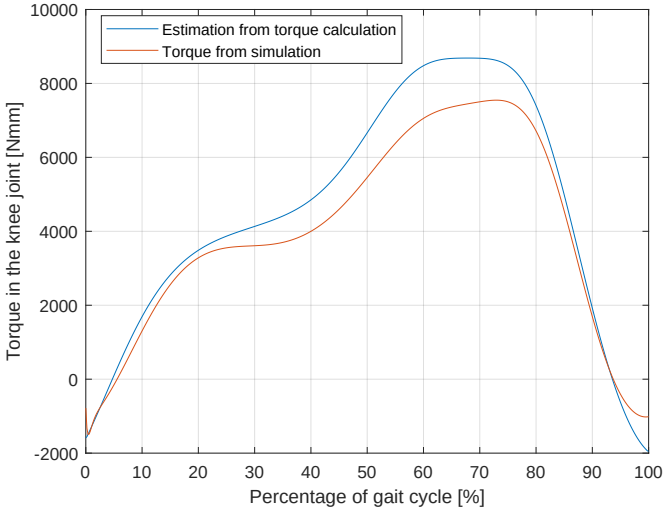

Figure 7.8: Knee profile from simulation, compared to the previously calculated torque profile.

From the figure it's clear that the torque produced by the exoskeleton knee joint follows almost exactly the same trend as was calculated beforehand. The difference is likely caused by the fact the simulation utilizes the characteristics of the physical spring and not its ideal values found from the optimization. The weight of the joint itself could be a contributing factor, in addition to simplifications done in the CAD modelling process.

7.3.2 Simulation of the Hip Exoskeleton Joint

The simulation of the exoskeleton was visualized in Simscape Multi-body as presented in Figure 7.9. The design parameters of the joint is presented in Table 7.2.

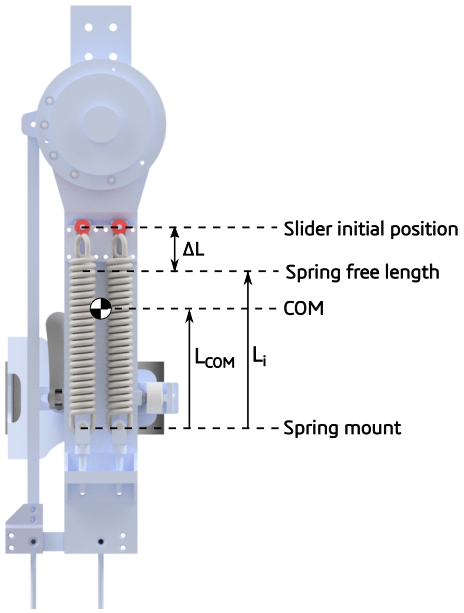

Figure 7.9: Illustration of design parameters utilized in hip joint simulation.

	Mass	L_{COM}	I_{zz}	k	L_i	ΔL
Unit	kg	mm	$kg * m^2$	$\frac{N}{mm}$	mm	mm
Value	2.03	152	0.0303	26.5 (x2)	138	24

Table 7.2: Design parameters in the exoskeleton knee.

The simulation of the hip joint resulted in the torque profile seen in Figure 7.10. The simulated profile is compared against the previously calculated hip profile in order investigate how well the concept have translated to the design implementation. From the figure it's clear that the design generates the expected behaviour. The slight difference from calculation is thought to be caused by the spring characteristics, weight and modelling simplifications in the same manner as with the knee joint.

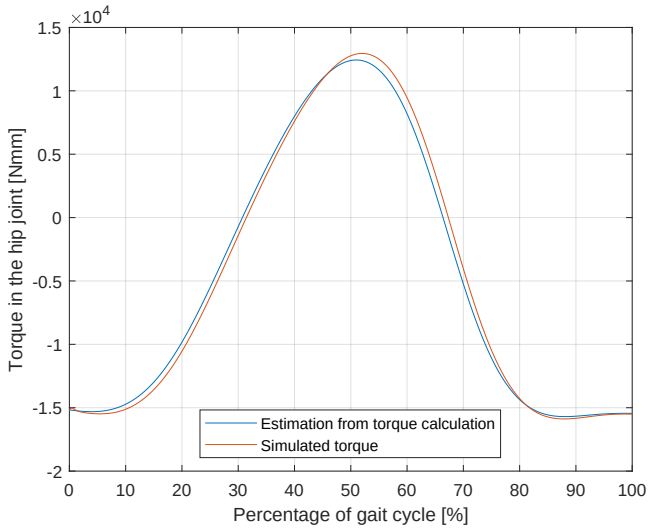

Figure 7.10: Hip profile from simulation, compared to the previously calculated torque profile.

7.3.3 Simulation of the Human Model

The simulation of the human model in Simscape multibody is visualized as presented in Figure 7.6. The design parameters of the human model is presented in Table 7.3.

	Unit	Thigh (human)	Calf (human)	Foot (human)
Mass	kg	10.5	4.75	1.43
Length	m	0.5	0.47	0.23
*COM	%	0.43	0.43	0.43
Inertia	kg*m2	0.1881	0.0831	0.0053

Table 7.3: Design parameters of the human leg. *COM is presented as % of total limb length.

Since the human leg simulation share the same design parameters and motion input as the simplified dynamic model, the two models presents almost identically the same torque profiles for both joints. The simulated profiles are presented later in Figure 7.12 and Figure 7.13.

7.4 Modelling and Simulation of an Exo-Human Model

A simulation of the human wearing the exoskeleton will be conducted, in order to assess the assistive performance. The full model is created in Solidworks, where the exoskeleton parts and human model are imported and constrained together. The central part of the exoskeleton hip is fixed to the ground and the rest of the assembly rotates with respect to the exoskeleton hip joint. Two small holes are drilled in the hip and knee joints of the human model, and these holes are aligned to fit the joints of the exoskeleton. The limbs are then aligned to the cuffs in order for the human to follow the motion of the exoskeleton. The exoskeleton joints are now constrained together by attaching the rods from the hip joint to the base of the knee joint. A screenshot of the model during simulation is presented in Figure 7.11.

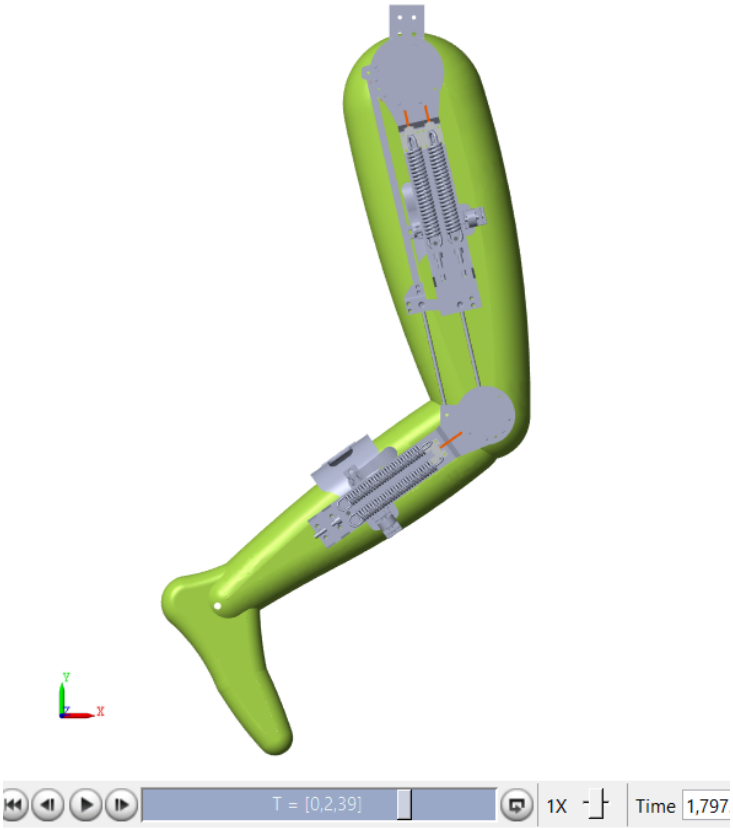

Figure 7.11: Screenshot taken of the full assembly during simulation.

The two exoskeleton joints are now actuated by the same procedure and angle input as done with the single exoskeleton joints. Since the exoskeleton is actuated are absolute angles utilized as input for both joints. The resulting balanced torque in each of the joints is compared against the torque profile from the human when not wearing the exoskeleton.

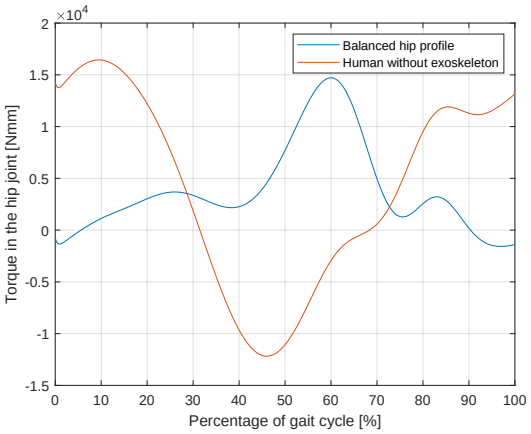

Figure 7.12: Balanced hip torque compared to an unassisted gait.

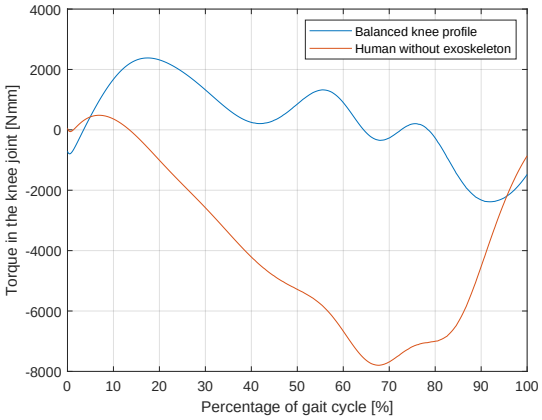

Figure 7.13: Balanced knee torque compared to an unassisted gait.

The overall trend of the two figures is a significant decrease of the required torque throughout the gait. By taking the average of the absolute torque values at each point during the gait, the hip joint sees a reduction of 53.5%, while the knee sees a reduction of 72% when wearing the exoskeleton.

7.5 Discussion on Simulation Results

In order to more clearly understand the behavior of the balanced torque profiles, has a line of investigations been conducted. An additional simulation of the full assembly was run without the spring force applied. In that way corresponds the output to the necessary torque for driving both the human and exoskeleton, which is the same as estimated in the simplified computational model. By comparing the output of the two models, can conclusions be drawn to the initial estimations of the torque requirements, and hence the utility of the simplified computational model.

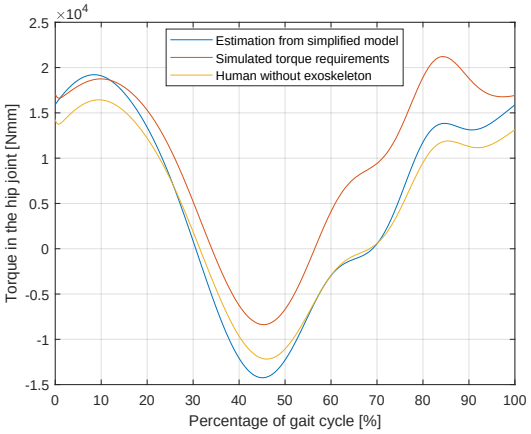

Figure 7.14: The torque requirements of the hip with and without the exoskeleton.

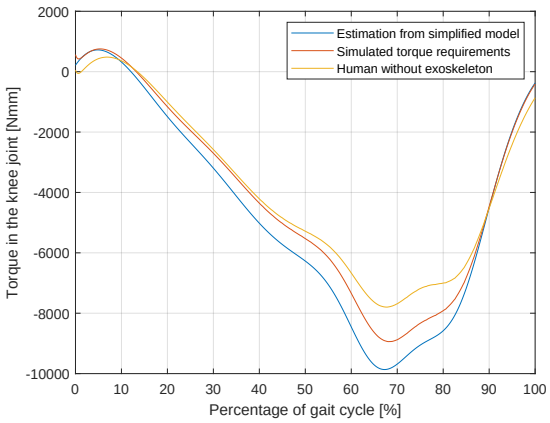

Figure 7.15: The torque requirements of the knee with and without the exoskeleton.

Figure 7.14 and 7.15 presents the torque requirements from the two models with and without the exoskeleton. The simulated hip torque of the human with exoskeleton (not actuated), can be seen to deviate from what was estimated by the simplified model. Even more interesting, the magnitude of the torque can be seen to be lower than the human without exoskeleton at around 35-56%. The difference from the simplified model is likely to come from the initial guess of mass, COM and MOI for the exoskeleton.

The profiles in the knee presents the expected behaviour of increasing magnitudes when the human is required to also carry the weight of the exoskeleton. In addition, it can be seen that the initial torque estimate present larger magnitudes than actually necessary.

From the above observation it's a clear difference between the estimated required torque and the more accurate simulated requirements. As presented in Section 7.3.1 and 7.3.2 is there also a difference in the generated torque from calculation and simulation. For these reasons is it necessary to compare the required torque and generated torque from the simulations to better explain the result of the balanced torque profiles. The simulated results are presented in Figure 7.16 and Figure 7.17, for the hip and knee joint respectively. The simulated requirements have been flipped for a simpler interpretation of the results.

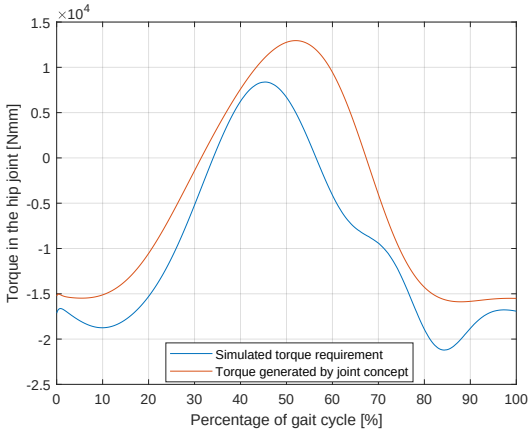

Figure 7.16: The generated torque vs. the required torque during one gait cycle in the hip joint.

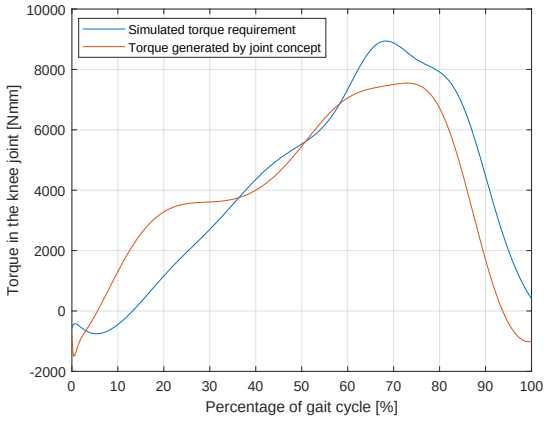

Figure 7.17: The generated torque vs. the required torque during one gait cycle in the knee joint.

The reason for the high peak seen in Figure 7.12 becomes obvious when comparing the two torque profiles in Figure 7.16 at 60% of the gait. Since the torque requirements in the hip joint turned out to be much lower than initially estimated is there a large residual between the two profiles in this region. The resulting balanced torque is far from optimal, and options for improving the performance with the current design are discussed in Section 7.6.

The simulated results in Figure 7.17 have seen a reduction in both the required torque and the generated torque from the concept in the knee joint. The result is a similar relationship between the two profiles compared to Figure 4.7 in Section 4.6, but with smaller peak magnitudes.

7.6 Influence of Spring Characteristics

Simulation of the full model with the initially stated design parameters presented an unfavorable peak in the hip joint torque plot. This was later discovered to be caused by a wrongful estimation of the torque requirements. Although the geometrical design parameters are set with this design, it's still possible to change the output torque by altering the spring characteristics. This is most easily achieved by adjusting the pretension of the spring, which is easily done by applying an adjustment wheel to the design. The second possibility would be to alter the spring stiffness, which in physical terms means to exchange the spring altogether.

In order to investigate the influence of pretension on the current design, is the same simulation carried out for different levels of pretension. The pretension is set to vary from 70-120% of the currently used pretension. The limit is set to 120% in order to not exceed the maximum allowed tension in the springs. The spring stiffness and all other geometrical parameters have remained constant in these simulations. The result of altering the pretension can be seen in Figure 7.18 and Figure 7.19 for the hip and knee joint respectively.

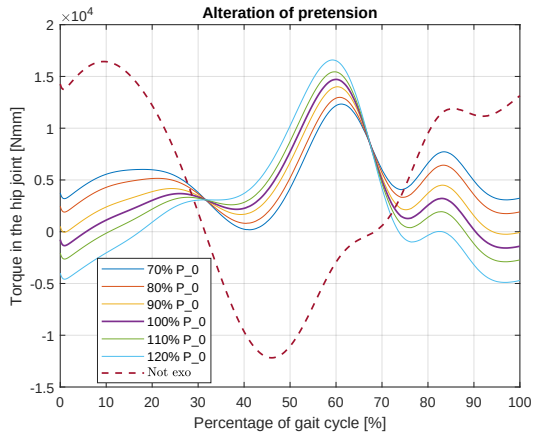

Figure 7.18: Torque performance in hip due to altering of pretension.

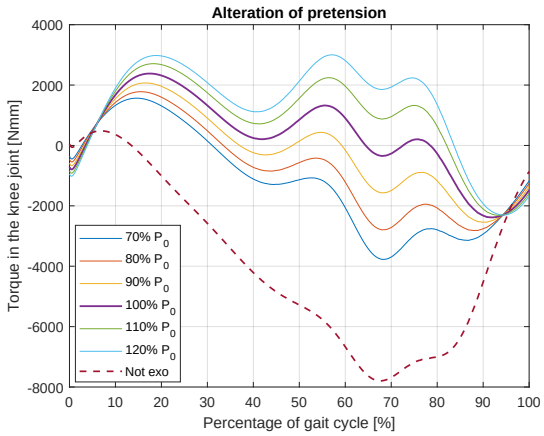

Figure 7.19: Torque performance in knee due to altering of pretension.

The hip joint originally saw a decrease of 53.5% in average torque with the current pretension. When only applying 90% ,the tension is this reduced to 52.3%. When only applying 80%, the average torque reduction drops to 45.7%. An increase of the tension by 110% will have the same effect and lead to a 52.5% reduction.

The knee joint originally saw a decrease of 72% in average torque with the current pretension. When only applying 90% of the pretension this is reduced to 71.5%. Decreasing the pretension further by 80% leads to a 64% decrease of average torque. An increase of 110% leads to a decrease of average torque to only 62%.

The results indicates that the average torque is lowest when the pretension is in its optimized value. The investigation also shows the ability of the design to obtain gravity balancing at different levels.

7.7 New Design Iteration for the Hip Joint

A new optimized configuration based on the simulated torque requirements is necessary for achieving more satisfying results in the hip joint. This is a time consuming and iterative process where the alterations to the design in turn will affect the simulated torque requirements as well. It has therefore been decided to investigate the influence of minor design alterations. The optimization algorithm previously used in Section 4.5 are again utilized by keeping most of the geometrical parameters fixed. The design parameters allowed to change are: the initial angle, spring stiffness and pretension. The result from the optimization can be seen in Figure 7.20.

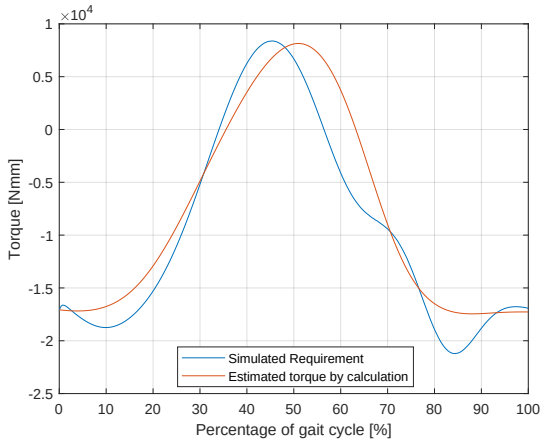

Optimized Configuration x2		
Parameter	Unit	Value
N	#	1
l_1	mm	30.0576
l_3	mm	46.0604
k	$\frac{N}{mm}$	25.14
F_0	N	617
R	mm	6.5
θ_0	rad	3.19

Figure 7.20: New optimized configuration based on the simulated requirements.

This configuration is similar to what is used in the current design, with the exception that the initial angle is increased from 3.09 rad to 3.19. Due to the similar spring characteristics has it been decided to only alter the initial angle in the current design and adjusting the pretension, while retaining the other design parameters. A complete exo-human simulation are then run with the new design. The new balanced torque curve in the hip is presented in Figure 7.21.

With this new design have the peak magnitude been reduced from 14 Nm to 9 Nm and the overall average torque reduction are increased from 53.5% to 65.7%.

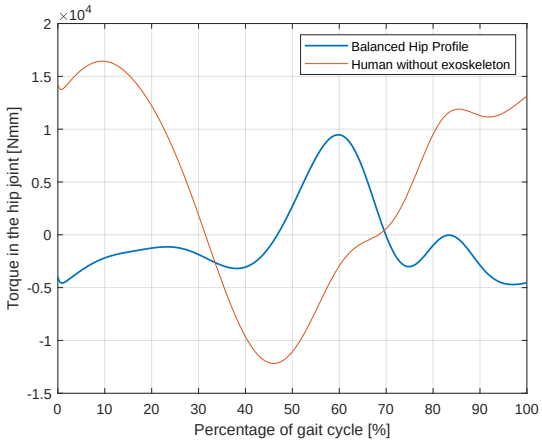

Figure 7.21: New design iteration.

8 Discussion and Conclusion

8.1 Discussion

The goal of this thesis was to propose a new method of passive actuation and implement this feature in a lower limb passive exoskeleton. Since the joint actuation is directly tied with the torque requirements of the limbs, it was decided to carry out a user specific approach. This has made the design optimized to a specific user in terms of actuation requirements and dimensions. Efforts have been made to generalize the design, by allowing for length adjustments and variable pretension. Experimental testing of multiple users is necessary in order to assess how the design performs on a general basis. The proposed design was in Chapter 7 seen to have a significant impact on the average joint torques when wearing the exoskeleton, with a reduction of about 66% in the hip and 72% in the knee. This shows great potential, but also represents the optimally balanced profiles of the user without altering the design.

The total weight of the exoskeleton was measured to be 2.8 kg. This is close to the max weight requirement, and is caused by the necessary spring tension force and size of the physical springs. This can be seen as a limitation to the design, as the torque generated from the design is dependent on the size of the pulley system and the tension force of the springs. If the exoskeleton outer frames are designed to withstand greater tension forces (i.e. by a stiffer material), the dimensions of the frame could be smaller. On the other hand, if the dimensions of the pulley system is increased, would the system require a smaller tension force. The last option is however in violation with the constraints set to the joint size. It is worth to mention that the torque requirements specified in this thesis is based on a test subject weighing 101 kg and a relatively fast gait (2.39s). The requirements are believed to be smaller for patients of lesser weight and slower gait, and as a result might smaller springs be utilized.

With the focus being on implementing the actuation system, less attention has been directed to components such as trunk attachment, cuffs and the auxiliary link etc. An additional material selection and structural analysis should be conducted with these parts, to ensure a safe and possibly lighter design.

Additionally, it's important to underline that this design only considers the loads due to the gravitational and inertial effects of the limbs during gait. Ground reaction forces and forces generated due to the passive elasticity of soft tissue and muscles are not accounted for.

Lastly, with respect to the dynamic modelling, it was observed some deviations between the calculated torque requirements and the later simulated profiles. This is believed to be rooted in the crude estimations of the simplified dynamic model. The model has still proven to be a valuable design tool, due to its ease of use and relatively accurate results. For utilization in the future should more attention be made to specify the initial design parameters.

8.2 Conclusion

This thesis has presented the design of a passive lower body exoskeleton, using novel compliant joints. The mechanism features compensation of the gravitational and inertial effects during walking, in the form of a novel pulley-configuration attached to springs. The full mechanism is contained within the frame of the exoskeleton links, and thereby unable to interact with environmental obstacles. The design can therefore be considered to fulfill the requirement of safety.

The torque requirements were used to formulate three critical load cases for each joint. The structural integrity of the design was evaluated by various simulations of the critical load cases. The deflection of outer frame was seen to be the main structural issue, leading to an initial bulky design. The topology of the frame was optimized with respect to stiffness and a mass constraint. The resulting frame designs where seen to withstand the critical load cases with a weight of 371g in the hip and 233g in the knee. This corresponds to a weight reduction of 58% and 49%, respectively, from the initial design.

The mechanism has been successfully validated by simulations in Simscape Multibody, where the human-exoskeleton performance also has been evaluated. Results showed a significant reduction in driving joint torques as a result of the assistance from the exoskeleton. Simulation of variations to the pretension also illustrated the designs ability to balance at different levels.

In addition, this thesis proposes an alternative approach to the typical engineering process by utilizing a simplified design tool for estimating the performance requirements of the exoskeleton design. The estimations from the simplified model was seen to deviate a little from the final simulation. More accurate initial guesses for the mass, inertia properties and COM is believed to help with this problem. The simplified model was improved to include the effects of ground reaction forces for future design cases. A refinement of the model is however necessary to accurately portray the double-support phases of the gait cycle.

8.3 Future Work

The thesis provides detailed simulations of the theoretical performance of the exoskeleton. The next step according to the engineering design process, presented in Section 2.6, is to experimentally validate these simulations.

Proof of Concept
The experimental validation should begin with manufacturing of the exoskeleton joints and then performing a static test, where the torque of each joint is obtained and compared to the simulated values.

Evaluation of the Metabolic Cost
While the balanced torque profiles in Section 7.4 presents a theoretical decrease in the necessary user assist during gait, this must be investigated under real conditions. Surface electromyography (sEMG) can be used to observe the reduction in metabolic cost of muscles during gait. This is typically done by placing the EMG electrodes on the skin directly above the muscles of interest. The change in metabolic cost can then be measured by comparing the recordings of the test user walking with and without the exoskeleton.

Lightweight Design
The exoskeleton design is considered too heavy in its current state, and it's believed that conducting a re-design process with focus on utilizing lightweight materials (e.g. composites) might improve the weight estimation of the current design.

Design of Sub-components
For the implementation of this concept in a real design, have several sub-components been proposed, but not evaluated in detail. This includes the auxiliary link (forming the parallel mechanism in the hip), the cuffs and pretension screws. Structural analysis and material evaluation of the sub-assemblies have to be carried out in order to ensure a safe and lightweight design.

Improvement of Computational Model
The computational model should be further refined in order to more accurately portray the performance requirements when including the influence of ground reaction forces. Future investigations could then assess how the compliant joint concept could be applied to more complex design scenarios.

Bibliography

ANSYS, 2019a. ANSYS. *ANSYS Mechanical APDL 2019 R2 - Theory Reference*. `https://ansyshelp.ansys.com/account/secured?returnurl=/Views/Secured/corp/v194/ans_thry/thy_el187.html`, 2019. Downloaded: 16-05-2020.

ANSYS, 1999. ANSYS. *ANSYS Theory Reference*. `http://research.me.udel.edu/~lwang/teaching/MEx81/ansys56manual.pdf`, 1999. Downloaded: 31.05.2020.

ANSYS, 2019b. ANSYS. *ANSYS Workbench 2019 R2 - User's Guide*. `https://ansyshelp.ansys.com/account/secured?returnurl=/Views/Secured/corp/v194/wb2_help/wb2h_topoptAN.html?q=topology%20optimization`, 2019. Downloaded: 31-05-2020.

Ashby, 2011. Michael F. Ashby. *Chapter 5 - Materials Selection—The Basics*. ebook. Butterworth-Heinemann, 2011.

Banala et al., Dec 2006. S. K. Banala, S. K. Agrawal, A. Fattah, V. Krishnamoorthy, W. Hsu, J. Scholz and K. Rudolph. *Gravity-Balancing Leg Orthosis and Its Performance Evaluation*. IEEE Transactions on Robotics, 22(6), 1228–1239, 2006. ISSN 1941-0468. doi: 10.1109/TRO.2006.882928.

Belda Lois et al., 12 2011. Juan Manuel Belda Lois, Silvia Horno, Ignacio Bermejo Bosch, Juan Moreno, José Pons, Dario Farina, Marco Iosa, Marco Molinari, Federica Tamburella, Ander Ramos-Murguialday, Andrea Caria, Teodoro Solis-Escalante, Clemens Brunner and Massimiliano Rea. *Rehabilitation of gait after stroke: a review towards a top-down approach. J Neuro Eng Rehabil 8(1):66*. Journal of neuroengineering and rehabilitation, 8, 66, 2011. doi: 10.1186/1743-0003-8-66.

Bjoner and Hole, 2019. Jørgen Bjoner and Roger Hole. *Development of a computational lower body exoskeleton-human model*, AAU, 2019.

Bosch et al., 05 2016. Tim Bosch, Jennifer Eck, Karlijn Knitel and Michiel Looze. *The effects of a passive exoskeleton on muscle activity, discomfort and endurance time in forward bending work*. Applied Ergonomics, 54, 212–217, 2016. doi: 10.1016/j.apergo.2015.12.003.

Bostelman and Hong, 2018. Roger Bostelman and Tsai Hong. *Test methods for exoskeletons—lessons learned from industrial and response robotics*. Institution of Engineering and Technology, Wearable Exoskeleton Systems: Design, control and applications, 2018. doi: 10.1049/PBCE108E_ch13.

Christensen et al., 01 2019. Simon Christensen, Shaoping Bai, Sajid Rafique, Magnus Isaksson, Leonard O'Sullivan, Valerie Power and Gurvinder Virk. *AXO-SUIT - A Modular Full-Body Exoskeleton for Physical Assistance: Proceedings of the 4th IFToMM Symposium on Mechanism*

Design for Robotics. Springer Nature Switzerland, 2019. ISBN 978-3-030-00364-7. doi: 10.1007/978-3-030-00365-4_52.

Cleve Moler, MathWorks, 2003. Cleve Moler, MathWorks. *Stiff Differential Equations*. `https://se.mathworks.com/company/newsletters/articles/stiff-differential-equations.html`, 2003. Downloaded: 25-05-2020.

Dežman et al., 2017. Miha Dežman, Tadej Debevec, Jan Babič, editor="Rodić Aleksandar Gams, Andrej" and Theodor Borangiu. *Effects of Passive Ankle Exoskeleton on Human Energy Expenditure: Pilot Evaluation*. Springer International Publishing, pages 491–498, 2017.

EN1999-1-1, 2007. EN1999-1-1. *Eurocode9: Design of aluminium structures - Par 1-1: General structural rule*, 2007.

Fukuchi et al., 04 2018. Claudiane Fukuchi, Reginaldo Fukuchi and Marcos Duarte. *A public dataset of overground and treadmill walking kinematics and kinetics in healthy individuals*. PeerJ, 6, e4640, 2018. doi: 10.7717/peerj.4640.

Hansen et al., 06 2004. Andrew Hansen, Dudley Childress and Erick Knox. *Roll-over shapes of human locomotor systems: Effects of walking speed*. Clinical biomechanics (Bristol, Avon), 19, 407–14, 2004. doi: 10.1016/j.clinbiomech.2003.12.001.

Herrero-Perez et al., 05 2013. David Herrero-Perez, Jesus Martinez-Frutos and Pascual Martí-Montrull. *An implementation of level set based topology optimization using GPU*. 2013.

Hung et al., 2017. Yu-Chun Hung, Kuo and Chin-Hsing. *A Novel One-DoF Gravity Balancer Based on Cardan Gear Mechanism*. Springer International Publishing, pages 261–268, 2017.

ISO, 2014. ISO. *ISO 13482 – 2014 Standard*. Online Article - `https://www.iso.org/standard/53820.html`, 2014.

Jain et al., 07 2015. Naman Jain, Rahul Joshi and Rakesh Saxena. *TOPOLOGICAL OPTIMIZATION TECHNIQUES FOR LINEAR ISOTROPIC STRUCTURES SUBJECTED TO STATIC AND SELF-WEIGHT LOADING CONDITIONS*. International Research Journal of Engineering and Technology, 2, 52–59, 2015.

Jansen et al., 06 2013. Karen Jansen, Friedl De Groote, Jacques Duysens and Ilse Jonkers. *How gravity and muscle action control mediolateral center of mass excursion during slow walking: A simulation study*. Gait and posture, 39, 2013. doi: 10.1016/j.gaitpost.2013.06.004.

Kanjanapas and Tomizuka, 2013. Kan Kanjanapas and Masayoshi Tomizuka. *7 Degrees of Freedom Passive Exoskeleton for Human Gait Analysis: Human Joint Motion Sensing and Torque Estimation during Walking*. IFAC Proceedings Volumes, 46(5), 285 – 292, 2013. ISSN 1474-6670. doi: https://doi.org/10.3182/20130410-3-CN-2034.00020. URL `http://www.sciencedirect.com/science/article/pii/S1474667015362285`. 6th IFAC Symposium on Mechatronic Systems.

Kintsch and Depaula, 01 2002. Anja Kintsch and Rogerio Depaula. *A framework for the adoption of assistive technology*. Proceedings of SWAAAC 2002: Supporting Learning Through Assistive Technology, 2002.

Kollen et al., 04 2006. Boudewijn Kollen, Gert Kwakkel and Eline Lindeman. *Hemiplegic Gait After Stroke: Is Measurement of Maximum Speed Required?* Archives of physical medicine and rehabilitation, 87, 358–63, 2006. doi: 10.1016/j.apmr.2005.11.007.

Li and Bai, 2019. Zhongyi Li and Shaoping Bai. *A novel revolute joint of variable stiffness with reconfigurability*. Mechanism and Machine Theory, 133, 720 – 736, 2019. ISSN 0094-114X. doi: https://doi.org/10.1016/j.mechmachtheory.2018.12.011. URL `http://www.sciencedirect.com/science/article/pii/S0094114X1831512X`.

Mahmoodi et al., 2013. P. Mahmoodi, R.S. Ransing and M.I. Friswell. *Modelling the effect of 'heel to toe' roll-over contact on the walking dynamics of passive biped robots*. Applied Mathematical Modelling, 37(12), 7352 – 7373, 2013. ISSN 0307-904X. doi: https://doi.org/10.1016/j.apm.2013.02.048. URL `http://www.sciencedirect.com/science/article/pii/S0307904X13001558`.

MatWeb, 2020. MatWeb. *Material property data*. `http://www.matweb.com/search/DataSheet.aspx?MatGUID=4f19a42be94546b686bbf43f79c51b7d`, 2020. Downloaded: 05-05-2020.

Näf * et al., 2 2019. Matthias Näf *, Karen Junius *, Marco Rossini, Carlos David Rodriguez Guerrero, Bram Vanderborght and Dirk Lefeber. *Misalignment Compensation for Full Human-Exoskeleton Kinematic Compatibility: State of the Art and Evaluation*. ASME Applied Mechanics Reviews, 70(5), 2019. ISSN 0003-6900. doi: 10.1115/1.4042523. * These authors contributed equally to this work.

Nakayama et al., 2009. T. Nakayama, Y. Araki and H. Fujimoto. *A new gravity compensation mechanism for lower limb rehabilitation*. 2009 International Conference on Mechatronics and Automation, pages 943–948, 2009. ISSN 2152-744X. doi: 10.1109/ICMA.2009.5246352.

Nikravesh, 1988. Pariz E. Nikravesh. *Computer-Aided Analysis of Mechanical Systems*. ebook. Prentice Hall, 1988.

Nikravesh, 09 2018. Parviz Nikravesh. *Planar Multibody Dynamics: Formulation, Programming with MATLAB®, and Applications*. 2018. ISBN 9781315105437. doi: 10.1201/b22302.

Pahl et al., 2007. Gerhard Pahl, Wolfgang Beitz, Jörg Feldhusen and Karl-Heinrich Grote. *Product Development Process*. Engineering Design: A Systematic Approach, pages 125–143, 2007. doi: 10.1007/978-1-84628-319-2_4. URL `https://doi.org/10.1007/978-1-84628-319-2_4`.

Perez, 2012. David Herrero Perez. *Level Set Method Applied to Topology Optimization*. Grupo de Optimizacion Estructural (GOE), 2012.

Ren et al., 05 2005. Lei Ren, Richard Jones and David Howard. *Dynamic analysis of load carriage biomechanics during level walking*. Journal of biomechanics, 38, 853–63, 2005. doi: 10.1016/j.jbiomech.2004.04.030.

Sanchez-Villamañan et al., 2018. M. Sanchez-Villamañan, J. Gonzalez-Vargas and Torricelli. *Compliant lower limb exoskeletons: a comprehensive review on mechanical design principles.* NeuroEngineering Rehabil, 16, 2018. doi: https://doi.org/10.1186/s12984-019-0517-9.

The MathWorks, Inc, 2020. The MathWorks, Inc. *Simscape User's Guide*. `https://se.mathworks.com/help/pdf_doc/physmod/simscape/simscape_ug.pdf`, 2020. Downloaded: 25-05-2020.

Torricelli et al., aug 2016. Diego Torricelli, Jose Gonzalez, Maarten Weckx, René Jiménez-Fabián, Bram Vanderborght, Massimo Sartori, Strahinja Dosen, Dario Farina, Dirk Lefeber and Jose L Pons. *Human-like compliant locomotion: state of the art of robotic implementations*. Bioinspiration & Biomimetics, 11(5), 051002, 2016. doi: 10.1088/1748-3190/11/5/051002. URL `https://doi.org/10.1088%2F1748-3190%2F11%2F5%2F051002`.

Wall et al., 06 2014. Anneli Wall, Katarina Skough Vreede, Vera Häglund, Hiroaki Kawamoto, Yoshiyuki Sankai and Jörgen Borg. *Gait training early after stroke with a new exoskeleton - The hybrid assistive limb: A study of safety and feasibility*. Journal of neuroengineering and rehabilitation, 11, 92, 2014. doi: 10.1186/1743-0003-11-92.

Zanotto et al., 08 2015. Damiano Zanotto, Yasuhiro Akiyama, Paul Stegall and Sunil Agrawal. *Knee Joint Misalignment in Exoskeletons for the Lower Extremities: Effects on User's Gait*. IEEE Transactions on Robotics, 31, 978–987, 2015. doi: 10.1109/TRO.2015.2450414.

Zhou et al., 08 2020. Libo Zhou, Weihai Chen, Wenjie Chen, Shaoping Bai, Jianbin Zhang and Jianhua Wang. *Design of a Passive Lower Limb Exoskeleton for Walking Assistance with Gravity Compensation*. Mechanism and Machine Theory, 150, 2020. doi: 10.1016/j.mechmachtheory.2020.103840.

Zoss et al., April 2006. A. B. Zoss, H. Kazerooni and A. Chu. *Biomechanical design of the Berkeley lower extremity exoskeleton (BLEEX)*. IEEE/ASME Transactions on Mechatronics, 11 (2), 128–138, 2006. ISSN 1941-014X. doi: 10.1109/TMECH.2006.871087.

A FEM Considerations

This chapter presents additional result from the analyses performed to ensure the structural integrity of the Exoskeleton, and a more detailed description of the level set based topology optimization method.

A.1 Structural Analysis Knee Exoskeleton - Initial Design

Stress Results Load Case 1

Load case 1 is observed to display larger maximum stress compared to the hip, but it is still yields a safety factor of about 4 when yield is assessed. The stress is higher even though the forces are smaller in magnitude, due to a thinner base. Again it is observed that the general stress level of the part is low compared to the material strength.

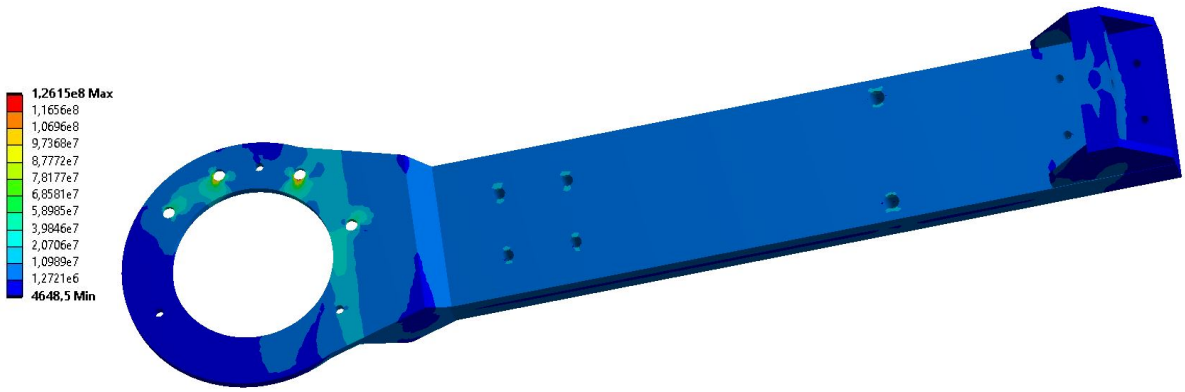

Figure A.1: Stress distribution of the initial design. The unit of the color bar is Pascals (Pa).

Deformation Results for Load Case 1

The total deformation occurs mainly in the positive z-direction, and the maximum deformation is observed to be $1mm$. The deformation distribution is very similar to the ones presented for the hip frame, and is therefore not presented.

Stress Results for Load Case 2

The setup of case 2 is identical to the setup in the hip joint, except for a smaller magnitude of loads. The resulting stress from load case 2 is presented in Figure A.2.

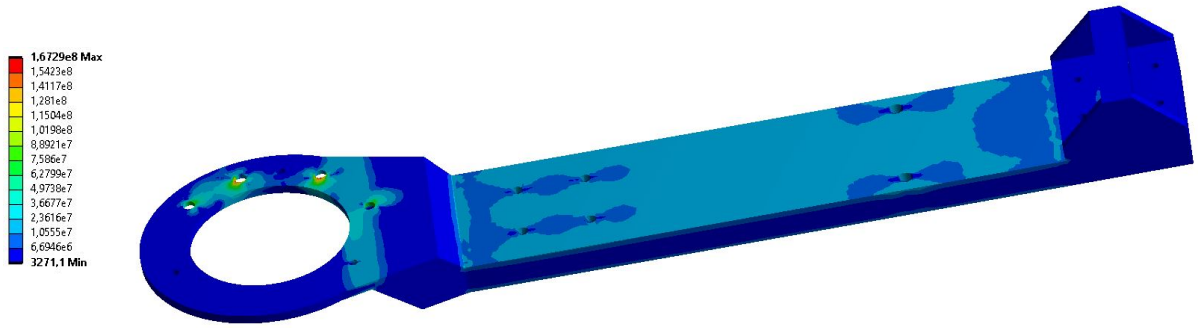

Figure A.2: Stress distribution of the calf limb resulting from load case 2. The unit of the color bar is Pascals (Pa)

Deformation results for Load Case 2

The maximum total deformation resulting from load case 2 is 1.24mm, and occurs mainly in the positive z-direction. Again the distribution is similar to that of the hip frame.

Results from Load Case 3

The deformation was observed to be less than 0.1mm, which is considered negligible, hence the deformation results are not presented. The stress distribution of the inner pin plate is presented in Figure A.3.

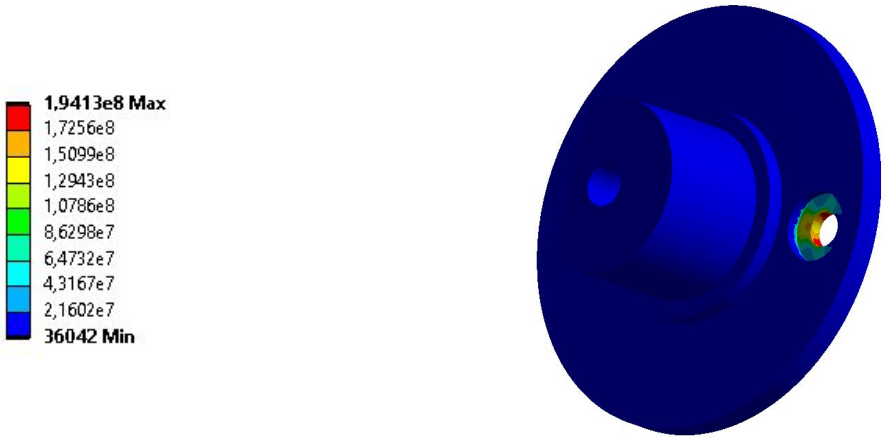

Figure A.3: Stress distribution of the inner pin plate resulting from load case 3. The unit of the color bar is Pascals (Pa)

A.2 Structural Integrity Final design - Load case 1

The total deformation of the final design, with a converged mesh, is shown in Figure A.4. The deformation can be seen to be maximum 1.178mm, which is within the failure criteria.

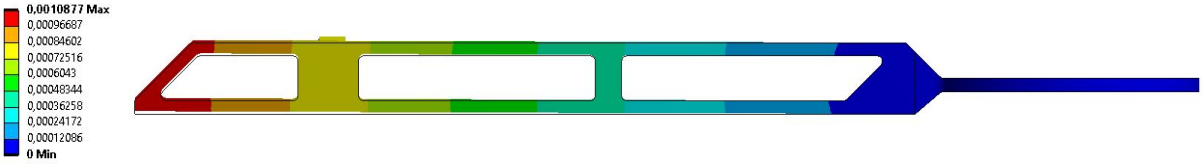

Figure A.4: Maximum deformation of the final design subjected to load case 1. The color bar is given with the unit meter.

The stress distribution of the final design is shown in Figure A.5. It is observed that the general stress level of the new design is generally higher than in the initial design. The maximum stress is still well below yield, and the part has a safety factor of about five.

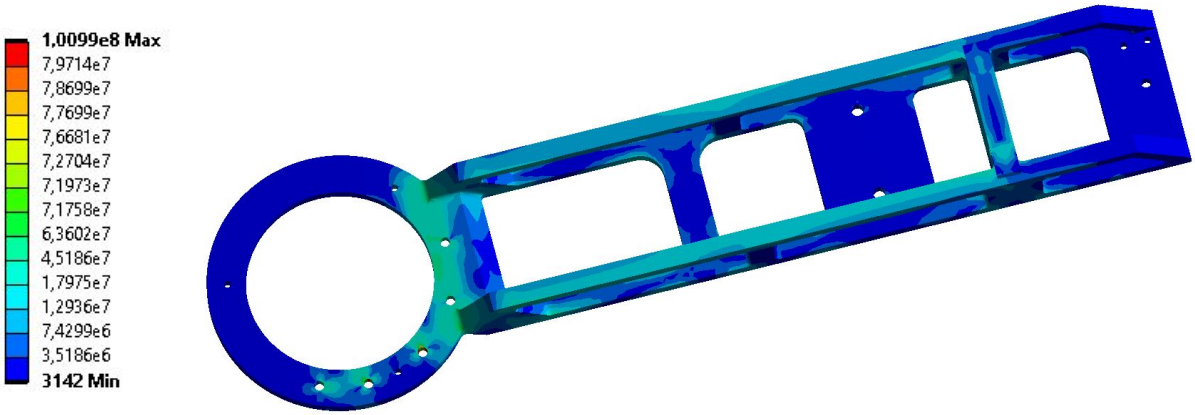

Figure A.5: Stress distribution of the final design subjected to load case 1. The color bar is given with the unit Pascals [Pa].

A.2.1 Knee Structural Integrity - load case 2

Analysis results from load case 2

To ensure the design has the required strength it was subjected to load case 2. Load case 2 yielded a maximum deformation of 0.566mm in the positive z-direction. The deformation distribution is similar to the one for the hip outer frame, (Figure 6.18). The stress in the part subjected to load case 2 is presented in Figure A.6.

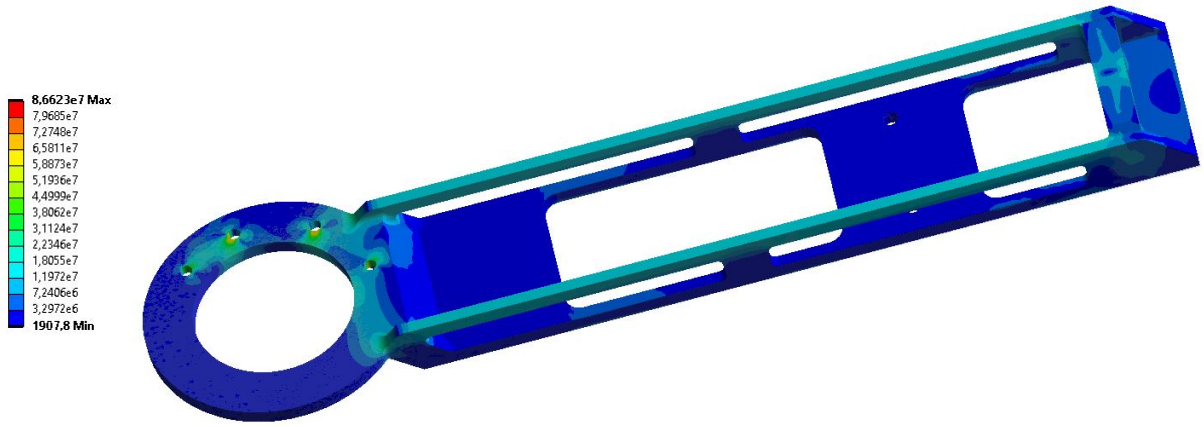

Figure A.6: Stress distribution of the calf limb resulting from load case 1. The unit of the color bar is Pascals (Pa)

A.3 Level Set Based Topology Optimization Theory

This section presents a more detailed description of the level set based based method for topology optimization. The section is based on the paper, Herrero-Perez et al. [2013] and the lecture slide Perez [2012].

A.3.1 Level Set Equation

A closed curve Γ can be represented by using an auxiliary variable φ called the level set function. This function represents the curve at a certain level. The function at the zero level is given as:

$$\Gamma = \{(x, y) | \varphi(x, y) = 0\} \tag{A.1}$$

The level set function is assumed to take positive values inside the region delimited by the curve and negative values outside. When the curve Γ moves in the normal direction with a speed v then the level set function satisfies the level set equation:

$$\frac{\partial \varphi}{\partial t} = v|\nabla \varphi| \tag{A.2}$$

Where the $||$ represents the Euclidean norm and t is the time. This equation is a partial differential equation, it is actually the equation known as the Hamilton-Jacobi equation. The equation can be solved by using a finite differences on a Cartesian grid. However using a simple finite difference method often fails, therefore upwind methods are recommended.

Evolution of the boundary

The level set method represents the boundary of the structure, $\partial\Omega$, using a scalar level set function defined in the design domain D, which contains the domain Ω. The level set function

is defined as:

$$\phi(\mathbf{x},t) = \begin{cases} > 0 & \mathbf{x},\mathbf{y} \in \Omega \\ = 0 & \mathbf{x},\mathbf{y} \in \partial\Omega \\ < 0 & \mathbf{x},\mathbf{y} \notin \partial\Omega \end{cases} \tag{A.3}$$

Where (x,y) is any point in the design domain. As mentioned above the evolution of the boundary. To ensure convergence of the differential equation the Courant-Friedrichs-Levy (CFL) condition must be satisfied:

$$\Delta t \leq \frac{h}{\max|v|} \tag{A.4}$$

where h is the minimum distance between points of the grid and max $|v|$ is the maximum value of the normal velocity. The normal velocity is what links the structural optimization to the level set method.

A.3.2 General level set topology optimization algorithm

This section explains the general algorithm of the level set method applied to the standard topology optimization problem of minimizing compliance of a solid structure, while subjected to a constraint on the material used. This standard problem is stated in mathematical terms below, and then used to explain the level set based topology optimization.

$$\begin{aligned} &\text{min :} && c(\eta) = U^T K U = \textstyle\sum_{i=1}^{N} u_i^T k_i u_i = \sum_{i=1}^{N} \eta_i u_i^T k_l u_i \\ &\text{Subjected to:} && V(\eta) = V_{req} \\ & && KU = F \\ &\left.\begin{matrix} \eta_i & = 0 \\ \eta_i & = 1 \end{matrix}\right\} && \forall \eta = 1,\ldots,N \end{aligned} \tag{A.5}$$

In the above formulation the symbols have the following meaning:

- $\eta = (\eta_1, ..., \eta_N)$ is the vector of pseudo densities, where one entry is assigned to each element. The pseudo density of an element (η_i) is either 0 or 1, where 0 represents a void element and 1 represents a solid element.
- $c(\eta)$ is the objective function for minimizing compliance.
- K, U and F are the global stiffness matrix, displacement vector and force vector, respectively. These are introduced from the equilibrium equation of FEM.
- k_i and u_i are the element stiffness matrix and the element displacement vector of element i.
- k_l is the element stiffness matrix of an element with a pseudo density of 1.
- N is the number of elements in the design domain.
- $V(\eta)$ is the total number of solid elements.
- V_{req} is the required number of solid elements.

Topology optimization using the level set method starts with the boundary of the part within the design domain and then itteratively updates this boundary until the objective function reaches an optimum. The boundary of the part is described by the level set function in the following way:

$$\phi(\mathbf{x},\mathbf{y}) = \begin{cases} > 0 & \text{if} \quad (\mathbf{x},\mathbf{y}) \in \Omega \\ = 0 & \text{if} \quad (\mathbf{x},\mathbf{y}) \in \partial\Omega \\ < 0 & \text{if} \quad (\mathbf{x},\mathbf{y}) \notin \partial\Omega \end{cases} \tag{A.6}$$

Here $(\mathbf{x},\mathbf{y})$ is a random point within the design domain, and the boundary is defined as $\partial\Omega$. The now defined boundary is then updated by the evolution equation:

$$\frac{\partial\varphi}{\partial t} = v|\nabla\varphi| - wg \tag{A.7}$$

Here t represents a fictitious time parameter that indicates the way of the evolution of the boundary, during the optimization. Both g and v are scalar fields within the design domain, and v determines the geometric motion of the boundary of the structure. This is chosen based on the shape derivative of the optimization object. The field g determines the nucleation of new holes within the boundary (structure), this is determined by the topological derivative of the optimization objective. And finally w is a positive parameters which determines the influence of g.

Now the level set function can be discretized with grid points centered on the elements of an FE mesh. The position of the center of the element is denoted c_i, and then the discretized level set function should satisfy:

$$\phi\left(c_\mathrm{i}\right) = \begin{cases} > 0 & \eta_\mathrm{i} = 1 \\ < 0 & \eta\mathrm{i} = 0 \end{cases} \tag{A.8}$$

The equations represent that all elements with a center outside the boundary are now considered void elements. Then the boundary is updated by numerically solving Equation A.7. To ensure convergence of the differential equation the Courant-Friedrichs-Levy (CFL) condition must be satisfied:

$$\Delta t \leq \frac{h}{\max|v|} \tag{A.9}$$

where h is the minimum distance between points of the grid and max $|v|$ is the maximum value of the normal velocity.

Constraints:
The volume constraint is set to ensure the volume of the structure is less than a determined requirement. The constraint is incorporated to the objective function using the agumented lagranian method, to obtain the augmented objective function.

$$L = c(\eta) + \lambda^k \left(V(x) - V_{req}\right) + \frac{1}{2\Lambda^k}\left[V(x) - V_{req}\right]^2 \tag{A.10}$$

Here λ^k and Λ^k are parameters which are updated for each iteration. The parameters are updated by the following scheme.

$$\lambda^{k+1} = \lambda^k + \frac{1}{\Lambda^k}\left(V(x) - V_{req}\right), \quad \Lambda^{k+1} = \alpha\Lambda^k \tag{A.11}$$

Where α is a fixed parameter between 0 and 1.

Normal velocity

The normal velocity is chosen as the decent direction of the Lagrangian L, which is found by taking the shape derivative. The shape sensitivity of the compliance objective $c(\eta)$ is the negative of the strain energy density, which for the discretized model becomes:

$$\left.\frac{\partial c}{\partial \Omega}\right|_{\mathrm{i}} = -u_{\mathrm{i}}^T k_{\mathrm{i}} u_{\mathrm{i}} \tag{A.12}$$

The shape sensitivity of the volume $V(\eta)$ is given as:

$$\frac{\partial V}{\partial \Omega}|_e = 1 \tag{A.13}$$

Now by using these sensitivities in combination with the Equations A.11 and A.10, the normal velocity within element i at the iteriation k can be expressed as:

$$v|_{\mathrm{i}} = -\left.\frac{\partial L}{\partial \Omega}\right|_{\mathrm{i}} = u_{\mathrm{i}}^T k_{\mathrm{i}} u_{\mathrm{i}} - \lambda^k - \frac{1}{\Lambda^k}\left(V(x) - V_{req}\right) \tag{A.14}$$

Nucleation of new holes in the structure

As mentioned above the scalar field g is used to determine when a new hole in the structure should be created. The field can be defined as:

$$g = -\operatorname{sign}(\varphi)\delta_T L \tag{A.15}$$

Where $\delta_T L$ is the topological sensitivity of the Lagrangian L. What is important to note here is that creating new holes outside the boundary (where there are only void elements) is pointless, therefore the topological sensitivity is set to zero, whenever the level set function takes on a values smaller than zero.

B | Supplement to the Dynamic Model Refinement

This Chapter is a supplement to the dynamic model refinements, and presents a more detailed description of the roller constraint, an initial trial with two legs and supplemental results to the presented model refinements.

B.1 Roll Over Shape Constraint

As presented in Chapter 3, the foot roller is based on a point follower cam constraint, as presented in Nikravesh [1988]. The general expanded form of the constraint is stated in Equation B.1, where the notations used are displayed in Figure B.1. From the figure it is observed that body i is the cam body and body j is the point follower body.

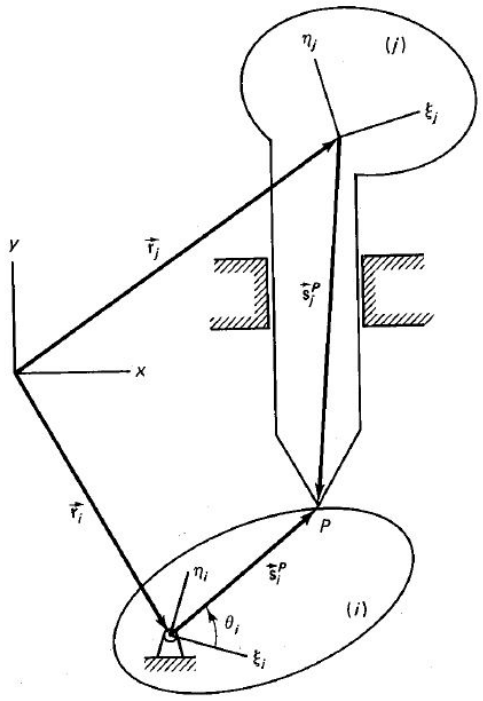

Figure B.1: Illustration of point follower cam, Nikravesh [1988].

$$\begin{bmatrix} x \\ y \end{bmatrix}_i + \begin{bmatrix} \cos\phi & -\sin\phi \\ \sin\phi & \cos\phi \end{bmatrix}_i \begin{bmatrix} s\cos\theta \\ s\sin\theta \end{bmatrix}_i - \begin{bmatrix} x \\ y \end{bmatrix}_j - \begin{bmatrix} \cos\phi & -\sin\phi \\ \sin\phi & \cos\phi \end{bmatrix}_j \begin{bmatrix} \xi^p \\ \eta^P \end{bmatrix}_j = \begin{bmatrix} 0 \\ 0 \end{bmatrix} \tag{B.1}$$

In the above equation two parameters are introduced, namely s and θ, which both are introduced as tools to describe the cam shape. The general expanded form lifted from

Nikravesh [1988], is then transformed into the notations used in Chapter 3, resulting in the following equation.

$$\mathbf{r}_i + \mathbf{A}_i \begin{bmatrix} s\cos\theta \\ s\sin\theta \end{bmatrix}_i - \mathbf{r}_j - \mathbf{A}_j \mathbf{s}_{jX} = \begin{bmatrix} 0 \\ 0 \end{bmatrix} \tag{B.2}$$

To implement this constraint to act as the roll over shape of the foot, it is desired that the cam shaped body rolls relative to a fixed point in space. Hence the point follower body is then set as the ground fixing point $\mathbf{r}_g$. Then from literature, Hansen et al. [2004], it is found that the roll over shape can be modeled as circle with a center located on the body of the foot. This point is defined as $\mathbf{r}_4 + \mathbf{A}_4 s_{4C}$. As the cam shape is represented by a circle s is transformed into a set radius $R = 0.2726m$. Then θ is defined as $\theta = -\phi_4$, to ensure no points of the cam shape penetrates the ground during the gait cycle. Then by applying the above mentioned changes the cam constraint becomes:

$$\mathbf{r}_g - \mathbf{r}_4 - \mathbf{A}_4 \left[\mathbf{s}_{4C} + \begin{bmatrix} R\cos\theta \\ R\sin\theta \end{bmatrix} \right] = \begin{bmatrix} 0 \\ 0 \end{bmatrix} \tag{B.3}$$

B.2 Jacobian Matrix

In this Section the Jacobian matrix of the model with a rollover foot and fixed ankle angle (see Eq:3.2 is presented. The notations presented in Chapter 3 is applied. Additionally the two notations given in equation B.4 is used.

$$curve = \begin{bmatrix} R\cos\theta \\ R\sin\theta \end{bmatrix} \qquad dcurve = \begin{bmatrix} -R\sin\theta \\ R\cos\theta \end{bmatrix} \tag{B.4}$$

	$\frac{\partial\Phi}{\partial x_1}$	$\frac{\partial\Phi}{\partial y_1}$	$\frac{\partial\Phi}{\partial\phi_1}$	$\frac{\partial\Phi}{\partial x_2}$	$\frac{\partial\Phi}{\partial y_2}$	$\frac{\partial\Phi}{\partial\phi_2}$	$\frac{\partial\Phi}{\partial x_3}$	$\frac{\partial\Phi}{\partial y_3}$	$\frac{\partial\Phi}{\partial\phi_3}$	$\frac{\partial\Phi}{\partial x_4}$	$\frac{\partial\Phi}{\partial y_4}$	$\frac{\partial\Phi}{\partial\phi_4}$
Φ_1	1	0	$B_1 s_{1H}(1)$	-1	0	$-B_2 s_{2H}(1)$	0	0	0	0	0	0
Φ_2	0	1	$1B_1 s_{1H}(2)$	0	-1	$-B_2 s_{2H}(2)$	0	0	0	0	0	0
Φ_3	0	0	0	1	0	$B_2 s_{2K}(1)$	-1	0	$-B_3 s_{3K}(1)$	0	0	0
Φ_4	0	0	0	0	1	$B_2 s_{2K}(2)$	0	-1	$-B_3 s_{3K}(2)$	0	0	0
Φ_5	0	0	0	0	0	0	1	0	$B_3 s_{3A}(1)$	-1	0	$-B_4 s_{4A}(1)$
Φ_6	0	0	0	0	0	0	0	1	$B_3 s_{3A}(2)$	0	-1	$-B_4 s_{4A}(2)$
Φ_7	0	0	0	0	0	0	0	0	0	-1	0	$B_4[s_{4C} + curve] - A_4 dcurve(1)$
Φ_8	0	0	0	0	0	0	0	0	0	0	-1	$B_4[s_{4C} + curve] - A_4 dcurve(2)$
Φ_9	0	0	1	0	0	0	0	0	0	0	0	0
Φ_{10}	0	0	0	0	0	0	0	0	1	0	0	0
Φ_{11}	0	0	0	0	0	-1	0	0	1	0	0	0
Φ_{12}	0	0	0	0	0	0	0	0	-1	0	0	1

C | Dimension of Design

This Chapter presents the main dimensions of the final design of the hip and knee frame, along with the dimensions of the hip and knee inner base plates.

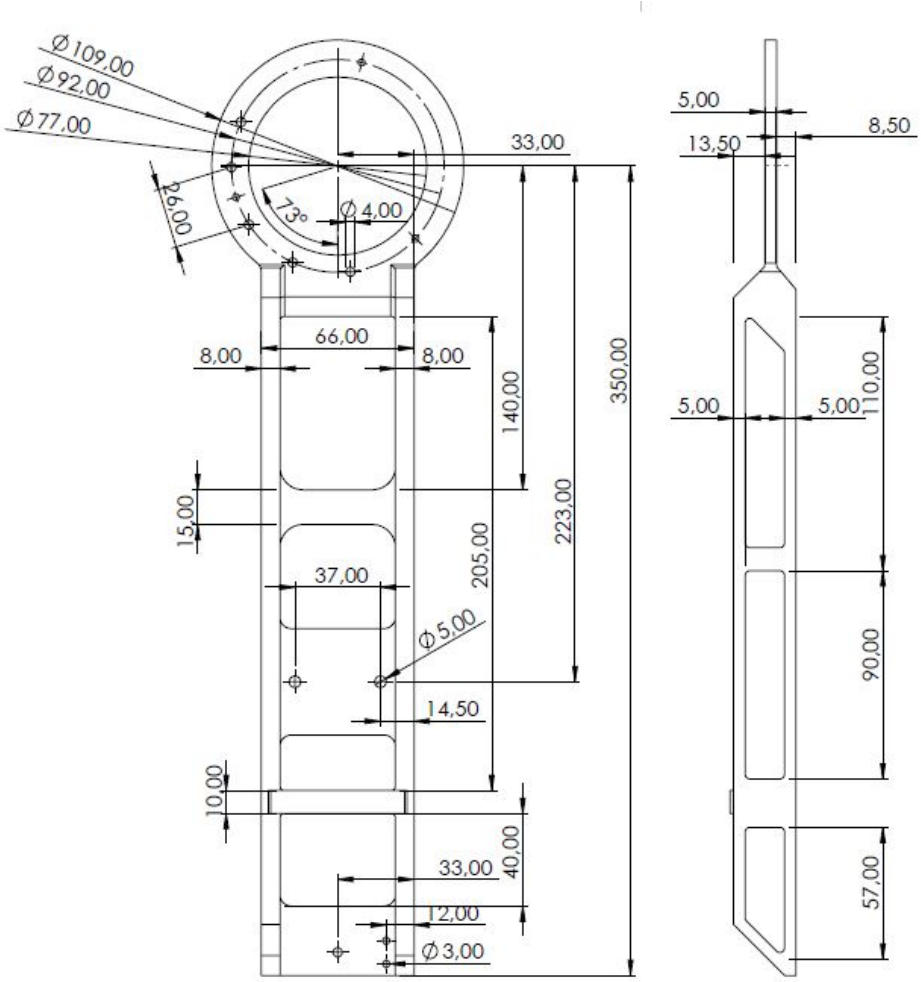

Figure C.1: Main dimensions of the hip frame

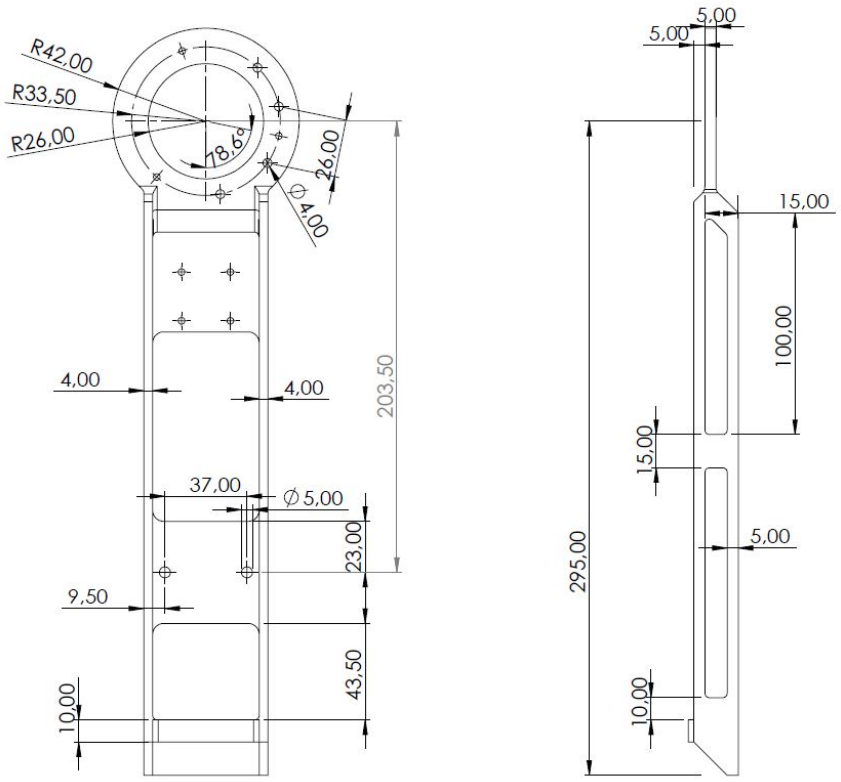

Figure C.2: Main dimensions of the knee frame

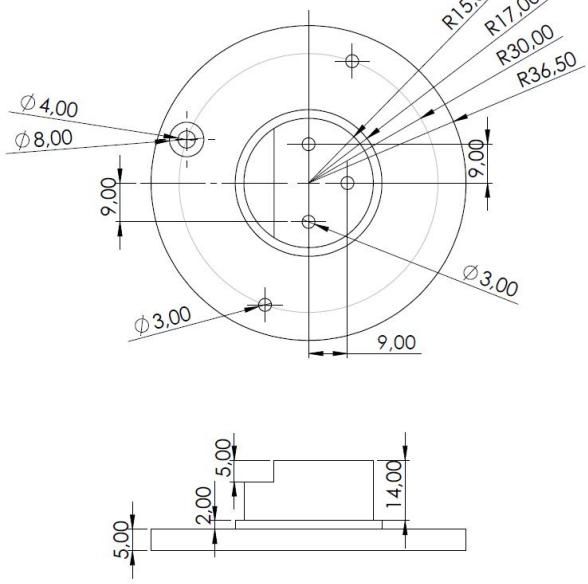

Figure C.3: Main dimensions of the hip inner base

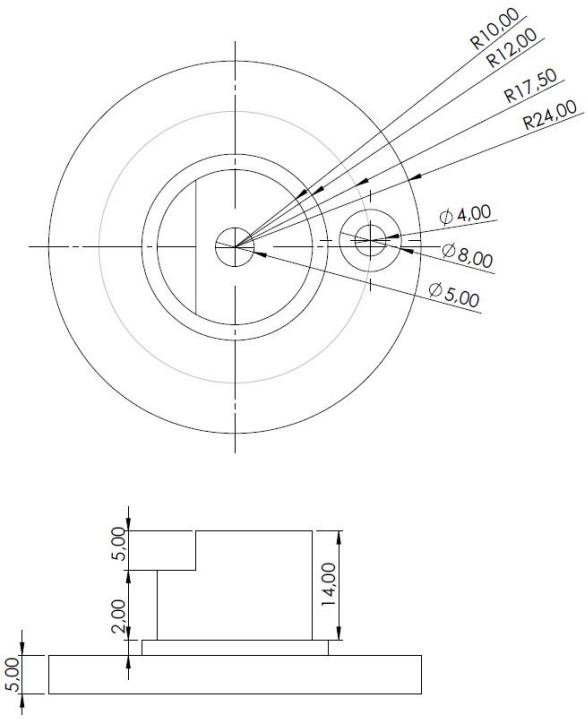

Figure C.4: Main dimension of the knee inner base

D | Dynamic Calculations

This chapter presents a more detailed view on the calculation approach for obtaining the positions, velocities and accelerations in the computational dynamic model. The solution approach has previously been presented in detail in a semester project by the authors, Bjoner and Hole [2019]. The sections D.1, D.2 and D.3, are lifted directly from, Bjoner and Hole [2019], and are only presented for continuity. The theory is fundamentally built on the works by Nikravesh [2018].

D.1 Newton-Raphson solution method

When solving a kinematic analysis of a mechanical system, one is required to find the solution of the position constraint equations:

$$\mathbf{\Phi}(\mathbf{q}) = 0 \tag{D.1}$$

As seen in Section 3.6 are these nonlinear functions. Newton- Raphson is a nonlinear iterative solver used for this purpose. The algorithm in terms of a kinematic system is given as follows, where i represents the iteration number.

1. An initial guess, $\mathbf{q_0}$, is stated for the solution; $\mathbf{q_i} = \mathbf{q_0}$
2. The constraints are evaluated at the initial guess: ${}^{i}\mathbf{\Phi} = \mathbf{\Phi}(\mathbf{q_i})$
3. If the $|\mathbf{\Phi}(\mathbf{q_i})| \leq \varepsilon$, then the iteration is stopped. $\varepsilon \approx 0$ (User defined tolerance)
4. If not, then evaluate the Jacobian ${}^{i}\mathbf{D} = \frac{\partial^{i}\mathbf{\Phi}}{\partial \mathbf{q_i}}$
5. The set of linear equations $\mathbf{D}^{i}\Delta\mathbf{q} = -{}^{i}\mathbf{\Phi}$ is then solved for $\Delta\mathbf{q}$
6. The corrections are added to the previous solution for a better estimate: ${}^{i}\mathbf{q} +^{i} \Delta\mathbf{q} \Rightarrow^{i+1} \mathbf{q}$
7. Return to step 2 with the new estimate.

D.2 Velocities and Accelerations

The system of velocity equations is found by taking the time derivative of the constraint matrix, which is given by the compact form, (Nikravesh [2018]):

$$\mathbf{D}\dot{\mathbf{q}} = \dot{\boldsymbol{\alpha}} \tag{D.2}$$

where the vector $\mathbf{D}$ is the constraint Jacobian matrix and $\dot{\boldsymbol{\alpha}}$ is given as $\dot{\boldsymbol{\alpha}} = -\frac{\partial \Phi}{\partial t} = \begin{bmatrix} 0 \\ \dot{\boldsymbol{d}}(t) \end{bmatrix}$.

Solving for $\dot{\mathbf{q}}$ yields the velocity with respect to time. The formulation of the Jacobian matrix is different for the different constraints utilized. For the deduction of Jacobian matrix, please see the documentation in the previous project by Bjoner and Hole [2019].

The system of acceleration equations are in the same manner found by taking the second time derivative of all constraint equations. In compact form this becomes:

$$\mathrm{D}\ddot{\mathrm{q}} + \dot{\mathrm{D}}\dot{\mathrm{q}} = \ddot{\alpha} \tag{D.3}$$

Solving for $\ddot{\mathrm{q}}$ yields the accelerations.

D.3 Inverse Dynamic Analysis

The dynamic equation of motion of the system can be formulated as presented in Nikravesh [2018]:

$$\mathbf{M}\ddot{\mathbf{q}} = {}^{(a)}\mathbf{h} + \mathbf{D}^T\lambda + {}^{(dr)}\mathbf{D}^{T\,(dr)}\lambda \tag{D.4}$$

Here the Jacobian and Lagrange multipliers associated with the driver constraints are included, (dr), but separated from the kinematic constraints. This equation is rearranged to:

$$\left[\begin{array}{cc} \mathbf{D}^T & {}^{(dr)}\mathbf{D}^T \end{array}\right] \left\{\begin{array}{c} \lambda \\ {}^{(dr)}\lambda \end{array}\right\} = \mathbf{M}\ddot{\mathbf{q}} - {}^{(a)}\mathbf{h} \tag{D.5}$$

The accelerations and Jacobian for all constraints are known from the kinematic analysis. The mass matrix is known and the external forces, $\mathbf{h}$, comes from the gravity. This means that Equation D.5 can be solved as a set of linear algebraic equations with respect to the Lagrange multipliers. These multipliers will have to be related to their respective components in the Jacobian. This will translate the set of multipliers to act in their respective reference systems. The result is the reaction forces and torques at the joints ($\mathbf{D}'\boldsymbol{\lambda}$) and rotary motors (${}^{(dr)}\mathbf{D}'\,{}^{(dr)}\boldsymbol{\lambda}$).

D.4 Inertia Estimations

The dynamic model is designed to be utilized in an early phase of the exoskeleton design process. At this phase is there no prototype to base the dimensions and weight properties on. An initial estimate is therefore necessary. As with the previous semester project has this estimation been based on an existing active exoskeleton at AAU. The methods used to estimate the moment of inertia for each part is described below:

Moment of Inertia of the Thigh

To simplify from 3D to 2D, the thigh is simplified into one rectangular plate and three disks. One disk at each end and one in the center, as seen in Figure D.1. The disk on the left side represents the inertia of the hip joint, the disk in the center represents the inertia of the cuff and the one on the left represent the inner knee joint. The estimated masses of the components are listed in Table D.1. The inertias of the disks is calculated using Equation D.6, where m is the mass of the given disk and r is the radius. For the two end disks the radius is $45mm$ and for the center one it is $20mm$.

$$I_{disk} = \frac{mr^2}{2} \tag{D.6}$$

The rectangular plate represents the frame connecting the hip and the knee joint, its inertia is calculated using Equation D.7, where $l = 0.507m$ is the length and $w = 0.035m$ is the width.

$$I_{rec} = \frac{1}{12} m(l^2 + w^2) \tag{D.7}$$

Then to add the inertias of the objects mentioned above, the parallel axis theorem is used. However to use the theorem the center off mass must be determined. The center of mass is determined by using Equation D.8, where m_{1-4} is the mass of the objects, and x_{1-4} is the distance from the object center of mass to the reference point, which for the thigh is chosen to be the hip mounting point.

$$x_{CM} = \frac{m_1 x_1 + m_2 x_2 + ...m_n x_n}{m_1 + m_2 + ...m_n} \tag{D.8}$$

After determining the center of mass the parallel axis theorem is applied to each of the objects. Equation D.9 is the parallel axis theorem, where I is the moment of inertia about the center of mass of the thigh, I_{CM} is the inertia of the object about its own center of mass and d is the distance from the object mass center to the selected point.

$$I = I_{CM} + md^2 \tag{D.9}$$

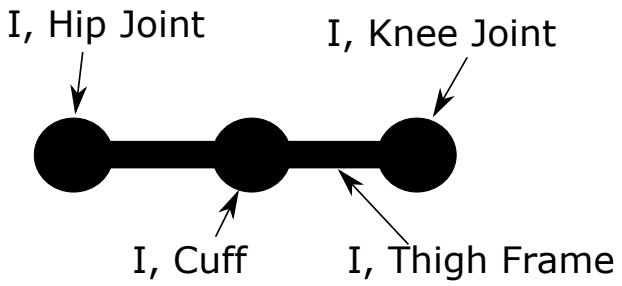

Figure D.1: Illustration of inertia simplification for the thigh

Moment of Inertia of the Calf part

The inertia of the calf is calculated similarly as for the thigh, by dividing it into two discs, placed at the knee end and in the center, and one rectangular plate. The discs at the knee end represents the knee joint and the center disk represent the cuff (see Tab. D.1 for the mass of each component). The inertia is then calculated by inserting the mass properties of the calf into Equations D.6, D.7, D.8 and D.9. The same width, and radii are used as for the thigh estimation.

Part	Hip Joint	Thigh Frame	Cuff	Knee Joint	Calf Frame
Mass [kg]	0.2	0.8	0.5	0.2	0.6

Table D.1: Mass of the representative disks used for inertia estimation

E | Simscape- Theoretical

This chapter provides additional insight into the solver, actuation and sending applied to the Simscape simulations detailed in Chapter 7.

E.1 Choice of Solver

The following background information is based on the userguide to Simscape provided by (The MathWorks, Inc [2020].)
The Simscape Multibody add-on software can be seen as a set of extra block libraries and special simulation features for modelling physical systems in the Simulink environment. Unlike Simulink does it however utilize what is labelled the "Physical Network Approach", which is a method well suited for simulating real physical systems. With this approach represents the block diagram a system of functional elements that interact with each other by connecting the ports of the blocks. Connecting these ports can be compared to connecting the real components of the assembly.

The block library can be considered to mainly include three families of blocks. These are physical elements (CAD import), building blocks (joints, engineering components etc.) and environmental blocks (coordinate frames etc.). The parameters of the building blocks can be altered to fit the physical requirements, and a big part of the modelling process lies in specifying these.

Simscape constructs the equations of motion based on the block network and block parameters. The mathematical representation of the physical system can consist of algebraic constraint equations for specifying the relationship between the system variables and/or Ordinary Differential Equations (ODE's) which governs the rate of change to the system variables, in other words the continuous states for the dynamic system. Together these form a set of Differential Algebraic equations (DAE's). Simscape applies a numerical method for solving the set of ODE's, and in this process also determines the time for the next simulation step. Simscape enables the use of a variety of solvers, both fixed-step and variable-step computations. The solver can further be explicit or implicit. This last choice is important dependent on whether the system id considered *stiff* or not.
A mathematical problem is considered stiff if:
"The solution sought after varies slowly, but there are other solutions within the error tolerances that vary rapidly" - Cleve Moler, MathWorks [2003].
A stiff physical system has one or more components that behaves in a "stiff" manner, such as springs with large spring constant. For stiff systems it is recommended to use an implicit solver.

The choice of solver should be based on computation time and if the specified tolerances are

met when solved. In this simulation has the option "VariableStepAuto" been used, where Simscape automatically suggest a solver with variable step computation. The solver suggested is the explicit solver "ode45", which is seen to present relatively accurate results and a short computational time. To verify this choice have also the implicit solver "ode23t" been used and seen to present the same result at a cost of higher computational time.

E.2 Actuation and Sensing

The block "From Workspace" is utilized to read the input angles from the Matlab workspace, where the input file is a matrix with a time stamp in the first column and corresponding angles in the second column. The input file is marked as "B" in Figure E.1 below. A simulink PS-converter (PS=physical signal) is then used to convert the unit-less input signal to a physical signal. The solver requires two derivaties of the input signal to calculate the dynamic response, i.e. the torque output. The "simulink PS-converter" block therefore has the option to turn on second order filtering, where the first and second time derivatives are calculated. A time filtering time constant of 0.01s has been applied as standard. The layout for actuation and sensing in Simscape Multi-Body is presented in Figure E.1.

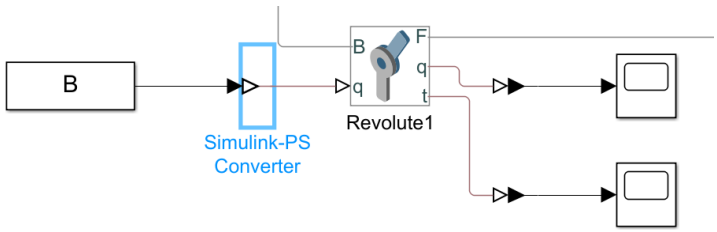

Figure E.1: Section of the block diagram providing the input and output signals.